TESIS DOCTORAL

ULPGC Universidad de Las Palmas de Gran Canaria | Escuela de Doctorado

NUEVAS ALEACIONES DE ALTA ENTROPÍA CREADAS EXPERIMENTALMENTE PARA USOS INDUSTRIALES

Doctorando en Ingenierías Química, mecánica y fabricación

Las Palmas de Gran Canaria.

Mayo de 2025.

Autor:

Alberto Daniel Rico Cano

Directora:

Dra. Julia Claudia Mirza Rosca

SHEng SMART HEALTHCARE ENGINEERING

UNIVERSIDAD DE LAS PALMAS DE GRAN CANARIA

ESCUELA DE DOCTORADO

Programa de doctorado en Ingenierías Química, Mecánica y de Fabricación

Departamento de Ingeniería Mecánica

Título de Tesis

NUEVAS ALEACIONES DE ALTA ENTROPÍA
CREADAS EXPERIMENTALMENTE PARA USOS INDUSTRIALES

Autor:
Alberto Daniel Rico Cano

Directora:
Dra. Julia Claudia Mirza Rosca

Las Palmas de Gran Canaria, a 7 de mayo de 2025

La Directora,

MIRZA ROSCA JULIANA CLAUDIA - 45360672A

Firmado digitalmente por MIRZA ROSCA JULIANA CLAUDIA - 45360672A
Fecha: 2025.05.13 13:29:53 +01'00'

El Doctorando,

RICO CANO ALBERTO DANIEL - 44727996B

Firmado digitalmente por RICO CANO ALBERTO DANIEL - 44727996B
Fecha: 2025.05.13 13:57:39 +01'00'

AGRADECIMIENTOS

Gracias a mi familia y amigos, a los que aún están y a los que ya no, me encantaría disfrutar de este reconocimiento con todos ustedes. Por el orgullo que me han mostrado siempre a lo largo de este camino, que ha tenido muchas subidas y bajadas, sonrisas y lágrimas. Gracias de corazón a mi padre, mi hermana y mi madre.

Agradecido a todo el equipo del laboratorio, a Pedro, Santiago y Miguel, que durante estos casi 5 años me han visto crecer y sus palabras han sido siempre de consejo y apoyo. Gracias especialmente a Cristina, compañera y mentora en el laboratorio, por su infinita paciencia aunque le preguntara lo mismo 4 veces, sin ella el laboratorio no sería el mismo. Suerte en la vida, conseguirás todo lo que te propongas.

Por último pero no menos importante, mis más sinceros agradecimientos a mi tutora y directora de tesis Julia. Por su infinito apoyo y asesoramiento. Esto no hubiese sido posible sin su constante dedicación, eternamente agradecido.

ULPGC Universidad de Las Palmas de Gran Canaria | Escuela de Doctorado

Resumen

Resumen

El objetivo principal de este trabajo de tesis es el estudio de la caracterización mecánica y electroquímica de cuatro novedosos compuestos elaborados a partir de una matriz de carburo de boro y distintos porcentajes de una aleación de alta entropía (CoCrFeNiMo), para determinar sus posibles aplicaciones industriales.

Este objetivo a su vez puede conseguirse mediante la superación de distintos objetivos específicos:

1. Estudiar y evaluar las propiedades mecánicas y electroquímicas de cada una de las muestras por separado.
2. Comparar como afecta el porcentaje de aleación de alta entropía (HEA) en la matriz cerámica a nivel mecánico y electroquímico.
3. Comparar las muestras con HEA con una muestra de carburo de boro puro (fabricado en las mismas condiciones) para determinar cuál es mejor y sus posibles aplicaciones industriales.

La tesis propuesta se encuentra enmarcada en el programa de doctorado en Ingenierías Química, Mecánica y de Fabricación (QUIMEFA) por la Universidad de Las Palmas de Gran Canaria, siendo su línea de investigación corrosión de los metales. La presentación de la presente tesis es bajo la modalidad de tesis por compendio de publicaciones, para su correcto desarrollo se han publicado 3 artículos.

En el primero de los artículos publicados “Corrosion Behavior of New B_4C Ceramic Doped with High-Entropy Alloy in an Aggressive Environment”, se realiza un estudio que explora el comportamiento frente a la corrosión de una nueva cerámica de carburo de boro (B_4C) dopada con 2% de una aleación de alta entropía (HEA) expuesta a un entorno marino agresivo. La investigación incluye la caracterización microestructural y ensayos electroquímicos, tratando de entender cómo afecta la influencia de la adición de HEA en las propiedades del material.

En el segundo de los artículos publicados “Corrosion Behavior and Microhardness of a New B_4C Ceramic Doped with 3% Volume High-Entropy Alloy in an Aggressive

Environment", se analiza el material, fabricado mediante sinterización por plasma de chispa, pero en este caso la muestra dopada con un 3% de HEA. Se analizó mediante microscopía electrónica de barrido (SEM), ensayos de microdureza Vickers y una serie de técnicas electroquímicas, como el potencial de corrosión, la polarización lineal y la espectroscopia de impedancia electroquímica (EIS), para realizar una completa caracterización mecánica y electroquímica del material. Se presta especial atención a la microestructura del material, la formación de películas pasivas y la resistencia a la corrosión en un entorno altamente corrosivo, de NaCl al 3,5%, lo que permite comprender mejor el comportamiento de las cerámicas dopadas con HEA en condiciones agresivas.

El tercero y último de los artículos publicados se titula "Impact of CoCrFeNiMo High-Entropy-Alloy Doping on the Mechanical and Electrochemical Properties of B_4C Ceramic" trata de evaluar y comparar las propiedades mecánicas y electroquímicas de estos cuatro nuevos materiales, compuestos por una matriz cerámica de B_4C dopada con volúmenes de HEA (0,5%, 1%, 2% y 3% de CoCrFeNiMo) frente a una quinta muestra de B_4C monolítico. Las muestras estudiadas se obtuvieron mediante la técnica de sinterización por plasma de chispa. La estructura y dureza de las muestras se analizaron mediante microscopía electrónica de barrido (SEM) y distintos ensayos de microdureza Vickers, del cual se obtuvo un estudio estadístico. Durante la inmersión en agua de mar artificial para simular un entorno marino corrosivo, se realizaron ensayos de potencial de corrosión, velocidad de corrosión y espectroscopia de impedancia electroquímica para determinar el comportamiento electroquímico de las muestras. Se obtuvieron las pendientes de Tafel y el circuito equivalente que se ajustaban a los datos experimentales de EIS.

ULPGC Universidad de Las Palmas de Gran Canaria | Escuela de Doctorado

Índice

Índice

1 Introducción

1. Introducción

El carburo de boro (B_4C) es un material cerámico con propiedades mecánicas excepcionales, como una buena estabilidad térmica y conductividad (30 W/m K), una baja densidad (2,52 g/cm3), un alto punto de fusión (2450 °C) y una elevada dureza (30 GPa) [1]. Estas propiedades garantizan que el B_4C sea un material versátil y ventajoso, utilizado para una amplia gama de aplicaciones industriales, como el sector balístico, refractario o electrónico [2]. El B_4C se comporta como un material termoeléctrico con un elevado coeficiente Seebeck de 300 µV/K. Esta característica lo convierte en un material extremadamente interesante para aplicaciones emergentes en termopares, diodos y transistores. El B_4C está reconocido como el tercer material más duro conocido, después del diamante y el nitruro de boro cúbico. Esta cerámica combina una dureza excepcional manteniendo una baja densidad, lo que lo convierte en una alternativa ligera al diamante (~3,51 g/cm3), sin embargo, su conductividad térmica es inferior. Eléctricamente, el B_4C se comporta como un semiconductor de baja conductividad, lo que contrasta con el diamante, que es un magnífico aislante eléctrico. El B_4C funciona bien en entornos agresivos gracias a su gran resistencia a la corrosión. El diamante, a pesar de su inercia química, puede oxidarse a temperaturas elevadas. El B_4C podría sustituir el uso del diamante por ser un material más rentable y fácilmente disponible en grandes cantidades, lo que lo hace atractivo para diversas aplicaciones industriales [3].

Las radiaciones ionizantes son muy importantes en los ámbitos médico e industrial. En medicina, se utiliza para técnicas de diagnóstico por imagen y tratamientos de medicina nuclear. En el campo industrial, la radiación se utiliza para aplicaciones como la esterilización, el ensayo de materiales y el control de calidad. La generación de energía nuclear contribuye significativamente a la producción mundial de energía, ofreciendo una alternativa con bajas emisiones de carbono a los combustibles fósiles. El reto consiste en determinar cómo aprovechar las ventajas de la radiación ionizante minimizando al mismo tiempo los riesgos asociados. En este contexto, el B_4C presenta una excepcional capacidad de absorción de neutrones (600 barns). Esto hace que se utilice ampliamente en los sistemas de protección y monitorización de reactores nucleares como blindaje eficaz [4,5].

Más allá de sus aplicaciones nucleares, el B_4C tiene una gran dureza y una densidad reducida en comparación con otras cerámicas, como el SiC, el Al2O3, el Si3N4 y el ZrO2. Estas características hacen que los polímeros reforzados con B_4C resulten muy atractivos para aplicaciones tribológicas [6].

El B_4C es un semiconductor prometedor con un comportamiento de transporte eléctrico de tipo salto. Su bandgap (aproximadamente 2,09 eV) está influido por su composición y orden estructural. Es un material de tipo p con potencial para aplicaciones innovadoras en dispositivos electrónicos [2].

Un aspecto crítico a la hora de procesar el B_4C es la densificación. A menudo se necesitan materiales densos para muchas aplicaciones avanzadas. Se han estudiado diferentes aditivos de sinterización para aumentar las tasas de densificación, controlar el crecimiento de grano y mejorar las propiedades mecánicas. El carbono ha demostrado su eficacia para reducir la capa de óxido de los polvos B_4C, lo que favorece la sinterización y limita el crecimiento de grano [7].

Por otro lado, las aleaciones de alta entropía (HEA) aparecieron en 2004 como resultado de la combinación de al menos cinco elementos metálicos en proporciones atómicas aproximadamente iguales [8,9]. Este tipo de aleaciones despertaron rápidamente un gran interés en el ámbito académico debido a sus notables propiedades y a sus posibles aplicaciones en ingeniería, donde se requiera alta resistencia, ductilidad, estabilidad térmica o resistencia a la corrosión [10]. Actualmente las HEAs se encuentran en una amplia gama de aplicaciones industriales, mostrando propiedades superiores a las aleaciones tradicionales (que normalmente consisten en sólo uno o dos elementos primarios), como son las aplicaciones biomédicas [11,12], nucleares [13,14,15] y refractarias, como motores a reacción y turbinas [16]. El enfoque de las HEAs está en constante desarrollo y crecimiento, estudios recientes intentan ampliar su uso a distintas aplicaciones como la magnéticas, la conversión energética, el almacenamiento de hidrógeno y la catálisis [17], dando respuesta a problemas sociales o industriales reales. En la actualidad se han estudiado y se siguen estudiando muchas HEAs, ya sea para obtener mejores propiedades o aumentar su campo de aplicación, como MoNbTiVTaW [18], Fe20Mn15Cr15V10Al10C2.5 [19], CoCrFeMnNi [20], TiNbTaZrMoHfWCr [21], Fe20Co30Ni10Cr20Mn20 [22] y CoCrFeNiMo [23,24,25].

La HEA CoCrFeNiMo se ha dopado con silicio [26], circonio [27], aluminio [28] o titanio [29], y se ha utilizado como recubrimiento [30,31], lo que aumenta la versatilidad de la HEA en diferentes aplicaciones de ingeniería. El efecto del Mo ha demostrado ser crucial no sólo en sus propiedades mecánicas, como la alta dureza [32], sino en la formación de una capa pasiva en el medio marino con la creación de Cr2O3 y MoO3, que aumenta la resistencia a la corrosión de la HEA [31,33]. Por otro lado, la adición de Ni y Cr sobre la HEA contribuye a la formación de una película protectora de óxido resistente sobre la capa externa del material, lo que implica también una mejora en la resistencia a la corrosión [34,35].

El objetivo por tanto de esta tesis doctoral es el de investigar las propiedades mecánicas y electroquímicas de estas nuevas muestras de B_4C dopado con HEA de CoCrFeNiMo al 0,5%, 1%, 2% y 3%, comparando y evaluando los resultados obtenidos entre las muestras dopadas con una quinta muestra de carburo de boro monolítico, para así determinar sus posibles aplicaciones industriales [36,37,38].

Así, en este estudio, se ha investigado el impacto del dopado con CoCrFeNiMo HEA en las propiedades electroquímicas y mecánicas de la cerámica B_4C. Los ensayos electroquímicos se realizaron en un ambiente artificial de agua de mar, una solución de NaCl al 3,5% de volumen. Además, se realizaron ensayos de microscopía electrónica de barrido (SEM) y un análisis estadístico de microdureza, para completar la caracterización mecánica.

Por tanto, el estudio se centra en evaluar y comparar cinco muestras de carburo de boro, cuatro de ellas dopadas con HEA, en un entorno marino y corrosivo. Este trabajo pretende proporcionar una comprensión más profunda de cómo el dopaje CoCrFeNiMo HEA afecta a la cerámica B_4C y cuál de estos compuestos tiene la composición óptima, haciendo hincapié en aplicaciones en las que factores como la durabilidad, la resistencia a la corrosión y la dureza mejorada son esenciales, para así determinar sus posibles aplicaciones industriales.

La tesis propuesta se encuentra enmarcada en el programa de doctorado en Ingenierías Química, Mecánica y de Fabricación (QUIMEFA) por la Universidad de Las Palmas de Gran Canaria, siendo su línea de investigación corrosión de los metales. Además, las publicaciones científicas elaboradas a raíz del desarrollo de esta tesis doctoral cubren los ensayos mencionados para caracterizar estos nuevos materiales a nivel mecánico y electroquímico. En total, se presentan 3 artículos publicados como primer autor, otro artículo pendiente de

publicación y distintas participaciones en congresos internacionales en las que se han realizado comunicaciones orales o posters. Todo ello forma parte del trabajo para el correcto desarrollo y reconocimiento de la tesis, justificando la unidad temática y permitiendo la presentación de la presente tesis bajo la modalidad de tesis por compendio de publicaciones.

2

Justificación del compendio

2. Justificación del compendio

El resultado de la elaboración de esta tesis doctoral por compendio es la publicación de 3 artículos en los que soy el primer autor. Además, he colaborado en otras publicaciones aun no publicadas, publicaciones en revistas no indexadas, participaciones en congresos y presentación de posters. Se muestra a continuación un resumen de cada una de las publicaciones en orden cronológico:

TÍTULO:	Corrosion Behavior of New B_4C Ceramic Doped with High-Entropy Alloy in an Aggressive Environment
AUTORES:	A D Rico-Cano, J C Mirza-Rosca, B C Ocak, G Goller
REVISTA:	Microscopy and Microanalysis
ÍNDICE DE IMPACTO:	2.9
CUARTIL:	Q1
DOI:	https://doi.org/10.1093/mam/ozae044.666
ISSN:	1431-9276
EDITORIAL:	Oxford University Press
MES Y AÑO:	Julio 2024
VOLUMEN:	30
PÁGINAS	3

Este primer artículo investiga un nuevo material cerámico compuesto de carburo de boro (B_4C) dopado con una aleación de alta entropía, centrándose en su comportamiento electroquímico en un ambiente salino y corrosivo (agua de mar artificial). De las 5 muestras

totales de las que se disponían para la elaboración de esta tesis, 4 de ellas dopadas HEA y otra que no, en este artículo se estudió la muestra que disponía de un 2% de contenido de HEA. El artículo incluye la síntesis del material, fabricado mediante sinterización por plasma de chispa, la preparación detallada de la muestra previa a los ensayos y las pruebas electroquímicas realizadas: potencial de circuito abierto, polarización lineal y espectroscopia de impedancia electroquímica. Además, se analiza a nivel microestructural mediante microscopia electrónica de barrido (SEM) para complementar la evaluación del comportamiento frente a la corrosión.

TÍTULO:	Corrosion Behavior and Microhardness of a New B_4C Ceramic Doped with 3% Volume High-Entropy Alloy in an Aggressive Environment
AUTORES:	A D Rico-Cano, J C Mirza-Rosca, B C Ocak, G Goller
REVISTA:	Metals
ÍNDICE DE IMPACTO:	2.6
CUARTIL:	Q2
DOI:	https://doi.org/10.3390/met15010079
eISSN:	2075-4701
EDITORIAL:	MDPI
MES Y AÑO:	Enero 2025
VOLUMEN:	15
PÁGINAS	16

El segundo de los artículos, al igual que el primero, buscaba estudiar la caracterización mecánica y electroquímica de otra de las muestras dopadas, en este caso la que disponía de un 3% de contenido de HEA. Buscando ampliar el conocimiento adquirido sobre este nuevo

material y obtener una caracterización más completa, además de los ensayos realizados en el artículo anterior, se procedió a realizar un estudio estadístico de la microdureza de la muestra (mediante un ensayo de microdureza Vickers) y además se obtuvo el circuito equivalente y parámetros eléctricos (profundizando más en los resultados de la espectroscopia de impedancia electroquímica).

TÍTULO:	Impact of CoCrFeNiMo High-Entropy-Alloy Doping on the Mechanical and Electrochemical Properties of B_4C Ceramic
AUTORES:	A D Rico-Cano, J C Mirza-Rosca, B C Ocak, G Goller
REVISTA:	Applied Sciences
ÍNDICE DE IMPACTO:	2.5
CUARTIL:	Q1
DOI:	https://doi.org/10.3390/app15094859
eISSN:	2076-3417
EDITORIAL:	MDPI
MES Y AÑO:	Abril 2025
VOLUMEN:	15
PÁGINAS	17

En el tercero y último de los artículos publicados, se realiza una comparación de la caracterización mecánica y electroquímica completa de todas las muestras del estudio, un total de 5. Para ello se recogieron todos los datos obtenidos del primer y segundo artículo para posteriormente compararlos con las otras muestras aun sin analizar; la dopada al 0,5% de HEA, al 1% de HEA y la muestra sin dopar (carburo de boro monolítico). Se realizan por tanto todos los ensayos nombrados en los anteriores artículos, pero además, el ensayo de polarización lineal

es ampliado para obtener las curvas de Tafel, necesarias para calcular la velocidad de corrosión de todas las muestras.

Estos 3 artículos, por tanto, obtenidos a través del estudio y ejecución de la tesis propuesta, son los que permiten la presentación de la presente tesis es bajo la modalidad de tesis por compendio de publicaciones, enmarcada en el programa de doctorado en Ingenierías Química, Mecánica y de Fabricación (QUIMEFA) por la Universidad de Las Palmas de Gran Canaria, siendo su línea de investigación corrosión de los metales.

3 Publicaciones

3. Publicaciones

3.1. Corrosion Behavior of New B_4C Ceramic Doped with High-Entropy Alloy in an Aggressive Environment

Microscopy and Microanalysis, **30** (Suppl 1), 2024, 1352–1354
https://doi.org/10.1093/mam/ozae044.666

Microscopy AND Microanalysis

Meeting-report

Corrosion Behavior of New B_4C Ceramic Doped with High-Entropy Alloy in an Aggressive Environment

A.D. Rico-Cano[1], J.C. Mirza-Rosca[1,2,*], B.C. Ocak[3], and G. Goller[3]

[1]*Mechanical Engineering Department, University of Las Palmas de Gran Canaria, Las Palmas de Gran Canaria, Spain*
[2]*Transylvania University of Brasov, Materials Engineering and Welding Department, Brasov, Romania*
[3]*Department of Metallurgical and Materials Engineering, Istanbul Technical University, Maslak, Istanbul, Turkey*
*Corresponding author: julia.mirza@ulpgc.es

TÍTULO:	Corrosion Behavior of New B_4C Ceramic Doped with High-Entropy Alloy in an Aggressive Environment
AUTORES:	A D Rico-Cano, J C Mirza-Rosca, B C Ocak, G Goller
REVISTA:	Microscopy and Microanalysis
ÍNDICE DE IMPACTO:	2.9
CUARTIL:	Q1
DOI:	https://doi.org/10.1093/mam/ozae044.666
ISSN:	1431-9276
EDITORIAL:	Oxford University Press
MES Y AÑO:	Julio 2024
VOLUMEN:	30
PÁGINAS	3

Corrosion Behavior of New B4C Ceramic Doped with High-Entropy Alloy in an Aggressive Environment

A D Rico-Cano, J C Mirza-Rosca, B C Ocak, G Goller

Microscopy and Microanalysis, **30** (Suppl 1), 2024, 1352–1354
https://doi.org/10.1093/mam/ozae044.666

Microscopy AND Microanalysis

Meeting-report

Corrosion Behavior of New B_4C Ceramic Doped with High-Entropy Alloy in an Aggressive Environment

A.D. Rico-Cano[1], J.C. Mirza-Rosca[1,2,*], B.C. Ocak[3], and G. Goller[3]

[1]*Mechanical Engineering Department, University of Las Palmas de Gran Canaria, Las Palmas de Gran Canaria, Spain*
[2]*Transylvania University of Brasov, Materials Engineering and Welding Department, Brasov, Romania*
[3]*Department of Metallurgical and Materials Engineering, Istanbul Technical University, Maslak, Istanbul, Turkey*

*Corresponding author: julia.mirza@ulpgc.es

Introduction

Boron carbide (B_4C) ceramic shows a unique combination of properties that make it a suitable material for multiple engineering applications, like refractory, electronic or ballistic industry [1]. Eligible properties such as low density, good thermal conductivity and high hardness and melting point makes B_4C an extremely competitive material [2].

High-entropy alloys (HEAs) are a new type of material that contain at least five distinct metallic elements in approximately equal atomic ratio, unlike the traditional metallic alloys, usually composed of one or two main elements [3]. Due to the exceptional properties of HEAs, such as high corrosion resistance, high strength, high ductility and high temperature stability, these materials have gained the scientific community interest [4, 5]. Some potential applications are energy [6, 7], nuclear [8, 9], and biomedical industries [10-12].

Thus, in this study, corrosion properties of new HEA doped B_4C has been investigated to determine its behavior in artificial sea water.

Experimental

Investigations were conducted on B_4C with 2 vol.% CoCrFeNiMo HEA addition, from now on doped sample. This new material was produced by the Metallurgical and Materials Engineering Department of Istanbul Technical University, using spark plasma sintering (SPS) technic (SPS-7.40 MK-VII, SPS Syntex Inc).

Before carrying out the electrochemical tests, the doped sample was encapsulated in a two-component epoxy resin to be easily handled. Afterwards, the sample was polished with the Struers TegraPol-11 polisher in two stages: first polishing with silicon carbide abrasive papers with progressively finer grain sizes varying from 240 to 2000 grit and secondly a final polishing with 0.1µm alpha alumina suspension to obtain a mirror finish polishing. The manufacturing process and sample preparation are shown in Fig.1.

After preparing the sample, three electrochemical tests were performed using the potentiostat BioLogic Essential SP-150 (Bio-Logic Science Instruments SAS, Seyssinet-Pariset, France) and an electrochemical cell: Open circuit potential, linear polarization and Electrochemical Impedance Spectroscopy in a 3.5% NaCl artificial sea water. The software used to set the test parameters and analyse the results it is EC - Lab® v-9.55 and aplicable standard ASTM G5-94(2004) was followed. The used conventional electrochemical cell has three electrodes: doped B_4C as working electrode, the platinum electrode as counter electrode, and the saturated calomel electrode as reference electrode.

Using the software "Ecorr vs. Time" approach, the 24 h open circuit potential of the sample was recorded at every 30 s or every time there was a 100 mV change in potential. The data obtained was analysed and plotted as a graph of potential against time, to determine whether the sample's corrosion potential is stable over time or exhibits a trend toward passivation or corrosion.

Electrochemical Impedance Spectroscopy (EIS) is a nondestructive test that measures electrochemical impedance. It works by applying an alternating current potential to an electrochemical cell while it measures the current through the cell main results. Applicable standard ISO 16773-1-4:2016 was followed.

The "Linear Polarisation" approach was used to carry out these measurements and its potential was stabilised by entering the sample surface area value and the test time of 110 minutes. The potential scanning showed a 10 mV/minute time-variation relationship from - 0.1 to 1 V vs open circuit potential, with data recorded of intensity during the potential variation scanning. After the plotting of these linear polarisation curves, the corrosion rate values of the sample were determined using EC-Lab's "Tafel Fit" technique.

Results and discussion

Fig. 2 illustrates scanning electron microscope (SEM) images of the surfaces of B_4C and doped B_4C-HEA ceramics that have been etched using electrochemical methods. The monolithic B_4C material exhibits a porous microstructure characterized by a non-uniform distribution of grain size and shape. The B_4C material exhibits the lowest relative density compared to doped ceramic sample. The triangular and uniformly dispersed pores were primarily found at the intersections of three boundaries and the interfaces between grains. Microstructural investigations indicate that the doping led to a more compact microstructure in comparison to the solid B_4C material.

The distribution of doping HEA has been shown to be homogeneous, with the majority positioned on the grain borders and filled pores at several grain junctions inside the B_4C matrix. According to German et al. [13], the liquid phase functions as a substance that fills the pores, rather than spreading over the solid grains, when there is no solubility between the solid and liquid phases. Due to inadequate liquid levels, the samples still retain holes as they were not completely filled. Based on the photos,

the incorporation of HEA phase leads to the removal of voids within the matrix through the process of liquid phase sintering. These tendencies are consistent with the shape of open circuit potential during immersion in artificial sea water (see Fig.3a).

The average grain size of the monolithic B_4C was determined to be 2.57 μm and an uneven distribution of grain sizes was found and was attributed to the rapid heating and melting of impurities that were already present in the initial powders. The doped ceramic yielded a more homogeneous distribution of particle sizes, with the smallest grain size measuring 2.16 μm. These observations suggest that the presence of HEA phases at the grain borders and triple junction locations inhibits grain expansion and results in a finer grain structure. As a result of the tendency of high-entropy alloys to gravitate towards the configuration with the lowest energy, HEA phases predominantly inhabited the smaller grains. It was found [13] that liquid phases have a tendency to occupy the configuration with the lowest energy, leading them to flow preferentially towards smaller grains and pores and in this way explain the linear polarization behavior (see Fig.3b).

The electrochemical impedance spectroscopy data (see Fig.4) showed a very high resistance to corrosion in artificial sea water. Nyquist diagram (Fig.4a) depicts three zones: one semicircle at high frequencies, another semicircle at medium frequencies and a diffusion line at high frequencies. The behavior is characterized by a process in two stages (Fig.4b): first the filling of the pores with sea water (with an important diffusional component) and second the formation of a passive film inside the pores and on the surface of the sample.

Conclusions

The behavior of a high entropy alloy doped B_4C in artificial sea water was studied and the main conclusions are listed as follows:

- The doping of B_4C ceramic with CoCrFeMoNi high entropy alloy led to a more compact microstructure in comparison to the solid B_4C material, inhibits grain expansion and results in a finer grain structure.
- The doped sample has a very high resistance to corrosion in artificial sea water.
- The chemical process which takes place at immersion of the doped sample in artificial sea water has two steps with an important diffusional component.

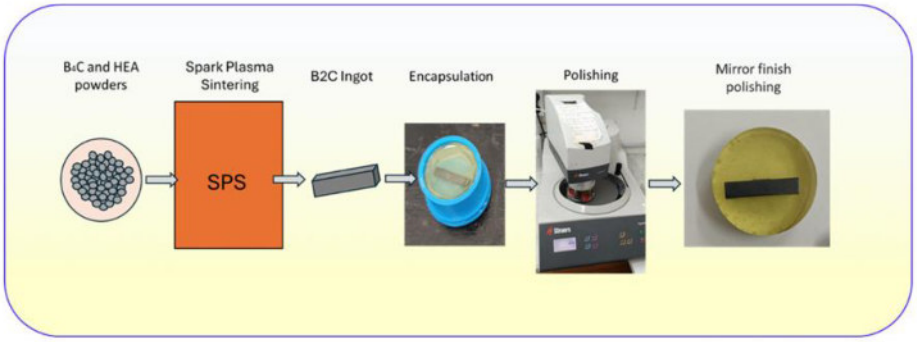

Fig. 1. Sample manufacturing process and preparation.

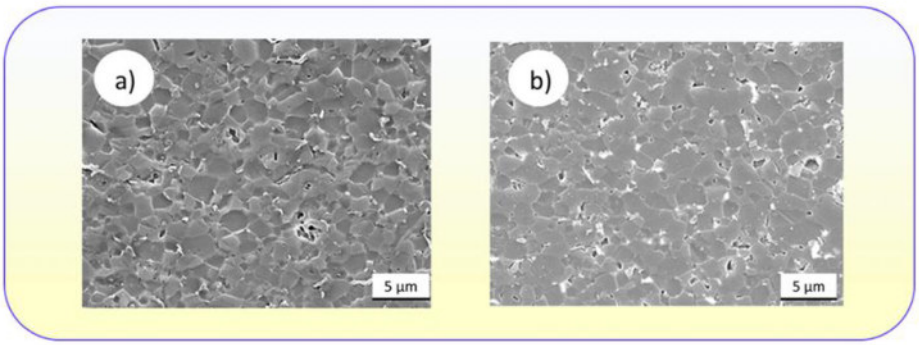

Fig. 2. SEM images of the a) B_4C ceramic and b) HEA doped ceramic.

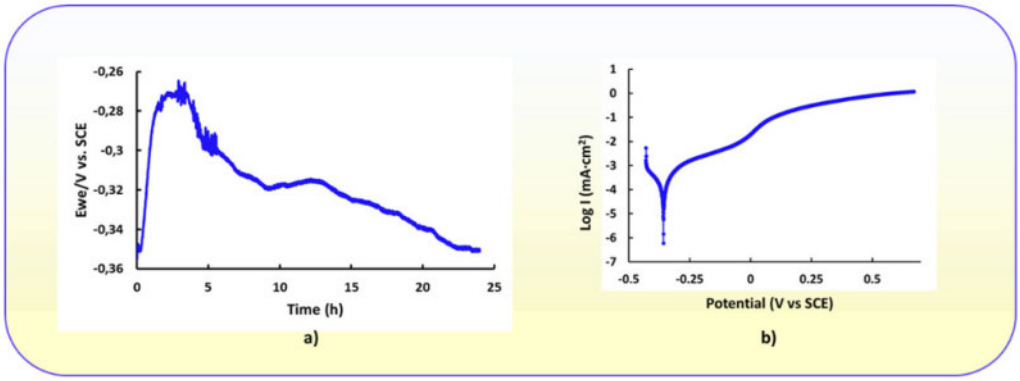

Fig. 3. a) Corrosion potential vs. time for 24 h of immersion and b) Linear polarization in 3.5% NaCl solution.

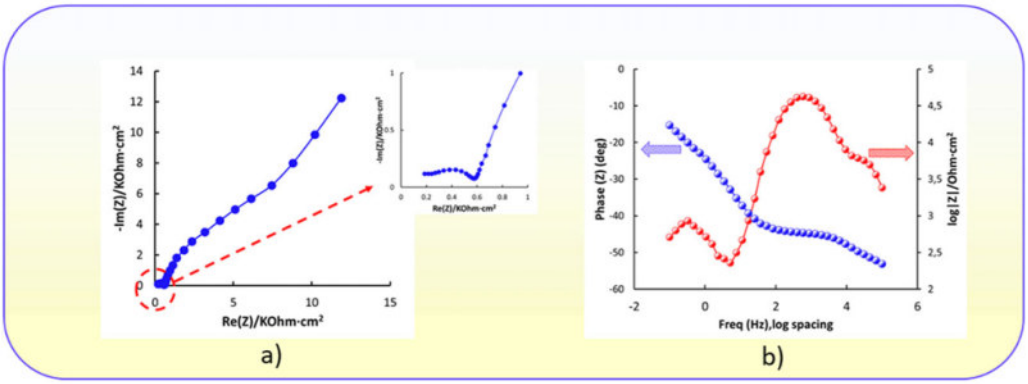

Fig. 4. Impedance diagrams: a) Nyquist; b) Bode-IZI and Bode-phase, for dopped sample in 3.5% NaCl

References

1. V. Domnich *et al.*, *Journal of the American Ceramic Society* **94**(11) (2011), p. 3605–3628. https://doi.org/10.1111/j.1551-2916.2011.04865.x.
2. B. Yavas *et al.*, *Ceram Int* **41**(7) (2015), p. 8936–8944. https://doi.org/10.1016/j.ceramint.2015.03.167.
3. G. Cui *et al.*, *Journal of Materials Research and Technology* **9**(2) (2020), p. 2598–2609. https://doi.org/10.1016/j.jmrt.2019.12.090.
4. S. J. Brito-Garcia *et al.*, *Metals (Basel)* **13**(5) (2023), p. 854. https://doi.org/10.3390/met13050854.
5. S. J. Brito-Garcia *et al.*, *Metals (Basel)* **13**(5) (2023), p. 883. https://doi.org/10.3390/met13050883.
6. F. Yang *et al.*, *International Journal of Hydrogen Energy* **47**(21) (2022), p. 11236–11249. https://doi.org/10.1016/j.ijhydene.2022.01.141.
7. M. Fu et al., *Iscience*, **24**(3) (2021). https://doi.org/10.1016/j.isci.2021.102177
8. M. L. Rios *et al.*, *Microscopy and Microanalysis* **26**(S2) (2020), p. 406–407. https://doi.org/10.1017/s1431927620014555.
9. T. Li *et al.*, *Metals* **13**(2) (2023), p. 363. https://doi.org/10.3390/met13020363.
10. P. Socorro-Perdomo *et al.*, *Microscopy and Microanalysis* **27**(S1) (2021), p. 1772–1774. https://doi.org/10.1017/s1431927621006486.
11. M. López Ríos *et al.*, *Scientific Reports* **10**(1) (2020), p. 21119. https://doi.org/10.1038/s41598-020-78108-5.
12. D. Castro *et al.*, *Metals* **11**(4) (2021), p. 648. https://doi.org/10.3390/met11040648.
13. R.M. German *et al.*, *Journal of materials science* **44** (2009), p. 1-39. https://doi.org/10.1007/s10853-008-3008-0.

3.2. Corrosion Behavior and Microhardness of a New B_4C Ceramic Doped with 3% Volume High-Entropy Alloy in an Aggressive Environment

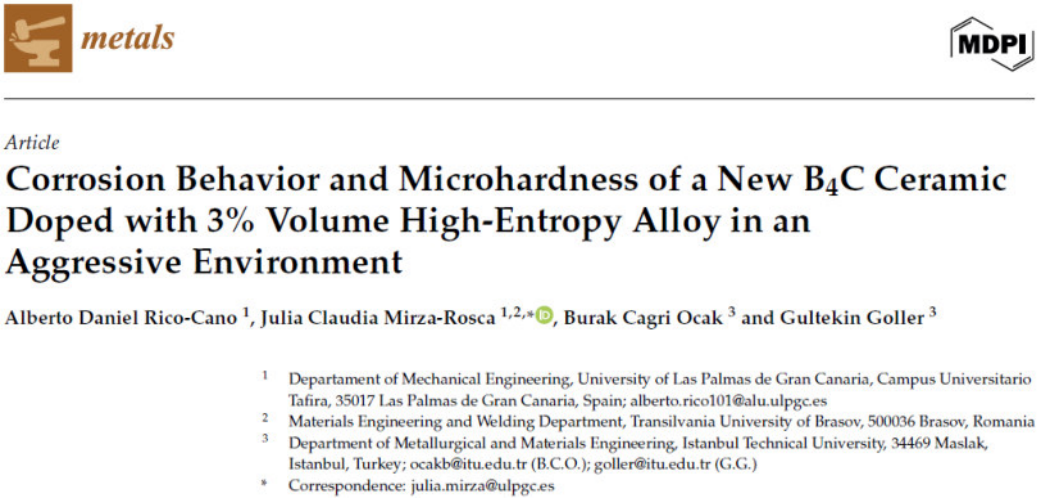

metals

MDPI

Article

Corrosion Behavior and Microhardness of a New B_4C Ceramic Doped with 3% Volume High-Entropy Alloy in an Aggressive Environment

Alberto Daniel Rico-Cano [1], Julia Claudia Mirza-Rosca [1,2,*], Burak Cagri Ocak [3] and Gultekin Goller [3]

[1] Departament of Mechanical Engineering, University of Las Palmas de Gran Canaria, Campus Universitario Tafira, 35017 Las Palmas de Gran Canaria, Spain; alberto.rico101@alu.ulpgc.es
[2] Materials Engineering and Welding Department, Transilvania University of Brasov, 500036 Brasov, Romania
[3] Department of Metallurgical and Materials Engineering, Istanbul Technical University, 34469 Maslak, Istanbul, Turkey; ocakb@itu.edu.tr (B.C.O.); goller@itu.edu.tr (G.G.)
* Correspondence: julia.mirza@ulpgc.es

TÍTULO:	Corrosion Behavior and Microhardness of a New B_4C Ceramic Doped with 3% Volume High-Entropy Alloy in an Aggressive Environment
AUTORES:	A D Rico-Cano, J C Mirza-Rosca, B C Ocak, G Goller
REVISTA:	Metals
ÍNDICE DE IMPACTO:	2.6
CUARTIL:	Q2
DOI:	https://doi.org/10.3390/met15010079
eISSN:	2075-4701
EDITORIAL:	MDPI
MES Y AÑO:	Enero 2025
VOLUMEN:	15
PÁGINAS	16

metals

MDPI

Article

Corrosion Behavior and Microhardness of a New B_4C Ceramic Doped with 3% Volume High-Entropy Alloy in an Aggressive Environment

Alberto Daniel Rico-Cano [1], Julia Claudia Mirza-Rosca [1,2,*], Burak Cagri Ocak [3] and Gultekin Goller [3]

[1] Departament of Mechanical Engineering, University of Las Palmas de Gran Canaria, Campus Universitario Tafira, 35017 Las Palmas de Gran Canaria, Spain; alberto.rico101@alu.ulpgc.es
[2] Materials Engineering and Welding Department, Transilvania University of Brasov, 500036 Brasov, Romania
[3] Department of Metallurgical and Materials Engineering, Istanbul Technical University, 34469 Maslak, Istanbul, Turkey; ocakb@itu.edu.tr (B.C.O.); goller@itu.edu.tr (G.G.)
* Correspondence: julia.mirza@ulpgc.es

Abstract: The aim of this paper is to study both the mechanical and chemical properties of a new material composed of B_4C doped with 3% volume of CoCrFeNiMo HEA by the spark plasma sintering technique. Scanning electron microscopy and microhardness were used to characterize the composite microstructure and hardness. Corrosion behavior was studied by corrosion potential, corrosion rate and electrochemical impedance spectroscopy, where the equivalent circuit was obtained, characterized by the presence of the Warburg element. The addition of HEA resulted in a more compact microstructure, filling pores and inhibiting ceramic grain growth. A microhardness statistical analysis revealed that the sample followed a normal distribution, which suggests that the sample has a homogeneous structure. The doped material exhibits excellent corrosion resistance in artificial seawater, where its chemical interaction occurs in two steps, with an important diffusional component. This study highlights the potential for use in environments where both corrosion resistance and mechanical strength are critical factors.

Keywords: ceramic; HEA; EIS; corrosion behavior; microhardness; SEM

Academic Editor: Thomas Fiedler

Received: 28 November 2024
Revised: 9 January 2025
Accepted: 15 January 2025
Published: 17 January 2025

Citation: Rico-Cano, A.D.; Mirza-Rosca, J.C.; Ocak, B.C.; Goller, G. Corrosion Behavior and Microhardness of a New B_4C Ceramic Doped with 3% Volume High-Entropy Alloy in an Aggressive Environment. *Metals* **2025**, *15*, 79. https://doi.org/10.3390/met15010079

1. Introduction

Boron carbide (B_4C) possesses a distinctive combination of characteristics that make it a preferred material for various technical applications. Boron carbide is utilized in refractory applications owing to its elevated melting point (2450 °C) and thermal stability and conductivity (30 W/m K). It serves as an abrasive powder and coating due to its exceptional abrasion resistance. Its elevated hardness renders it appropriate for grinding and cutting tools, ceramic bearings, wire drawing dies, and similar applications. It demonstrates superior ballistic performance due to its high hardness (30 GPa) and low density (2.52 g/cm^3). Boron carbide is an exceptional thermoelectric material due to its elevated Seebeck coefficient of 300 μV K^{-1}, and novel uses in thermocouples, diodes, and transistor devices are being discovered [1]. B_4C is extremely hard, ranked third after diamond and cubic boron nitride. B_4C has lower density, making it lightweight compared with diamond, which has higher density (~3.51 g/cm^3). Boron carbide is a good thermal conductor, though not as high as diamond that has exceptional thermal conductivity, the highest among known materials. B_4C is generally a semiconductor with low electrical conductivity, while diamond is an excellent electrical insulator; however, doped diamonds can exhibit semiconducting properties. B_4C is highly resistant to chemical corrosion, making it suitable

for harsh environments, while diamond is chemically inert and resistant to most acids and alkalis but can be oxidized at high temperatures. B_4C is less expensive and more readily available in large quantities for industrial applications [1].

In medicine, ionizing radiation is essential for diagnostic imaging techniques, including X-rays, CT scans, and nuclear medicine treatments. In industrial applications, radiation is employed in sterilizing, material testing, and quality control, thereby improving safety and efficiency. Furthermore, electricity generation by nuclear power constitutes a significant share of global energy output, offering a low-carbon alternative to traditional fossil fuels. The difficulty resides in utilizing the advantages of ionizing radiation while limiting the related dangers. Under these conditions, shielding is an essential element in radiation protection measures, and boron carbide possesses significant neutron absorption capacity (600 barns). B_4C ceramics are extensively utilized in nuclear applications, such as the protection and supervision of nuclear reactors [2,3].

Moreover, B_4C exhibits superior hardness and reduced density in comparison to ceramic materials such as Al_2O_3, ZrO_2, SiC, and Si_3N_4. Boron carbide-reinforced polymer composites are increasingly being recognized for tribological applications that necessitate low friction and minimal wear [4].

Boron carbide is a semiconductor characterized by hopping-type electrical transport features. The energy band gap is dependent on composition and the extent of order. Reports indicate a band gap of 2.09 eV, which includes several mid-bandgap states that complicate the photoluminescence spectra. The material is generally p-type with potential uses in innovative electronic devices [5].

The densification of boron carbide is crucial due to the necessity for dense bodies in many specific applications. Numerous sinter additives have been evaluated for their ability to increase the rate of densification, control grain development, and improve the mechanical characteristics of boron carbide. Carbon has been highly useful in decreasing the oxide layer of boron carbide powders, hence facilitating sintering and inhibiting grain development [6]. The same authors conducted a systematic study on the effects of the addition of the same weight percent of different sintering additives (C, B, TiB2, and CSi) on the density, hardness and wear resistance of B_4C compacts, produced by pressureless sintering.

Many research efforts have been undertaken to improve the fracture toughness and mechanical properties of B_4C ceramics through the incorporation of metallic sintering additives such as Co [7], Fe [8,9], Si [10], Ti [11], and Ni [12].

While the reduction in sintering temperature has been documented with the incorporation of metallic aids, these metals may result in diminished hardness values. Considering the aforementioned factors, a novel strategy may be implemented to tackle these challenges with the incorporation of HEAs as sintering additives.

HEAs, or high-entropy alloys, are a relatively new family of materials, characterized by the inclusion of at least five different metallic elements in nearly equal atomic ratios, unlike traditional alloys, which typically consist of only one or two primary elements [13]. HEAs possess remarkable properties, such as excellent corrosion resistance, high strength, and impressive ductility and stability at elevated temperatures, which have captured the interest of the scientific community [14]. Potential applications for HEAs include energy systems [15,16], nuclear technology [17,18], and biomedical fields [19,20].

Doping high-entropy alloys (HEAs) involves the deliberate introduction of small amounts of additional chemical elements into the base alloy composition [21]. This process can significantly impact the alloy's mechanical and physical properties. The impact of doping is primarily influenced by the types of elements introduced, their concentrations, and the specific application intended for the alloy. By strategically adjusting the doping

process, HEAs can be tailored to possess properties that meet the requirements of particular operating conditions.

CoCrFeNiMo HEA has been used as coating on 304 stainless steel [22–24] and 316 stainless steel [25] or doped with other metals such as titanium [14], zirconium [26], and aluminum [27]. The inclusion of Cr and Ni significantly enhances the corrosion resistance of the FeNiCoCrMo high-entropy alloy (HEA) by forming a dense, protective oxide layer over the substrate [28,29]. Additionally, Mo, with its high melting point [30,31], contributes to the formation of Mo-rich phases, imparting higher hardness and reducing pitting corrosion due to lattice distortion [32]. In previous studies, the effects of varying Mo concentrations (CoCrFeNiMox, $x \leq 0.25$) on the corrosion resistance of HEA coatings in acidic environments, such as 3.5 wt% NaCl solutions, have been explored, concluding that the passivation film, composed mainly of Cr_2O_3 and MoO_3, was the key factor in enhancing the corrosion resistance [25]. In similar studies it was demonstrated that the formation of a passivation film in CoCr2FeNiMox ($x \leq 0.4$) coatings improved corrosion resistance in acidic 3.5 wt% NaCl solutions [33].

In this context, combining CoCrFeNiMo HEA with B_4C as a composite seeks to benefit from the remarkable mechanical strength and corrosion resistance offered by the HEA while utilizing the high hardness and thermal stability of B_4C.

Thus, in this study, the corrosion behavior of a novel B_4C ceramic material doped with CoCrFeNiMo HEA is investigated to assess its performance in an artificial seawater environment—a 3.5% in volume NaCl solution. In addition to corrosion testing, this study aims to conduct a statistical analysis of the microhardness behavior of the material. This research aims to assess the potential of these materials for use in harsh and corrosive environments, with a particular focus on applications where durability, corrosion resistance, and improved hardness are critical factors.

2. Materials and Methods

2.1. Material Preparation

This investigation focused on a B_4C ceramic sample doped with 3 vol.% CoCrFeNiMo HEA. This material was synthesized at Istanbul Technical University by the Department of Metallurgical and Materials Engineering. First, the starting powders were weighed accurately and mixed for 6 h using a tubular mixer (T2F Bachofen, Bachofen AG, Muttenz, Switzerland) to ensure homogeneity. The mixed powders were then placed into a hollow graphite die with an inner diameter of 50 mm and a thickness of 4 mm. To enhance electrical and thermal conductivity and facilitate easy removal after sintering, a graphite sheet was inserted between the punches and the powder. Additionally, the graphite die was insulated with carbon felt to minimize heat loss.

The sintering process was conducted in a vacuum atmosphere using an SPS apparatus (SPS-7.40 MK-VII, SPS Syntex Inc., Saitama, Japan). A pulsed direct current (12 ms/on, 2 ms/off) and uniaxial pressure of 40 MPa were applied throughout the process. The temperature was monitored with an optical pyrometer (Chino, IR-AH, Tokyo, Japan) capable of measuring temperatures above 570 °C, focusing on a small hole in the graphite die. The process was temperature-controlled, and the shrinkage behavior of the samples was tracked continuously via punch rod displacement. To account for the thermal expansion of the graphite punches, a blank test was conducted, and the expansion values were subtracted from the measured shrinkage data.

The optimized SPS parameters were set as follows: sintering temperature of 1600 °C, heating rate of 100 °C/min, and a holding time of 5 min. The final samples had a diameter of 50 mm and a thickness of 4 mm.

Before performing mechanical and electrochemical tests, the ingot was embedded in two-component epoxy resin for easier handling. The sample was then polished in two stages using a Struers TegraPol-11 (Copenhague, Denmark) polisher: first, with silicon carbide abrasive papers (from 240 to 2000 grit) and later with a 0.1 µm alpha alumina suspension to achieve a mirror-like finish. The whole manufacturing of the sample and preparation process is illustrated in Figure 1.

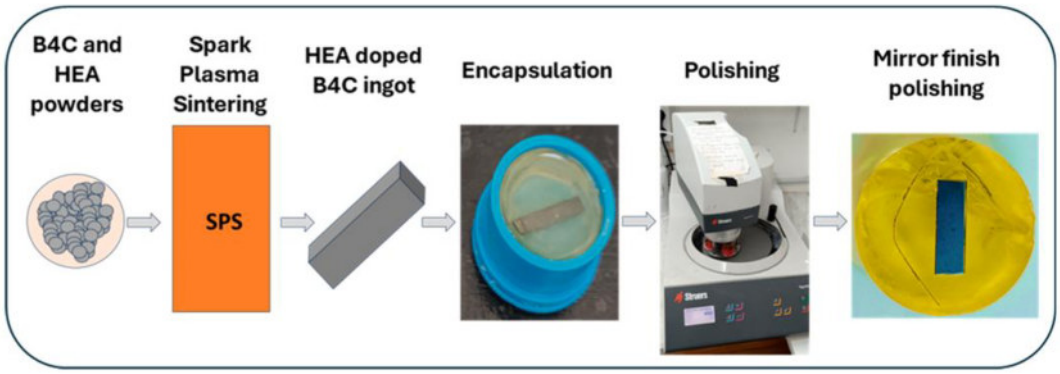

Figure 1. Schematic representation of the material preparation.

2.2. Scanning Electron Microscopy (SEM)

The microstructure of the sintered sample was analyzed through scanning electron microscopy model, FESEM JSM 7000 F (JEOL Ltd., Tokyo, Japan). To visualize effectively the microstructural features and facilitate the interpretation of the results obtained, the samples were etched using an electrolytic process to reveal the grain boundaries, employing a 10% NaOH solution for 15 s under conditions of 10 V and a current density of 0.25 A/cm^2.

2.3. Electrochemical Tests

After sample preparation, three different electrochemical tests were conducted using a BioLogic Essential SP-150 potentiostat (Bio-Logic Science Instruments SAS, Seyssinet-Pariset, France) and an electrochemical cell. These tests included open circuit potential (OCP), linear polarization, and electrochemical impedance spectroscopy (EIS) in an acidic environment—a 3.5% NaCl artificial seawater solution. The EC-Lab® v-9.55 software was used to set test parameters and analyze the results, following the ASTM G5-94(2004) standard [34]. The conventional electrochemical cell had three electrodes: the doped B_4C as the working electrode, a saturated calomel reference electrode, and a platinum counter electrode.

2.3.1. Corrosion Potential

Using the "Ecorr vs. Time" technique, for 24 h, the open circuit potential of the sample was recorded, with measurements taken every 30 s or when a 100 mV change in potential occurred. To determine whether the sample's corrosion potential remained stable, indicated passivation, or showed signs of corrosion over time, the recorded data were plotted.

2.3.2. Corrosion Rate

For linear polarization measurements, the sample's potential was stabilized by inputting the surface area and test duration (110 min). The potential was scanned at a rate of 10 mV/min, ranging from −0.1 to 1 V versus the open circuit potential. The resulting data were used to generate polarization curves, and the corrosion rate of the sample was calculated using the EC-Lab's "Tafel Fit" technique.

2.3.3. EIS

EIS, or electrochemical impedance spectroscopy, is a nondestructive test and was used to measure the sample's electrochemical impedance by applying an alternating current to the electrochemical cell at different frequencies and recording the resulting current. The test followed the ISO 16773-1-4:2016 standard [35]. To visualize the collected data, Nyquist and Bode diagrams were used. For further analysis and to simulate the electrochemical behavior of the materials, equivalent circuits (EC) were applied. These circuits helped in accurately modeling and understanding the complex impedance characteristics observed during the tests.

2.4. Microhardness

The Vickers microhardness of the sample was evaluated using an indentation test on a FM-810 Microhardness Tester (Future Tech, Kawasaki, Japan). The surface was polished to a mirror finish to ensure clear visibility of the indentation marks. Indentations were made with a prudent distance between them to avoid interference with the measurements. The test was conducted following the ISO 14577-1:2015 standard [36]. However, due to the high hardness of the material, a load of 2 kgf was applied to measure the indentation marks accurately. A total of 45 indentations were made on different regions of both the monolithic and doped B_4C samples, and the average Vickers hardness (HV_2) value was then calculated.

3. Results and Discussion

3.1. Scanning Electron Microscope (SEM)

Figure 2 shows, at low and high-magnification (3500× and 5000×), how a much denser microstructure is obtained by adding CoCrFeNiMo HEA to monolithic B_4C, as theoretical density suggested (monolithic B_4C: 2.52 g/cm^3; 3% HEA B_4C: 2.71 g/cm^3) and measured density corroborated (monolithic B_4C: 2.43 g/cm^3; 3% HEA B_4C: 2.66 g/cm^3) [37].

According to German et al. [38], liquid phases naturally tend to occupy configurations with the lowest energy, preferentially flowing into pores or smaller grains. This behavior, combined with the presence of CoCrFeNiMo HEA phases at triple junctions and grain boundaries, inhibits grain growth and results in finer grains. For instance, the microstructure of the 3% B_4C HEA demonstrates only a slight reduction in grain size (2.52 μm) compared to monolithic B_4C (2.57 μm) [37].

3.2. Electrochemical Tests

3.2.1. Corrosion Potential

The corrosion potential indicates the voltage at which the cathodic current density shifts to anodic when a metal is immersed in a solution. In accordance with the Mixed Potential Theory proposed by Wagner and Traud [39], oxidation and reduction reactions involved in corrosion occur at equal rates on the metal's surface. The change in corrosion potential as time passes serves as an accurate measure of corrosion behavior, although it is not sufficient for a comprehensive analysis.

In our observations, the corrosion potential of the sample first decreased but rapidly increased in two steps with the immersion time, indicating that the sample became passivated in the solution. The curve did not display any potential drops that would typically be inherent in surface activation during exposure to the corrosive solution, which implies that the passive film of the outer layers is thermodynamically stable under these conditions (see Figure 3).

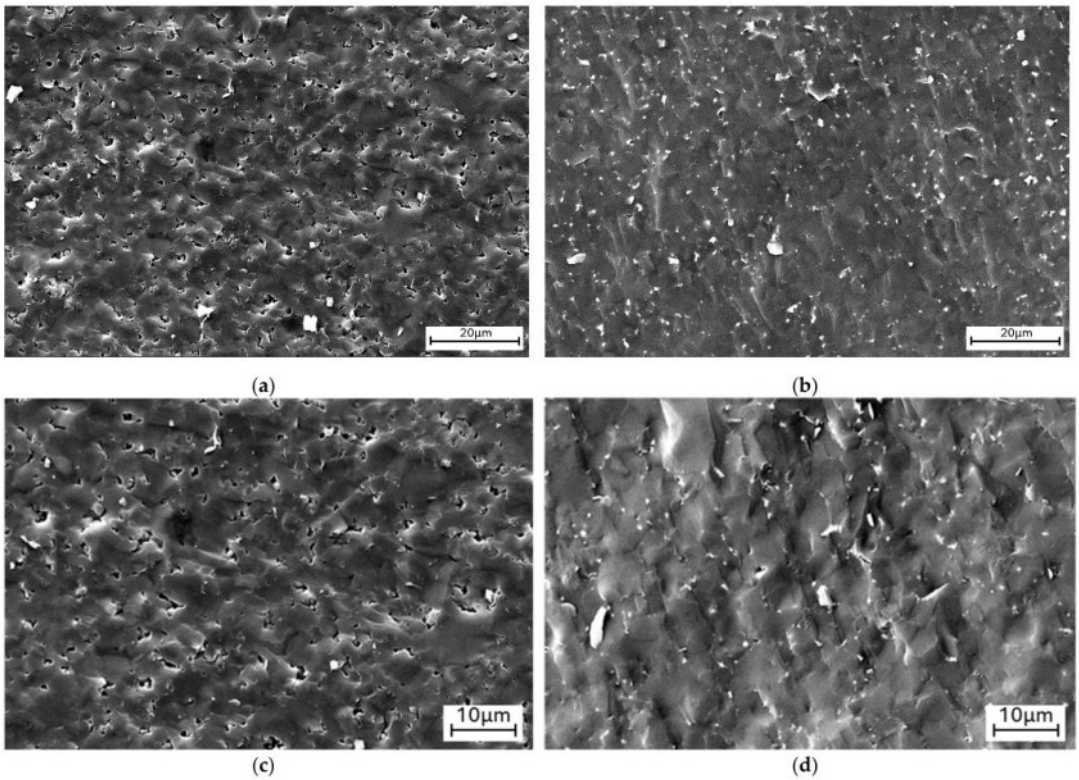

Figure 2. SEM images of (**a**) monolithic B_4C at 3500× magnification, (**b**) 3% HEA-doped B_4C at 3500× magnification, (**c**) monolithic B_4C at 5000× magnification, and (**d**) 3% HEA-doped B_4C at 5000× magnification.

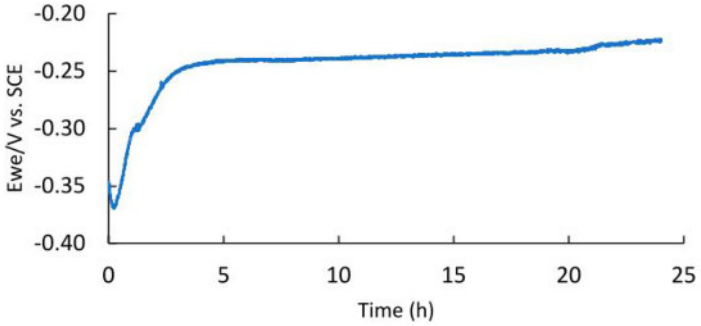

Figure 3. Corrosion potential vs. time for 24 h of immersion in 3.5% NaCl solution.

3.2.2. Corrosion Rate

It was found that liquid phases [38] generally favor the lowest energy configuration, causing them to move preferentially toward smaller grains and pores, which helps account for the observed linear polarization behavior (see Figure 4).

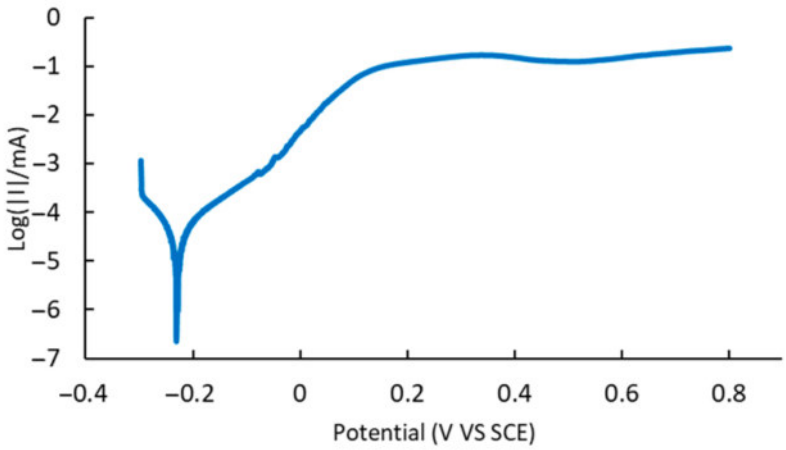

Figure 4. Polarization curve of B_4C 3% HEA-doped sample in 3.5% NaCl solution.

3.2.3. Electrochemical Impedance Spectroscopy (EIS)

This advanced technique is particularly useful for investigating the interfacial characteristics related to processes occurring on the surfaces of metallic alloys. Compared to other electrochemical methods, EIS offers several advantages, as it operates in a stationary state, measuring small signals effectively and is capable of probing frequencies ranging from 100 mHz to 100 kHz.

The selection of a frequency range from 100 mHz to 100 kHz for electrochemical impedance spectroscopy (EIS) measurements is driven by the necessity to encompass a broad spectrum of electrochemical processes and system characteristics. The high frequency ranges (10 kHz to 100 kHz) allow for the capture of information pertaining to the bulk properties of the electrolyte, including ionic conductivity. This also illustrates the high-frequency response of the system, including capacitive behaviors and dielectric properties. The mid frequencies range (1 Hz to 10 kHz) offers valuable insights into charge transfer resistance and double-layer capacitance, helping in the comprehension of processes such as ion diffusion and interfacial phenomena at the electrode/electrolyte interface. The low frequencies range (100 mHz to 1 Hz) indicates slow processes such as diffusion (Warburg impedance) and long-term stability, playing a vital role in analyzing phenomena like mass transport limitations, electrode porosity, and faradaic reactions.

Frequencies below 100 mHz are typically avoided because of the considerable time needed for stable measurements and the possibility of noise interference. Frequencies exceeding 100 kHz are unlikely to provide substantial additional helpful data for numerous electrochemical systems and were also constrained by the limitations of our equipment's capabilities.

Bode and Nyquist Diagrams in 3.5% NaCl Solution

The results from electrochemical impedance spectroscopy are displayed in Bode phase impedance plots, recorded at the same potential in a 3.5% NaCl solution. The highest impedance value was 60.047 kΩ, and the maximum phase angle was 70.5° (see Figure 5). The electrochemical impedance spectroscopy data collected showed incredibly high resistance to corrosion in a 3.5% NaCl solution.

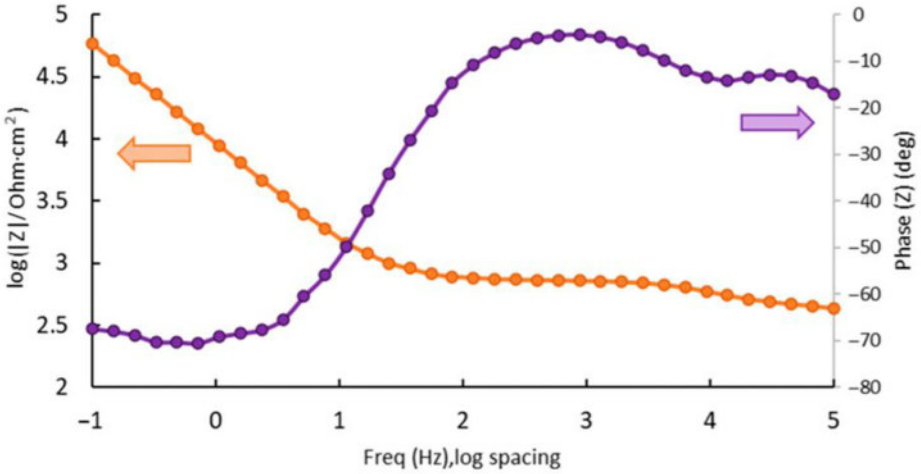

Figure 5. Bode-IZI and Bode phase for doped samples at Ecorr after 24 h of immersion in 3.5% NaCl solution.

The Nyquist diagram (see Figure 6) depicts three zones: high frequencies describe one semicircle, a second semicircle is described at medium frequencies, and finally at high frequencies, a straight line revealing diffusion appears. The behavior is determined by a two stages process: first, the filling of the pores and cracks with a 3.5% NaCl solution (with a remarkable diffusional component), followed by the creation of a passive film within those pores and on the material's surface. Similar results were obtained with B_4C doped with 2% CoCrFeNiMo HEA [40].

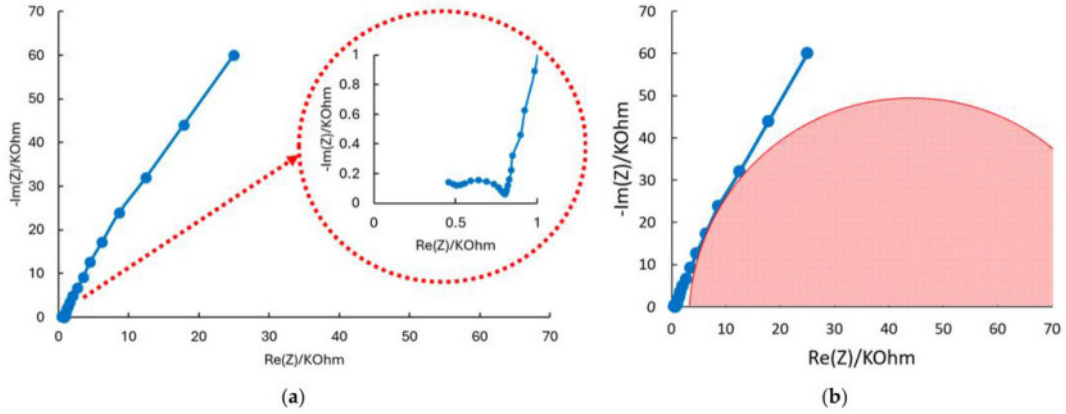

Figure 6. Nyquist diagrams for doped samples at Ecorr after 24 h of immersion in 3.5% NaCl solution with (**a**) higher detail at low frequencies and (**b**) higher detail at medium frequencies.

The equivalent circuit model R(Q(R(QR)Q(RW))), which most accurately aligns with the experimental results for sample B_4C 3% HEA, is illustrated in Figure 7. This circuit indicates that until the alloy film is reached, the outer layer of the sample demonstrates dissolution resistance, featuring a both porous and dense passive layer.

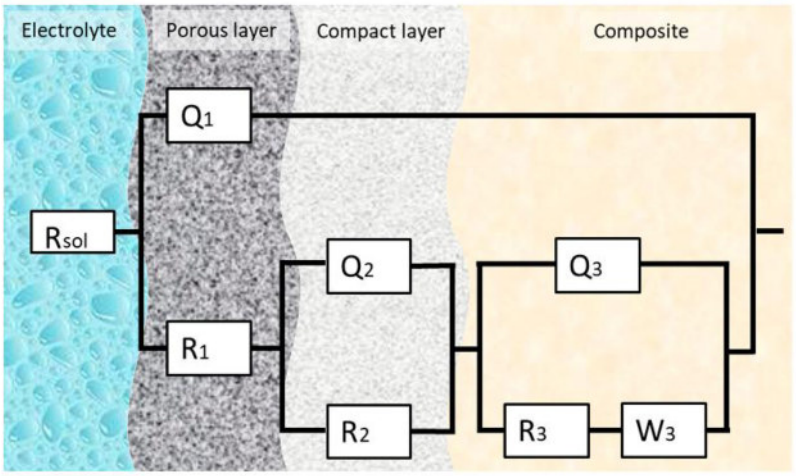

Figure 7. Equivalent circuit R(Q(R(QR)Q(RW))).

The electrical equivalent circuit was employed to model the experimental EIS data. The impedance spectra were processed by using the software ZSimpWin 3.6 (Informer Technologies, Los Angeles, CA, USA). The accuracy of the fit was determined by comparing the simulated results with the experimental data collected, where the chi-square value is calculated. A chi-square value near 10^{-5} indicates a highly precise fit with only a few components required for the model [41].

The formula obtained by applying Kirchhoff's circuit laws to this new circuit is as follows:

$$Z_{circuit} = R_{sol} + \frac{1}{\frac{1}{Q_1} + \frac{1}{R_1 + \frac{1}{\frac{1}{R_2}+\frac{1}{Q_2}} + \frac{1}{\frac{1}{R_3+W_3}+\frac{1}{Q_3}}}} \quad (1)$$

After obtaining Equation (1), it is simplified to yield the following equation:

$$Z_{circuit} = R_{sol} + \frac{Q_1 \cdot \left(R_1 + \frac{R_2 \cdot Q_2}{R_2+Q_2} + \frac{(R_3+W_3)\cdot Q_3}{(R_3+W_3)+Q_3}\right)}{Q_1 + R_1 + \frac{R_2 \cdot Q_2}{R_2+Q_2} + \frac{(R_3+W_3)\cdot Q_3}{(R_3+W_3)+Q_3}} \quad (2)$$

The letter "Q" stands for a constant phase element (CPE).It is normally used when the impedance data are not adequate for basic circuits elements and therefore, allow for the consideration of the passivated surface. The impedance provided by a CPE is described by the following equation [41]:

$$Z_{CPE} = \frac{1}{Y_0(jw)^n} \quad (3)$$

The letter "W" on the equivalent circuit stands for the Warburg element, which represents the movement or diffusion of electrons or ions in solid or liquid phases. It is represented by the following equation [42]:

$$Z_W = \frac{1}{Y_0(jw)^{0.5}} \quad (4)$$

Replacing the Equation (2) Warburg element and the constant phase elements, we create the following equation for the equivalent circuit obtained:

$$Z_{circuit} = R_{sol} + \frac{\frac{1}{Y_1(jw)^{n_1}} \cdot \left[R_1 + \frac{R_2 \cdot \frac{1}{Y_2(jw)^{n_2}}}{R_2 + \frac{1}{Y_2(jw)^{n_2}}} + \frac{\left(R_3 + \frac{1}{Y_W(jw)^{0.5}}\right) \cdot \frac{1}{Y_3(jw)^{n_3}}}{\left(R_3 + \frac{1}{Y_W(jw)^{0.5}}\right) + \frac{1}{Y_3(jw)^{n_3}}} \right]}{\frac{1}{Y_1(jw)^{n_1}} + R_1 + \frac{R_2 \cdot \frac{1}{Y_2(jw)^{n_2}}}{R_2 + \frac{1}{Y_2(jw)^{n_2}}} + \frac{\left(R_3 + \frac{1}{Y_W(jw)^{0.5}}\right) \cdot \frac{1}{Y_3(jw)^{n_3}}}{\left(R_3 + \frac{1}{Y_W(jw)^{0.5}}\right) + \frac{1}{Y_3(jw)^{n_3}}}} \quad (5)$$

Table 1 shows the circuit equivalent parameters for the sample under study.

Table 1. R(Q(R(QR)Q(RW))) circuit equivalent parameters for B_4C doped sample.

Parameters	Results
Y_1 ($S \cdot sec^n/cm^2$)	$1.001 \cdot 10^{-8}$
n_1	0.856
R_1 ($ohm \cdot cm^2$)	378.6
Y_2 ($S \cdot sec^n/cm^2$)	$1.226 \cdot 10^{-7}$
n_2	0.968
R_2 ($ohm \cdot cm^2$)	209.8
Y_3 ($S \cdot sec^n/cm^2$)	$2.061 \cdot 10^{-5}$
n_3	0.894
R_3 ($ohm \cdot cm^2$)	6363
Y_W ($S \cdot sec^5/cm^2$)	$8.952 \cdot 10^{-6}$
Chi-square	$1.22 \cdot 10^{-4}$

This model captures the processes occurring in the outer and inner layers of the material during electrochemical testing, specifically in relation to its corrosion resistance and passive film characteristics. When observing a bi-layer passive film consisting of a porous layer in contact with the electrolyte and a compact layer in contact with the underlying metal sample, several key characteristics and mechanisms influence the film's performance, especially regarding diffusion and long-term corrosion resistance.

The porous outer layer exhibits greater permeability to ions and water from the electrolyte, potentially acting as a barrier while facilitating the entrance of hostile species, such as chloride ions, from the environment. Ions, such as corrosive chlorides, may pass through the porous outer layer, with the diffusion rate dependent upon the layer's porosity, thickness, and rugosity. Oxygen may also penetrate the porous layer, contributing to oxidation reactions at the interface of the compact layer.

The compact layer (inner layer) is dense and provides the main barrier by restricting ion and electron transit. It attaches firmly to the metal surface, offering a more efficient barrier against corrosion. The compact layer exhibits reduced permeability and serves as a principal defense mechanism by markedly impeding the diffusion of aggressive ions, resulting in decreasing the rate of metal dissolution. The integrity and stability of this layer are essential for prolonged corrosion resistance.

The diffusion process affects long-term corrosion resistance, since the persistent access of hostile ions through the porous layer might result in the localized degradation of the compact layer over time. The compromise of the compact layer may accelerate corrosion rates, resulting in pitting or crevice corrosion. The system's capacity to re-passivate by generating a new compact layer is essential for long-term resistance if the compact layer is compromised. The migration of metal ions (e.g., Fe^{2+}, Cr^{3+}) from the metal substrate to the outer layer can facilitate the development of protective oxides. Oxygen diffusion through the porous layer is essential for sustaining passivity by facilitating the creation and

repair of oxide layers; insufficient oxygen supply can impede the re-passivation process, increasing the danger of corrosion in low-oxygen environments.

The results obtained suggest multiple layers of corrosion products, from a porous outer film to a more compact intermediate layer, and capture the impedance characteristics of the alloy surface. The presence of Warburg impedance on the layer closer to the alloy suggests that diffusion plays a significant role in the corrosion dynamics, improving the protective properties of the HEA system.

3.3. Microhardness

This test involves applying a vertical load onto the surface of the sample under study. In this case, the B_4C sample doped with a 3% volume of HEA was compared to monolithic B_4C by using a 136° edge angle pyramidal tetrahedral indenter from the hardness tester. The process continues for 15 s until an indentation was formed and, according to the Vickers method, a relationship was established between the applied load and the two diagonal measurements that describe the area of the indentation.

When analyzing the results from this technique, it is important to consider that the SEM images showed a porous microstructure with cracks appearing along the grain boundaries related to the presence of agglomerated HEA phases on the grain unions, as was corroborated by the equivalent circuit obtained from the electrochemical tests [37].

For this study, Vickers hardness was calculated using a fixed load of 2 kgf, as lower loads were insufficient to indent the sample effectively. The Vickers hardness values of indentation on the B_4C sample doped with a 3% volume of HEA can be seen in Figure 8.

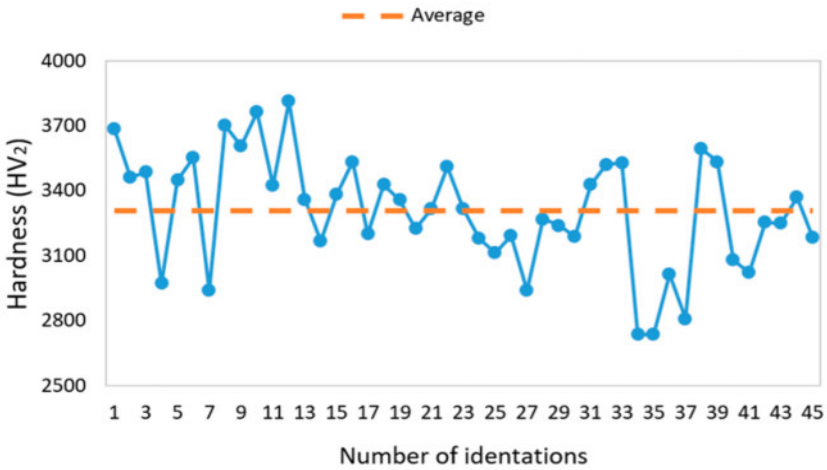

Figure 8. Microhardness values of each indentation for B_4C 3% HEA sample.

This variation can be attributed to the differing hardness levels of both the main phases seen in the SEM, B_4C and HEA, or the cracks noticed on the microstructure, as seen in other B_4C composite microhardness studies [43–45]. Therefore, a statistics study was applied to analyze and compare the distribution and variability of the Vickers hardness measurements of both samples. The results are summarized in Table 2, and various plots (boxplots, scatter plots, histograms, and normal distribution) are generated to visualize the distribution and comparison of hardness values across both samples (see Figure 9).

Table 2. Statistical parameters of Vickers hardness measurements for both B_4C doped and monolithic samples.

Statistical Parameter	Monolithic B_4C (HV_2)	Doped B_4C (HV_2)
Mean	2966.67	3308.57
Median	2990.0	3319.0
Standard Deviation	181.09	258.8
Minimum	2621.0	2737.0
Maximum	3381.0	3813.0
Quartile 25	2812.0	3182.0
Quartile 50 (Median)	2990.0	3319.0
Quartile 75	3074.0	3514.0

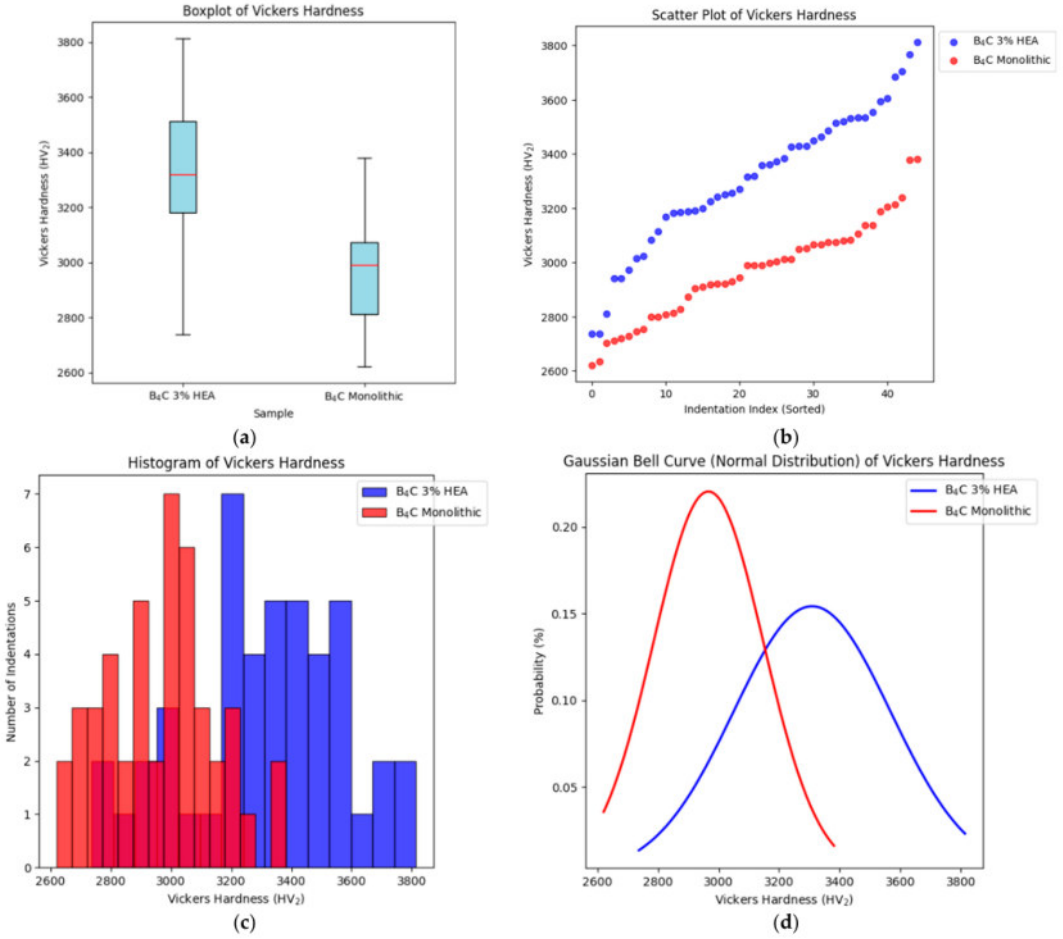

Figure 9. Vickers hardness for both B_4C monolithic and doped samples comparison: (**a**) distribution of Vickers hardness data through its quartiles; (**b**) dispersion of Vickers hardness values; (**c**) frequency of Vickers hardness values within certain intervals (bins); (**d**) probability distribution of the hardness values.

Through statistical analysis and the generated graphs, we can observe key trends in the hardness distribution of both samples. The B_4C doped sample results are harder than that of monolithic B_4C. Although there is a notable difference between the minimum and maximum values of both samples, most indentations are concentrated within a narrower range, especially in monolithic B_4C. This concentration suggests that both samples have a homogeneous structure and follow a normal distribution. The Vickers indentation led to radial cracks (see Figure 10), as seen in other B_4C composite studies [37,45].

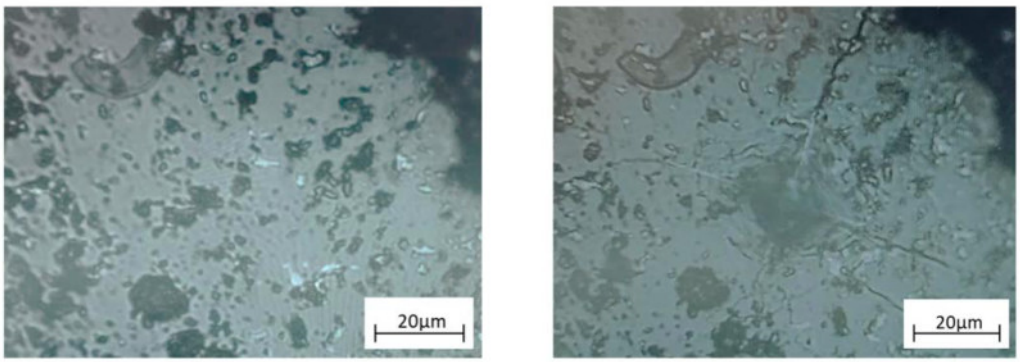

(**a**) (**b**)

Figure 10. B_4C doped sample (**a**) before Vickers indentation and (**b**) after Vicker indentation.

Densification leads to increased hardness as it results in a reduction of voids and defects within the microstructure. Increased density enhances the load-bearing capacity, as evidenced by the elevated microhardness values.

Hardness is influenced by grain boundary strengthening, as the increase in grain boundary area from grain refinement due to HEA doping leads to enhanced resistance and plastic deformation.

Secondary phases resulting from HEA doping can serve as reinforcement, thereby improving the overall strength and hardness of the material. The phases may also act to pin dislocations, thereby hindering plastic deformation and enhancing hardness.

The enhancement in microhardness resulting from the HEA doping of B_4C can be ascribed to improved densification, grain refinement, and the development of reinforcing secondary phases. The microstructural alterations decrease porosity, improve grain boundary strengthening, and obstruct dislocation movement, collectively leading to increased hardness values.

4. Conclusions

The behavior of 3% HEA B_4C ceramic in an artificial seawater environment was thoroughly investigated and the key findings can be summarized as follows:

- The addition of the CoCrFeMoNi high-entropy alloy to the B_4C ceramic significantly changed its microstructure, leading to a denser and more compact configuration when compared to undoped B_4C. This doping process effectively inhibited grain expansion, resulting in a more refined grain structure.
- The doped sample exhibited remarkable resistance to corrosion in the artificial seawater, making it suitable for applications in marine or corrosive environments conditions.
- The chemical reactions that occur when the doped sample was immersed in artificial seawater followed a two-step process, with a significant diffusional component involved. Initially, the seawater penetrated the material's surface, followed by the

formation of protective films or layers that prevent further degradation, contributing to the observed high corrosion resistance.

In addition, the statistical microhardness analysis revealed the probability distribution of the hardness values, indicating that the sample followed a normal distribution, which suggests that the sample has a homogeneous structure. The Vickers hardness of 3% HEA B_4C ceramic was higher than that of monolithic B_4C.

This study highlights the potential of HEA-doped B_4C for use in environments where both mechanical strength and corrosion resistance are critical factors. Future research lines to further investigate the material's properties and its applications include the following: (1) examining the effects of doping B_4C with elevated concentrations of HEAs (e.g., 4%, 5%, or higher) to find the saturation point or optimal concentration for improved attributes such as corrosion resistance, hardness, toughness, or thermal stability; (2) testing various HEA compositions to determine how specific elements within the HEA affect the properties of B_4C, thereby identifying the HEA composition that provides enhanced corrosion resistance, mechanical, thermal, or electrical properties.

Author Contributions: Conceptualization, A.D.R.-C.; methodology, A.D.R.-C.; software, A.D.R.-C.; validation, A.D.R.-C., B.C.O., J.C.M.-R. and G.G.; formal analysis, A.D.R.-C. and B.C.O.; investigation, A.D.R.-C.; resources, J.C.M.-R. and G.G.; data curation, A.D.R.-C.; writing—original draft preparation, A.D.R.-C.; writing—review and editing, A.D.R.-C.; visualization, A.D.R.-C.; supervision, J.C.M.-R. and G.G. All authors have read and agreed to the published version of the manuscript.

Funding: This research received no external funding.

Data Availability Statement: The original contributions presented in this study are included in the article. Further inquiries can be directed to the corresponding author.

Acknowledgments: We hereby acknowledge the European project 2023-1-RO01-KA220-HED-000159985: Smart Healthcare Engineering and Cabildo of Gran Canaria project with the reference Cabildo22-01.

Conflicts of Interest: The authors declare no conflicts of interest.

References

1. Suri, A.K.; Subramanian, C.; Sonber, J.K.; Ch Murthy, T.S.R. Synthesis and Consolidation of Boron Carbide: A Review. *Int. Mater. Rev.* **2010**, *55*, 4–38. [CrossRef]
2. Pérez, S.; Tamayo, P.; Rico, J.; Alonso, J.; Thomas, C. Effect of Fibers and Boron Carbide on the Radiation Shielding Properties of Limestone and Magnetite Aggregate Concrete. *Prog. Nucl. Energy* **2024**, *175*, 105320. [CrossRef]
3. Tamayo, P.; Thomas, C.; Rico, J.; Pérez, S.; Mañanes, A. Radiation Shielding Properties of Siderurgical Aggregate Concrete. *Constr. Build. Mater.* **2022**, *319*, 126098. [CrossRef]
4. Zhang, W. A Review of Tribological Properties for Boron Carbide Ceramics. *Prog. Mater. Sci.* **2021**, *116*, 100718. [CrossRef]
5. Domnich, V.; Reynaud, S.; Haber, R.A.; Chhowalla, M. Boron Carbide: Structure, Properties, and Stability under Stress. *J. Am. Ceram. Soc.* **2011**, *94*, 3605–3628. [CrossRef]
6. Zorzi, J.E.; Perottoni, C.A.; Da Jornada, J.A.H. Hardness and Wear Resistance of B4C Ceramics Prepared with Several Additives. *Mater. Lett.* **2005**, *59*, 2932–2935. [CrossRef]
7. Ortiz, A.L.; Candelario, V.M.; Moreno, R.; Guiberteau, F. Near-Net Shape Manufacture of B4C–Co and ZrC–Co Composites by Slip Casting and Pressureless Sintering. *J. Eur. Ceram. Soc.* **2017**, *37*, 4577–4584. [CrossRef]
8. Frage, N.; Hayun, S.; Kalabukhov, S.; Dariel, M.P. The effect of Fe addition on the densification of B 4 C powder by spark plasma sintering. *Powder Metall. Met. Ceram.* **2007**, *46*, 533–538. [CrossRef]
9. Ebrahimi, S.; Heydari, M.S.; Baharvandi, H.R.; Ehsani, N. Effect of Iron on the Wetting, Sintering Ability, and the Physical and Mechanical Properties of Boron Carbide Composites: A Review. *Int. J. Refract. Met. Hard Mater.* **2016**, *57*, 78–92. [CrossRef]
10. Larsson, P.; Axéax'axé, N.N.; Hogmark, S. Improvements of the Microstructure and Erosion Resistance of Boron Carbide with Additives. *J. Mater. Sci.* **2000**, *35*, 3433–3440. [CrossRef]
11. Levin, L.; Frage, N.; Dariel, M.P. The Effect of Ti and TiO 2 Additions on the Pressureless Sintering of B 4 C. *Metall. Mater. Trans. A* **1999**, *30*, 3201–3210. [CrossRef]

12. Rodríguez-Rojas, F.; Moreno, R.; Guiberteau, F.; Ortiz, A.L. Aqueous Colloidal Processing of Near-Net Shape B4C-Ni Cermet Compacts. *J. Eur. Ceram. Soc.* **2016**, *36*, 1915–1921. [CrossRef]
13. Cui, G.; Han, B.; Yang, Y.; Wang, Y.; Chunyang, H. Microstructure and Tribological Property of CoCrFeMoNi High Entropy Alloy Treated by Ion Sulfurization. *J. Mater. Res. Technol.* **2020**, *9*, 2598–2609. [CrossRef]
14. Brito-Garcia, S.J.; Mirza-Rosca, J.C.; Jimenez-Marcos, C.; Voiculescu, I. Impact of Ti Doping on the Microstructure and Mechanical Properties of CoCrFeMoNi High-Entropy Alloy. *Metals* **2023**, *13*, 854. [CrossRef]
15. Yang, F.; Wang, J.; Zhang, Y.; Wu, Z.; Zhang, Z.; Zhao, F.; Huot, J.; Grobivć Novaković, J.; Novaković, N. Recent Progress on the Development of High Entropy Alloys (HEAs) for Solid Hydrogen Storage: A Review. *Int. J. Hydrogen Energy* **2022**, *47*, 11236–11249. [CrossRef]
16. Fu, M.; Ma, X.; Zhao, K.; Li, X.; Su, D. High-Entropy Materials for Energy-Related Applications. *iScience* **2021**, *24*, 102177. [CrossRef]
17. Rios, M.L.; Baldevenites, V.L.; Voiculescu, I.; Rosca, J.M. AlCoCrFeNi High Entropy Alloys as Possible Nuclear Materials. *Microsc. Microanal.* **2020**, *26*, 406–407. [CrossRef]
18. Li, T.; Wang, D.; Zhang, S.; Wang, J. Corrosion Behavior of High Entropy Alloys and Their Application in the Nuclear Industry—An Overview. *Metals* **2023**, *13*, 363. [CrossRef]
19. Socorro-Perdomo, P.; Florido-Suarez, N.; Voiculescu, I.; Mirza-Rosca, J. Biocompatibility of New High-Entropy Alloys with Non-Cytotoxic Elements. *Microsc. Microanal.* **2021**, *27*, 1772–1774. [CrossRef]
20. Castro, D.; Jaeger, P.; Baptista, A.C.; Oliveira, J.P. An Overview of High-entropy Alloys as Biomaterials. *Metals* **2021**, *11*, 648. [CrossRef]
21. Zhang, J.; Tse, K.; Wong, M.; Zhang, Y.; Zhu, J. A Brief Review of Co-Doping. *Front. Phys.* **2016**, *11*, 117405. [CrossRef]
22. Dai, C.; Zhao, T.; Du, C.; Liu, Z.; Zhang, D. Effect of Molybdenum Content on the Microstructure and Corrosion Behavior of FeCoCrNiMox High-Entropy Alloys. *J. Mater. Sci. Technol.* **2020**, *46*, 64–73. [CrossRef]
23. Li, Y.; Zhang, J.; Huang, X.; Liu, J.; Deng, L.; Han, P. Influence of Laser Power on Microstructure Evolution and Properties of Laser Cladded FeNiCoCrMo HEA Coatings. *Mater. Today Commun.* **2023**, *35*, 105615t. [CrossRef]
24. Shang, C.; Axinte, E.; Sun, J.; Li, X.; Li, P.; Du, J.; Qiao, P.; Wang, Y. CoCrFeNi(W1 − XMox) High-Entropy Alloy Coatings with Excellent Mechanical Properties and Corrosion Resistance Prepared by Mechanical Alloying and Hot Pressing Sintering. *Mater. Des.* **2017**, *117*, 193–202. [CrossRef]
25. Wu, H.; Zhang, S.; Wang, Z.Y.; Zhang, C.H.; Chen, H.T.; Chen, J. New Studies on Wear and Corrosion Behavior of Laser Cladding FeNiCoCrMox High Entropy Alloy Coating: The Role of Mo. *Int. J. Refract. Metals Hard Mater.* **2022**, *102*, 105721. [CrossRef]
26. Brito-Garcia, S.; Mirza-Rosca, J.; Geanta, V.; Voiculescu, I. Mechanical and Corrosion Behavior of Zr-Doped High-Entropy Alloy from CoCrFeMoNi System. *Materials* **2023**, *16*, 1832. [CrossRef]
27. Semikolenov, A.; Shalnova, S.; Klinkov, V.; Andreeva, V.; Salynova, M.; Larionova, T.; Tolochko, O. Effect of al Content on Phase Compositions of Fenicocrmo0.5alx High Entropy Alloy. *Metals* **2021**, *11*, 1734. [CrossRef]
28. Dai, C.; Luo, H.; Li, J.; Du, C.; Liu, Z.; Yao, J. X-Ray Photoelectron Spectroscopy and Electrochemical Investigation of the Passive Behavior of High-Entropy FeCoCrNiMox Alloys in Sulfuric Acid. *Appl. Surf. Sci.* **2020**, *499*, 143903. [CrossRef]
29. Wang, L.; Mercier, D.; Zanna, S.; Seyeux, A.; Laurent-Brocq, M.; Perrière, L.; Guillot, I.; Marcus, P. Study of the Surface Oxides and Corrosion Behaviour of an Equiatomic CoCrFeMnNi High Entropy Alloy by XPS and ToF-SIMS. *Corros. Sci.* **2020**, *167*, 108507. [CrossRef]
30. Szymczak, T.; Gumienny, G.; Klimek, L.; Goły, M.; Szymszal, J.; Pacyniak, T. Characteristics of Al-Si Alloys with High Melting Point Elements for High Pressure Die Casting. *Materials* **2020**, *13*, 4861. [CrossRef]
31. Rajkumar, V.B.; Du, Y.; Liu, S.; Cheng, K.; Srivastav, A.K. Measurements of the Melting Points, Liquidus, and Solidus of the Mo, Ta, and MoTa Binary Alloys Using a Novel High-Speed Pyrometric Technique. *Int. J. Refract. Metals Hard Mater.* **2020**, *93*, 105335. [CrossRef]
32. Wang, W.; Wang, J.; Sun, Z.; Li, J.; Li, L.; Song, X.; Wen, X.; Xie, L.; Yang, X. Effect of Mo and Aging Temperature on Corrosion Behavior of (CoCrFeNi)100-XMox High-Entropy Alloys. *J. Alloys Compd.* **2020**, *812*, 152139. [CrossRef]
33. Fu, Y.; Huang, C.; Du, C.; Li, J.; Dai, C.; Luo, H.; Liu, Z.; Li, X. Evolution in Microstructure, Wear, Corrosion, and Tribocorrosion Behavior of Mo-Containing High-Entropy Alloy Coatings Fabricated by Laser Cladding. *Corros. Sci.* **2021**, *191*, 109727. [CrossRef]
34. *ASTM G5-94(2004)*; Standard Reference Test Method for Making Potentiostatic and Potentiodynamic Anodic. ASTM International: West Conshohocken, PA, USA, 2004.
35. *ISO 16773-1-4:2016*; Electrochemical Impedance Spectroscopy (EIS) on Coated and Uncoated Metallic Specimens. ISO: Geneva, Switzerland, 2016.
36. *ISO 14577-1:2015*; Metallic Materials—Instrumented Indentation Test for Hardness and Materials Parameters—Part 1: Test Method. ISO: Geneva, Switzerland, 2015.
37. Ocak, B.C.; Goller, G. Investigation the Effect of FeNiCoCrMo HEA Addition on Properties of B4C Ceramic Prepared by Spark Plasma Sintering. *J. Eur. Ceram. Soc.* **2021**, *41*, 6290–6301. [CrossRef]

38. German, R.M.; Suri, P.; Park, S.J. Review: Liquid Phase Sintering. *J. Mater. Sci.* **2009**, *44*, 1–39. [CrossRef]
39. Wagner, C.; Traud, W. "On the Interpretation of Corrosion Processes through the Superposition of Electrochemical Partial Processes and on the Potential of Mixed Electrodes", with a Perspective by F. Mansfeld. *Corrosion* **2006**, *62*, 843–855. [CrossRef]
40. Rico-Cano, A.D.; Mirza-Rosca, J.C.; Ocak, B.C.; Goller, G. Corrosion Behavior of New B4C Ceramic Doped with High-Entropy Alloy in an Aggressive Environment. *Microsc. Microanal.* **2024**, *30*, ozae044.666. [CrossRef]
41. Boukamp, B.A. A Nonlinear Least Squares Fit Procedure for Analysis of Immittance Data of Electrochemical Systems. *Solid State Ion.* **1986**, *20*, 31–44. [CrossRef]
42. Jáquez-Muñoz, J.M.; Gaona-Tiburcio, C.; Méndez-Ramírez, C.T.; Baltazar-Zamora, M.Á.; Estupinán-López, F.; Bautista-Margulis, R.G.; Cuevas-Rodríguez, J.; Flores-De los Rios, J.P.; Almeraya-Calderón, F. Corrosion of Titanium Alloys Anodized Using Electrochemical Techniques. *Metals* **2023**, *13*, 476. [CrossRef]
43. Uzun, A.; Asikuzun, E.; Gokmen, U.; Cinici, H. Vickers Microhardness Studies on B4C Reinforced/Unreinforced Foamable Aluminium Composites. *Trans. Indian Inst. Met.* **2018**, *71*, 327–337. [CrossRef]
44. Cramer, C.L.; Cakmak, E.; Unocic, K.A. Hardness Measurements and Interface Behavior of SiC-B4C-Si Multiple Phase Particulate Composites Made with Melt Infiltration and Additive Manufacturing. *J. Compos. Sci.* **2023**, *7*, 172. [CrossRef]
45. Ma, H.; Liang, Y.; Fu, H. Effect of B4C Addition on Microstructure and Wear Resistance of Laser Cladding NiCrBSi Coatings. *JOM* **2023**, *75*, 515–525. [CrossRef]

3.3. Impact of CoCrFeNiMo High-Entropy-Alloy Doping on the Mechanical and Electrochemical Properties of B_4C Ceramic

applied sciences

MDPI

Article

Impact of CoCrFeNiMo High-Entropy-Alloy Doping on the Mechanical and Electrochemical Properties of B_4C Ceramic

Alberto Daniel Rico-Cano [1], Julia Claudia Mirza-Rosca [1,2,*], Burak Cagri Ocak [3] and Gultekin Goller [3]

[1] Departamento de Ingeniería Mecánica, Campus Universitario Tafira, Universidad de Las Palmas de Gran Canaria, 35017 Las Palmas de gran Canaria, Spain; alberto.rico101@alu.ulpgc.es
[2] Materials Engineering and Welding Department, Transilvania University of Brasov, 500036 Brasov, Romania
[3] Department of Metallurgical and Materials Engineering, Istanbul Technical University, Maslak, 34469 Istanbul, Turkey; goller@itu.edu.tr (G.G.)
* Correspondence: julia.mirza@ulpgc.es

TÍTULO:	Impact of CoCrFeNiMo High-Entropy-Alloy Doping on the Mechanical and Electrochemical Properties of B_4C Ceramic
AUTORES:	A D Rico-Cano, J C Mirza-Rosca, B C Ocak, G Goller
REVISTA:	Applied Sciences
ÍNDICE DE IMPACTO:	2.5
CUARTIL:	Q1
DOI:	https://doi.org/10.3390/app15094859
eISSN:	2076-3417
EDITORIAL:	MDPI
MES Y AÑO:	Abril 2025
VOLUMEN:	15
PÁGINAS	17

applied sciences

MDPI

Article

Impact of CoCrFeNiMo High-Entropy-Alloy Doping on the Mechanical and Electrochemical Properties of B_4C Ceramic

Alberto Daniel Rico-Cano [1], Julia Claudia Mirza-Rosca [1,2,*], Burak Cagri Ocak [3] and Gultekin Goller [3]

[1] Departamento de Ingeniería Mecánica, Campus Universitario Tafira, Universidad de Las Palmas de Gran Canaria, 35017 Las Palmas de gran Canaria, Spain; alberto.rico101@alu.ulpgc.es
[2] Materials Engineering and Welding Department, Transilvania University of Brasov, 500036 Brasov, Romania
[3] Department of Metallurgical and Materials Engineering, Istanbul Technical University, Maslak, 34469 Istanbul, Turkey; goller@itu.edu.tr (G.G.)
* Correspondence: julia.mirza@ulpgc.es

Abstract: The purpose of this article is to evaluate and compare the mechanical and electrochemical properties of four new materials, composed of a B_4C ceramic matrix doped with 0.5%, 1%, 2% and 3% volumes of CoCrFeNiMo HEA with monolithic B_4C. The studied samples were obtained using the spark plasma sintering technique. The structure and hardness of the samples were analyzed via scanning electron microscopy (SEM) and a Vickers microhardness test. After immersion in artificial sea water to simulate a corrosive marine environment, corrosion potential, corrosion rate and electrochemical impedance spectroscopy tests were carried out to determine the samples' electrochemical behavior. Tafel slopes and the equivalent circuit that fit the EIS experimental data were obtained. A denser microstructure and smaller grain size was achieved as the HEA content increase. According to the Vickers measurements, every sample showed a normal distribution. All studied samples exhibit great corrosion resistance in a two-step chemical interaction, influenced by the presence of the Warburg element. The research demonstrates that increasing the HEA content implies better performance of corrosion resistance and mechanical properties, confirming the materials' potential use in corrosive environments and harsh mechanical applications.

Keywords: boron carbide; ceramic; HEA; EIS; corrosion behavior; microhardness; SEM

Academic Editor: Hyeonseok Yoon

Received: 13 March 2025
Revised: 16 April 2025
Accepted: 25 April 2025
Published: 27 April 2025

Citation: Rico-Cano, A.D.; Mirza-Rosca, J.C.; Ocak, B.C.; Goller, G. Impact of CoCrFeNiMo High-Entropy-Alloy Doping on the Mechanical and Electrochemical Properties of B_4C Ceramic. *Appl. Sci.* **2025**, *15*, 4859. https://doi.org/10.3390/app15094859

1. Introduction

Boron carbide (B_4C) is a ceramic material with outstanding mechanical properties, such as good thermal stability and conductivity (30 W/m K), a low density (2.52 g/cm^3), a high melting point (2450 °C) and high hardness (30 GPa) [1]. These properties guarantee B_4C as an extremely competitive material for a wide range of industrial applications, such as ballistic, refractory or electronics fields [2]. B_4C behaves as a thermoelectric material with a high Seebeck coefficient of 300 µV/K. This characteristic makes it a very interesting material for emerging applications in thermocouples, diodes and transistors. B_4C is recognized as the third-hardest material, after diamond and cubic boron nitride. It combines exceptional hardness, maintaining a low density, which makes it a lightweight alternative to diamond (~3.51 g/cm^3). B_4C exhibits good thermal conductivity but lower than diamond's. Electrically, B_4C behaves as a semiconductor with low conductivity, contrasting with diamond, which is a magnificent electrical insulator. B_4C works good in harsh environments due to its high resistance to corrosion. Diamond, despite its chemical inertness, can oxidize at elevated temperatures. B_4C could replace the use of diamond as a more

cost-effective and readily-available-in-larger-quantities material, making it attractive for industrial applications [3].

Ionizing radiation is very important in medical and industrial fields. In medicine, it is used for diagnostic imaging techniques and nuclear medicine treatments. In the industrial field, radiation is used for applications such as sterilization, material testing and quality control. Nuclear power generation contributes significantly to global energy production, offering a low-carbon alternative to fossil fuels. The challenge is determining how to take advantage of the benefits of ionizing radiation while minimizing the associated risks. In this context, B_4C exhibits exceptional neutron absorption capacity (600 barns). This makes it extensively used in nuclear reactor protection and monitoring systems as effective shielding [4,5].

Beyond its nuclear applications, B_4C has high hardness and reduced density compared to other ceramics, like SiC, Al_2O_3, Si_3N_4 and ZrO_2. These characteristics make polymers reinforced with B_4C highly attractive for tribological applications [6].

B_4C is a promising semiconductor with a hopping-type electrical transport behavior. Its bandgap (approximately 2.09 eV) is influenced by its composition and structural order. It is a p-type material with potential for innovative electronic device applications [2].

A critical aspect when processing B_4C is densification. Dense materials are often needed for many advanced applications. Different sintering additives have been explored to increase densification rates, control grain growth and improve mechanical properties. Carbon has proven effective in reducing the oxide layer on B_4C powders, which helps sintering and limits grain growth [7].

High-entropy alloys (HEAs) appeared in 2004 as a result of at least five different metallic elements being combined at approximately equal atomic ratios [8,9]. This kind of alloy rapidly became of high interest in the academic field due to their remarkable properties and their possible engineering applications, where high strength, ductility, thermal stability or corrosion resistance are required [10]. HEAs are found in a wide range of industrial applications, exhibiting superior properties to traditional alloys, which typically consist of only one or two primary elements, in biomedical [11,12], nuclear [13–15] and refractory applications, such as jet engines and turbines [16]. The actual focus of HEAs has appeared to expand to magnetic applications, energy conversion, hydrogen storage and catalysis [17], answering actual social or industrial problems. Many HEAs have been and are being studied nowadays in order to obtain better properties or increase their application range, such as MoNbTiVTaW [18], Fe20Mn15Cr15V10Al10C2.5 [19], CoCrFeMnNi [20], TiNbTaZrMoHfWCr [21], Fe20Co30Ni10Cr20Mn20 [22] and CoCrFeNiMo [23–25].

CoCrFeNiMo HEA has been doped with silicium [26], zirconium [27], aluminum [28] or titanium [29], as well as used as a coating [30,31], which enhance the HEA's versatility in different engineering applications. The effect of Mo has proven to be crucial not just on its mechanical properties, such as high hardness [32], but in the formation of a passive layer in the marine environment with the creation of Cr_2O_3 and MoO_3, which increases the HEA's corrosion resistance [31,33]. On the other hand, the addition of Ni and Cr on the HEA contributes to the formation of a resistant protective oxide film over the outer layer of the material, implying also an improvement in corrosion resistance [34,35].

This paper aims to investigate the mechanical and electrochemical properties of B_4C materials doped with 0.5% and 1% CoCrFeNiMo HEA and compare the results with those of B_4C doped with 2% and 3% CoCrFeNiMo [36,37].

Thus, in this study, the impact of CoCrFeNiMo HEA doping on the electrochemical and mechanical properties of B_4C ceramic has been investigated. Electrochemical tests were conducted in an artificial seawater environment, a 3.5% volume of NaCl solution. Additionally, scanning electron microscopy (SEM) and a microhardness statistical anal-

ysis were conducted. The study focuses on evaluating and comparing these two new compositions against the previously analyzed compounds under a marine and corrosive environment. By expanding the scope of the investigation, this work seeks to provide a deeper understanding of how CoCrFeNiMo HEA doping affects B_4C ceramic and which of these compounds have the optimal composition, with an emphasis on applications where factors such as durability, corrosion resistance and enhanced hardness are essential.

2. Materials and Methods

2.1. Material Preparation

The investigation was conducted on 4 different composites of B_4C ceramic doped with 0.5%, 1%, 2% and 3% volumes of CoCrFeNiMo HEA, created by the Department of Metallurgical and Materials Engineering of Istanbul Technical University. The preparation of the samples starting from raw materials is presented in our previous articles [37]. A graphite sheet was inserted between the punches and the powder to improve conductivity and facilitate post-sintering removal. Carbon felt insulation was used to minimize heat dissipation.

Sintering was carried out under vacuum using a Spark Plasma Sintering (SPS) system (SPS-7.40 MK-VII, SPS Syntex Inc., Saitama, Japan), applying a uniaxial pressure of 40 MPa and a pulsed direct current (12 ms/on, 2 ms/off). The temperatures during the whole process were measured with an optical pyrometer (Chino, IR-AH, Tokyo, Japan) on a designated spot in the graphite die. Continuous shrinkage tracking was conducted through punch rod displacement, with thermal expansion corrections based on a blank test. The holding time (5 min), heating rate (100 °C/min) and sintering temperature (1600 °C) were the established SPS conditions.

Then, the manufactured samples were embedded in a two-component epoxy resin. Using a Struers TegraPol-11 system (Struers, Copenhagen, Denmark), the surface was prepared via a two-step polishing procedure that included initial grinding with silicon carbide abrasive sheets (240–2000 grit) and final polishing with a 0.1 µm alpha alumina suspension to achieve a mirror-like sheen. The fabrication and preparation procedure of all studied samples is described in Figure 1.

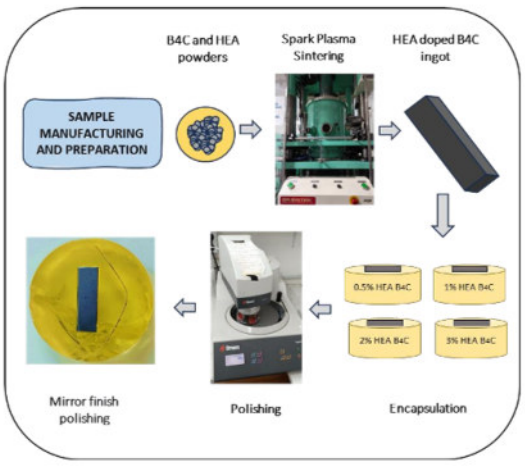

Figure 1. Schematic representation of the material preparation.

2.2. Scanning Electron Microscopy (SEM)

The scanning electron microscope model FESEM JSM 7000 F (JEOL Ltd., Tokyo, Japan) was used to analyze the microstructures of the samples under study. For a precise and easier evaluation of the images, the composites were electrochemically attacked for 15 s with a 10% NaOH solution. This process helps to reveal grain boundaries and other microstructural features, using, to maximize the results, a potential of 10 V and a current density of 0.25 A/cm^2. The linear intercept method (ASTM E112-96 [38]) was used to calculate the average grain size.

2.3. Electrochemical Tests

After finishing the sample preparation, electrochemical evaluations were carried out on the four different B_4C variants. Potentiostat BioLogic Essential SP-150 (Bio-Logic Science Instruments SAS, Seyssinet-Pariset, France) and an electrochemical cell were used to carry out the different tests. A total of 3 electrochemical tests were performed: direct-current open-circuit potential (OCP) and linear polarization and alternative-current electrochemical impedance spectroscopy (EIS). All tests were conducted in a 3.5% NaCl artificial seawater solution to simulate a marine environment. Test parameters were configured, and data analysis was conducted using EC-Lab® v-9.55 software, in accordance with the ASTM G5-94(2004) standard [39]. Each experiment utilized a conventional three-electrode electrochemical setup, where the doped B_4C samples served as the working electrodes, a saturated calomel electrode acted as the reference, and a platinum electrode functioned as the counter electrode.

2.3.1. Corrosion Potential

The open-circuit potential (OCP) was monitored over 24 h using the "Ecorr vs. Time" technique, with data recorded every 30 s or when a potential shift of 100 mV occurred. The results were analyzed to determine whether the material exhibited stable corrosion potential, passivation behavior or progressive degradation over time.

2.3.2. Corrosion Rate

The Tafel slope is utilized to establish the corrosion rate. Tafel slopes for both anodic (b_a) and cathodic (b_c) processes were determined by shifting the linear polarization curves. The ASTM G5-87 [40] Standard Reference Test Method for Conducting Potentiostatic and Potentiodynamic Anodic Polarization Measurements has been followed properly.

2.3.3. Electrochemical Impedance Spectroscopy (EIS)

EIS is a non-destructive alternative current technique with which the electrochemical impedance of all studied samples was evaluated in a wide frequency range (100 mHz to 100 kHz).

Electrochemical processes that happen slowly, like long-term stability or diffusion, can often be seen at low frequencies (100 mHz to 1 Hz). This helps to identify mass-transport limitations, electrode porosity or faradaic reactions. Medium frequencies (1 Hz to 10 kHz) are crucial for analyzing double-layer capacitance and charge-transfer resistance. This frequency range offers important information about ion diffusion and interfacial interactions at the electrode–electrolyte boundary. High frequencies (10 kHz to 100 kHz) provide information on the bulk electrolyte properties, including ionic conductivity, capacitive behavior and dielectric response.

Frequencies below 100 mHz were excluded because they prolong the measurement times and are often affected by noise interference. Frequencies above 100 kHz were not

considered either, as they provide minimal additional information for most electrochemical systems. This frequency is also beyond the operational limits of the available equipment.

This test followed the ISO 16773-1-4:2016 standard [41]. The obtained impedance data were represented using Nyquist and Bode diagrams. Additionally, equivalent circuits (ECs) were utilized to model and interpret the electrochemical behavior of the material, providing insights into its impedance characteristics.

2.4. Microhardness

With the use of an FM-810 Microhardness Tester (Future Tech, Kawasaki, Japan), the Vickers microhardness of all the composites under study was established using an indentation test. To guarantee precise measurements, the surface was polished to a mirror finish for clear visibility of the indentations. The test was performed according to the ISO 14577-1:2015 standard [42], with 19.61 N load applied due to the material's high hardness. A minimum of 45 indentations were created in various areas of all doped B_4C composites and the monolithic B_4C surface. Then, the average Vickers hardness (HV2) was calculated like all other statistical parameters.

3. Results

For clarity and ease of reference, the B_4C ceramic samples doped with 0.5%, 1%, 2% and 3% volumes of CoCrFeNiMo HEA will be, on occasion, designated as B4C.05, B4C.1, B4C.2 and B4C.3, respectively.

3.1. Scanning Electron Microscope (SEM)

SEM images of the samples after the electrochemical attack are shown in Figure 2.

When analyzing the etched microstructures of the composites, the grain size was measured: B4C.05 (2.53 $\pm$ 0.32 µm), B4C.1 (2.51 $\pm$ 0.35 µm), B4C.2 (2.16 $\pm$ 0.20 µm) and B4C.3 (2.52 $\pm$ 0.27 µm). All samples presented smaller average grain sizes compared to monolithic B_4C (2.57 $\pm$ 0.11 µm). It can be observed that the sample with 2% HEA content exhibits the smallest average grain size. It can be observed how the CoCrFeNiMo addition phase is clearly localized at the triple junctions and along the grain boundaries, contributing to understanding the high-entropy behavior within the B_4C matrix. HEA is observed as mainly filling pores or smaller grains, due to natural liquid-phase behavior, that tend to occupy configurations with the lowest energy [43]. The theoretical density of all samples increases with the HEA content: monolithic B_4C (2.52 g/cm^3), B4C.05 (2.55 g/cm^3), B4C.1 (2.58 g/cm^3), B4C.2 (2.64 g/cm^3) and B4C.3 (2.71 g/cm^3). The measured density also increases as the HEA content of the samples increases: monolithic B_4C (2.43 g/cm^3), B4C.05 (2.49 g/cm^3), B4C.1 (2.54 g/cm^3), B4C.2 (2.61 g/cm^3) and B4C.3 (2.66 g/cm^3). Finally, the porosity was measured: monolithic B_4C (3.57%), B4C.05 (2.42%), B4C.1 (1.42%), B4C.2 (0.78%) and B4C.3 (1.95%).

3.2. Electrochemical Tests

3.2.1. Corrosion Potential

The voltage at which the cathodic current density transitions to anodic when a metal is submerged in a solution, artificial sea water in this case, is called corrosion potential. The variation in corrosion potential over time provides a reliable indicator of the corrosion behavior, where oxidation and reduction reactions take place at equal rates on the samples surface [44].

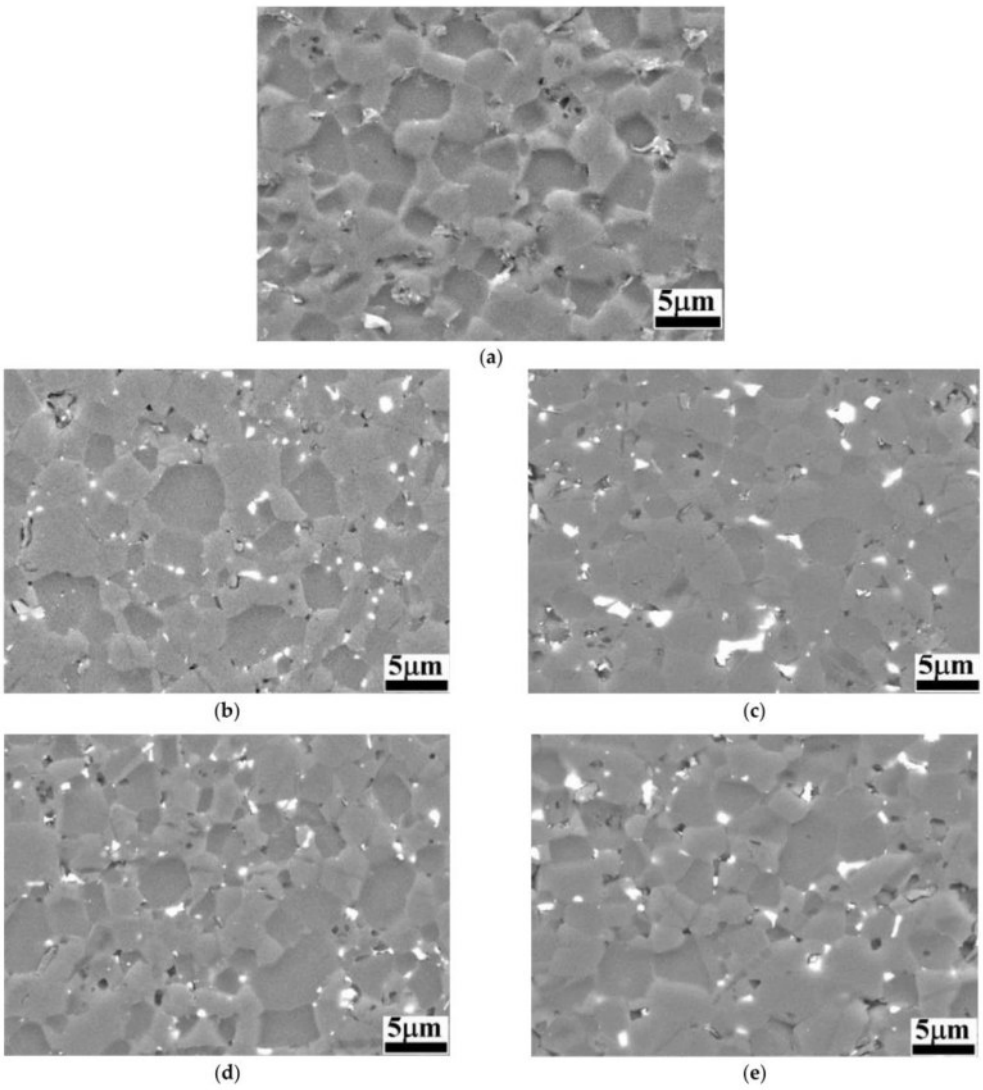

Figure 2. BSE-SEM images of B_4C and B_4C-doped composites: (**a**) monolithic B_4C; (**b**) B4C.05; (**c**) B4C.1; (**d**) B4C.2; (**e**) B4C.3.

Figure 3 presents a clear tendency towards higher corrosion potential as the HEA volume percentage increases. The B4C.05 sample shows a remarkable drop close to 5 h of immersion, which indicates a surface activation during exposure to 3.5% NaCl solution; however, after 13 h of immersion its corrosion potential began to increase, inherent to the creation of a passive film on the outer layers of the composite, suggesting that it becomes thermodynamically stable under a marine environment. Sample B4C.1, at close to 8 h of immersion, shows another potential drop, followed by a slight tendency to a potential decrease. Sample B4C.3's corrosion potential first decreased but rapidly increased, just like sample B4C.2's corrosion potential; however, during exposure, B4C.3's corrosion potential shows a clear positive tendency.

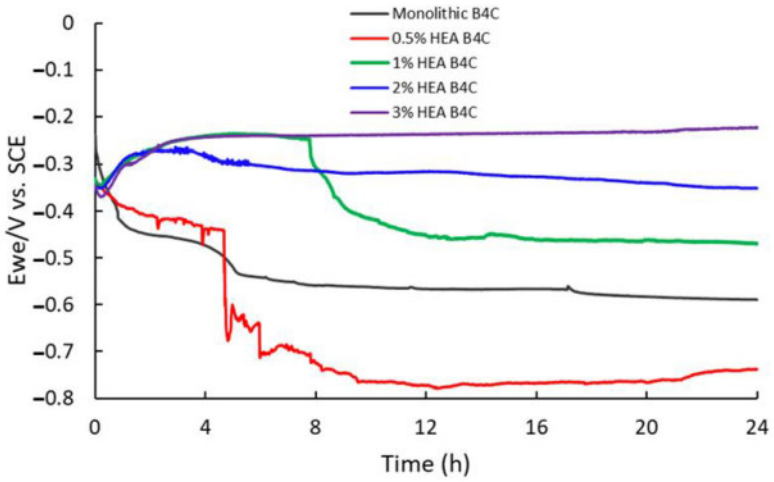

Figure 3. Comparison of corrosion potentials vs. time for 24 h of immersion in 3.5% NaCl solution of studied samples.

3.2.2. Corrosion Rate

The corrosion rate procedure offers insight into the effect of the environment on a material and can be determined through linear polarization curves, which relate potential to current. Figure 4 illustrates the linear polarization test performed to measure the corrosion rate of the composites immersed in artificial seawater, represented on a semi-logarithmic scale of current values.

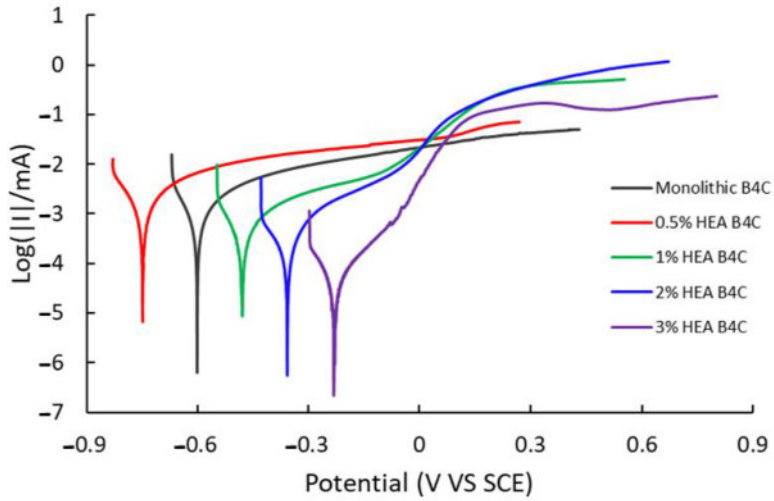

Figure 4. Polarization curve of studied samples in 3.5% NaCl solution.

The 0.5% HEA B_4C sample shows the most negative corrosion potential (E_{corr}) and the highest corrosion current (I_{corr}) of all the composites under study, as can be seen in Table 1. It was observed to be oxidized the most among all samples. To obtain the corrosion rate, first, the Tafel slopes (βc and βa), equivalent weight, density and surface were calculated.

Table 1. Corrosion parameters for all samples tested.

Parameters	Monolithic B4C	0.5% HEA B4C	1% HEA B4C	2% HEA B4C	3% HEA B4C
E_{corr} (mV vs. Ref)	−600.665	−749.920	−478.421	−357.533	−230.693
I_{corr} (μA/cm^2)	0.296	0.834	0.161	0.111	0.041
β_c (mV)	49.7	84.2	55.9	77.0	91.1
β_a (mV)	65.6	108.4	66.3	60.3	125.2
Equivalent weight (g/eq)	3.946	3.963	3.980	4.014	4.049
Measured density (g/cm^3)	2.43 ± 0.02	2.49 ± 0.01	2.54 ± 0.01	2.61 ± 0.02	2.66 ± 0.02
Surface (cm^2)	0.996	1.035	0.843	0.935	0.898
Corrosion rate (mpy)	62.158×10^{-3}	165.183×10^{-3}	38.544×10^{-3}	23.516×10^{-3}	8.951×10^{-3}

As the HEA content of composites increases, their corrosion rate decreases, indicating a higher corrosion resistance. Of all samples, B4C.3 presented the lowest corrosion potential, corrosion current and corrosion rate values, confirming that increasing the HEA content implies better performance regarding corrosion resistance. All four of the samples in our study tend to passivate, probably due to the creation of a passive film on their surface.

3.2.3. Electrochemical Impedance Spectroscopy (EIS)

EIS is an advanced method, being highly effective and accurate for analyzing interfacial properties associated with surface processes in metallic alloys. Unlike other electrochemical techniques, EIS offers significant advantages, such as operating under steady-state conditions, efficiently measuring small signals and covering a broad frequency range from 100 mHz up to 100 kHz.

Electrochemical impedance spectroscopy results of the different composites are presented as Bode-phase impedance plots, recorded at a consistent potential in a 3.5% NaCl solution. Due to the high number of samples under study, the Bode impedance plot is presented in Figure 5 and the Bode-phase plot in Figure 6; this way, the conducted test can be interpreted easier.

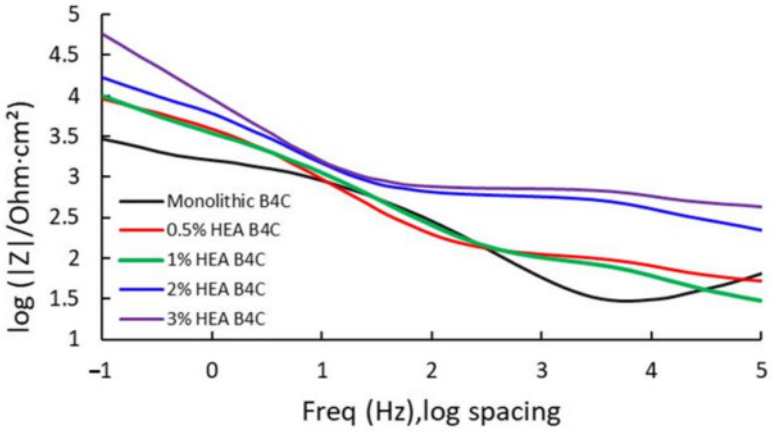

Figure 5. Bode impedance for the studied samples at Ecorr after 24 h of immersion in 3.5% NaCl solution.

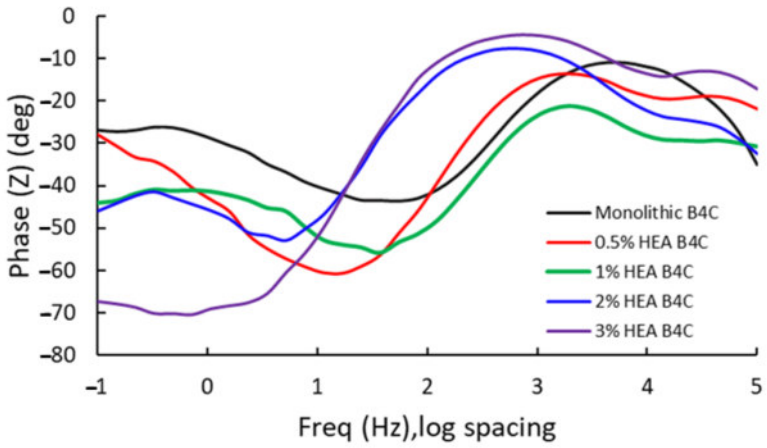

Figure 6. Bode phase for the studied samples at E_{corr} after 24 h of immersion in 3.5% NaCl solution.

In Figure 5, it is observed that the highest measure of impedance is attributed to B4C.3, which registered a value of 60.047 kΩ. This indicates that the 3% HEA composite has higher corrosion resistance as result of its capacity to oppose electric current. This is followed by B4C.2, presenting a similar result as obtained for the corrosion potential, as when the HEA volume percentage increases in the sample composition, the higher its corrosion resistance behavior. B4C.05 and B4C.1 presented similar results, indicating a very similar behavior.

The data obtained from the EIS measurements of B_4C composites demonstrated a very high resistance to corrosion in artificial seawater, especially B4C.3. On the other hand, Bode-phase analysis of B_4C-reinforced samples reveals significant differences in their electrochemical behaviors across frequency ranges (see Figure 7).

At low frequencies, the B4C.3 sample shows the most negative phase angle (−75°), which indicates a strong capacitive behavior and a strong passive layer. The B4C.05 sample shows a lower phase shift (~−30°), which implies a higher charge transfer rate and lower capacitive response. These results suggest that lower HEA concentrations lead to a thinner or less effective passive layer.

At medium frequencies, all the samples transition towards a mix between capacitive and resistive response. The 3% HEA B_4C sample maintains the highest phase shift. This indicates superior electrochemical stability, which matches the corrosion potential and corrosion rate test results.

At high frequencies, it can be seen how all composites converge towards lower phase angles (~−10° to −30°), dominated by electrolyte resistance. The B4C.3 sample consistently demonstrates the best capacitive properties, implying improved corrosion resistance. On the other hand, the 0.5% and 1% B_4C samples show the weakest capacitive response. This suggests that lower HEA concentrations result in a less effective passive layer. The intermediate behavior of the 2% B_4C sample implies a balance between resistive and capacitive contributions.

The Nyquist diagram reveals, for every sample, three remarkable zones, as seen in Figure 7. High and medium frequencies are described with semicircles, and low frequencies are defined by a straight line, which indicates Warburg element appearance. This indicates that the corrosion mechanism of the samples is changing, from charge transfer to diffusion, with the B4C.3 sample exhibiting the most pronounced Warburg impedance [45,46]. The overall trend indicates that increasing the HEA content enhances resistance behavior. This can be explained potentially due to agglomeration effects or altered charge

transport mechanisms. This must be considered when optimizing these materials for electrochemical applications.

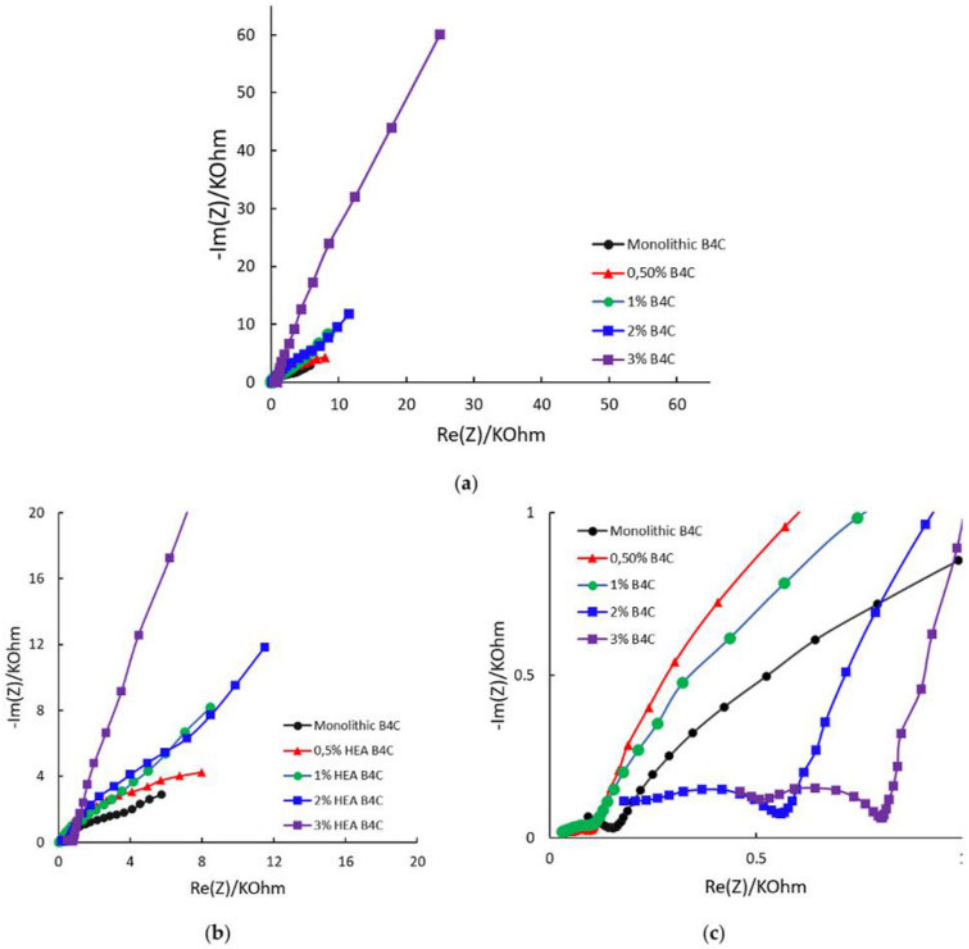

Figure 7. Nyquist diagrams for the studied samples at E_{corr} after 24 h of immersion in 3.5% NaCl solution: (**a**) complete plot; (**b**) detail at medium frequencies; (**c**) detail at low frequencies.

A more vertical line in the low-frequency region suggests that the system behaves more like an ideal capacitor. This behavior may be associated with the formation of protective layers or barriers that restrict corrosion, confirming that of all composites, B4C.3 has the highest resistance to corrosion under the studied situation.

The experimental EIS data were analyzed using an electrical equivalent-circuit model, and ZSimpWin 3.6 software (Informer Technologies, Los Angeles, CA, USA) was used to accurately represent the impedance response. The equivalent-circuit model that provided the best fit for all studied samples can be seen in Figure 8. A chi-square (χ^2) parameter close to 10^{-4} suggests a highly accurate fit between experimental and simulated data.

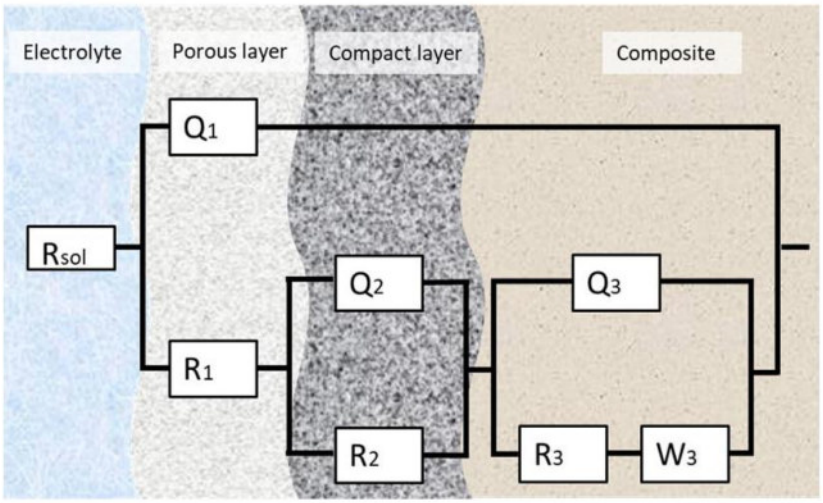

Figure 8. The equivalent circuit for the fitting of the EIS data.

In contexts where the passivated surface is considered, the letter "Q" stands for a Constant Phase Element (CPE). When it comes to the diffusion of ions or electrons in solids or liquids, the "W" stands for the Warburg element.

This configuration suggests that before reaching the alloy film, the outer layers of the samples offer resistance to dissolution, characterized by a dual-layer passive structure, consisting of both porous and compact regions. After applying Kirchhoff's circuit laws to the circuit and replacing the CPE and Warburg element, we obtained the following equation:

$$Z_{circuit} = R_{sol} + \frac{A \cdot \left[R_1 + \frac{R_2 \cdot B}{R_2 + B} + \frac{(R_3 + C) \cdot D}{(R_3 + C) + D}\right]}{A + R_1 + \frac{R_2 \cdot B}{R_2 + B} + \frac{(R_3 + C) \cdot D}{(R_3 + C) + D}} \quad (1)$$

where the letters "*A*", "*B*", "*C*" and "*D*" stand for

$$A = \frac{1}{Y_1 (jw)^{n_1}} \quad (2)$$

$$B = \frac{1}{Y_2 (jw)^{n_2}} \quad (3)$$

$$C = \frac{1}{Y_W (jw)^{0.5}} \quad (4)$$

$$D = \frac{1}{Y_3 (jw)^{n_3}} \quad (5)$$

The equivalent-circuit parameters for all samples can be seen in Table 2.

This study evaluates the electrochemical behavior of the composites under study, which suggests the appearance of a two-layer passive film. First, a porous outer layer, and secondly, a more compact inner layer, both play a role in the corrosion resistance of the samples.

Table 2. R(Q(R(QR)Q(RW))) equivalent-circuit parameters for all B_4C-doped samples under study.

Parameters	Monolithic B4C	0.5% HEA B4C	1% HEA B4C	2% HEA B4C	3% HEA B4C
Y_1 ($S{\cdot}s^n/cm^2$)	4.472×10^{-8}	5.218×10^{-5}	4.927×10^{-5}	8.268×10^{-9}	1.001×10^{-8}
n1	0.876	0.460	0.516	0.940	0.856
R_1 ($ohm{\cdot}cm^2$)	147.3	120.4	115.1	226.9	378.6
Y_2 ($S{\cdot}s^n/cm^2$)	2.302×10^{-14}	1.200×10^{-4}	2.617×10^{-5}	5.700×10^{-7}	1.226×10^{-7}
n2	0.999	0.772	0.968	0.797	0.968
R_2 ($ohm{\cdot}cm^2$)	2.635×10^{-3}	13.910	1.398	317.2	209.8
Y_3 ($S{\cdot}s^n/cm^2$)	3.284×10^{-5}	1.972×10^{-5}	8.002×10^{-6}	2.118×10^{-5}	2.061×10^{-5}
n3	0.8	0.948	0.987	0.889	0.894
R_3 ($ohm{\cdot}cm^2$)	3.397	7.797	204.2	4.918	6.363
Y_W ($S{\cdot}s^5/cm^2$)	2.916×10^{-4}	1.179×10^{-3}	1.095×10^{-4}	8.396×10^{-5}	8.952×10^{-6}
Chi-square	9.92×10^{-4}	7.75×10^{-4}	7.02×10^{-4}	5.18×10^{-4}	1.22×10^{-4}

In the first place, protective and corrosive processes are facilitated by the porous layer, which controls the diffusion of ions and oxygen. Its porosity, thickness and roughness play an important role in chloride ion penetration, which directly affects the compact layer.

Finally, the compact layer works as the primary corrosion barrier. It ensures surface passivation by limiting ion and electron transport. Its stability is crucial for long-term protection, as degradation may lead to localized corrosion. Metal ion migration (e.g., Fe^{2+} or Cr^{3+}) and oxygen diffusion contribute to passivity maintenance by the formation of protective oxides.

The EIS analysis confirms the existence of multiple corrosion layers. The appearance of the Warburg element on both Nyquist diagrams and the equivalent circuit indicates that the corrosion process is controlled by diffusion. This implies the creation of a protective film that helps with the passivation of the alloy.

3.3. Microhardness

The aggregation of HEA phases at grain junctions, frequently observed in earlier B_4C composite microhardness studies, was responsible for the identification of a porous microstructure and various fissures on the SEM images, primarily along the grain borders [47–49]. This suggested the need to perform a microhardness statistical analysis.

In order to perform this analysis, a fixed load of 19.61 N was applied on numerous occasions along different regions of the surface of all studied samples. With the use of a diamond point pyramidal indenter (136° edge angle), an indentation was developed after applying a vertical load for 15 s. The hardness of all studied samples as a relation between the applied load and the indentation mark was determined using the Vickers method.

Table 3 provides a summary of the findings of all studied samples, accompanied by different visual representations (boxplots, histograms and normal distribution curves) to provide a comprehensive comparison of hardness values across the different composites.

In the analysis of the statistical values, it can be seen how 2% and 3% HEA samples exhibit the greatest hardness values, which confirms that HEA doping positively influences the hardness of B_4C ceramics. Lower HEA concentrations (0.5% and 1%) showed lower hardness values. This relation can be explained with the microstructure analysis seen in the SEM images, where the porosity of the lower HEA concentration composites was not completely filled, leading to an incomplete phase integration with the ceramic matrix and microstructural inconsistencies.

Table 3. Statistical parameters of Vickers hardness measurements for B_4C composites and monolithic B_4C sample.

Statistical Parameters	Hardness (HV_2)				
	B_4C monolithic	B_4C 0.5% HEA	B_4C 1% HEA	B_4C 2% HEA	B_4C 3% HEA
Mean	2966.67	3079.52	3016.71	3268.00	3308.57
Median	2990.00	3073.00	3011.00	3288.00	3319.00
Standard deviation	181.09	296.82	211.32	225.16	258.80
Minimum	2621.00	2432.00	2568.00	2799.00	2737.00
Maximum	3381.00	3862.00	3550.00	3859.00	3813.00
Quartile 25	2812.00	2876.00	2913.00	3112.00	3182.00
Quartile 50	2990.00	3073.00	3011.00	3288.00	3319.00
Quartile 75	3074.00	3288.75	3100.00	3405.00	3514.00

The histogram provides a visual representation of the frequency distribution of Vickers hardness values for each B_4C sample under study. This allows for an easy and intuitive comparison of the hardness variations among different compositions. By analyzing the histograms, it is possible to identify the spread, central tendency and asymmetries of the hardness distributions among HEA additions (see Figure 9).

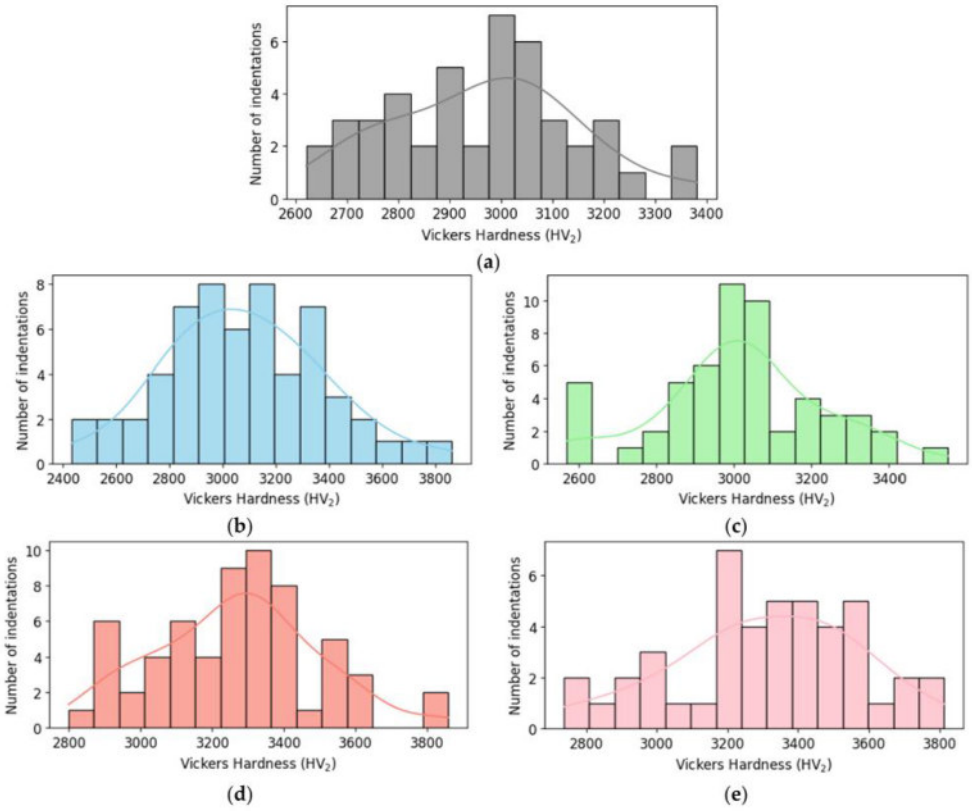

Figure 9. Histogram of Vickers hardness for (**a**) monolithic B_4C; (**b**) B4C.05; (**c**) B4C.1; (**d**) B4C.2; and (**e**) B4C.3.

Histograms charts reveal how the addition of HEA affects the hardness distribution. They show the hardness values of all indentations classified into different ranges. Composites with high HEA doping show higher hardness measures and smaller spread, suggesting a more homogenous hardness profile. The 0.5% HEA composite shows lower hardness measures and a wider distribution, which indicates greater variability.

In addition, box plots and normal distribution graphs of the Vickers hardness values obtained (see Figure 10) were generated in order to complete the statistical analysis. Information about the mechanical behavior of all composites and the impact of varying doping concentrations is obtained.

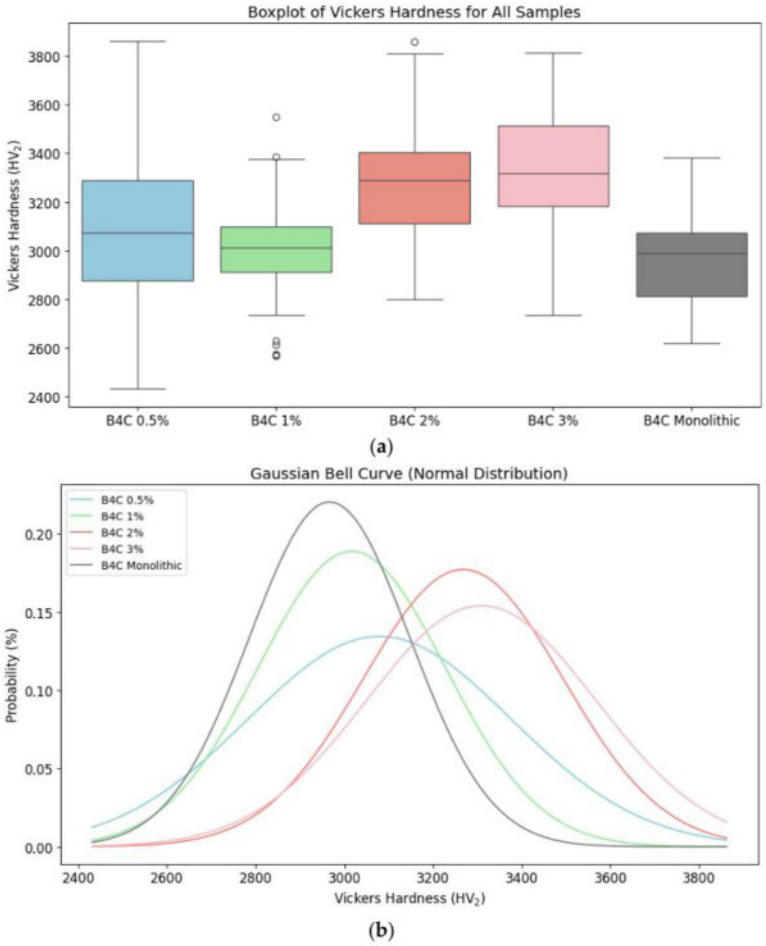

Figure 10. Vickers hardness for B_4C composites and monolithic sample comparison: (**a**) distribution of Vickers hardness data through its quartiles; (**b**) probability distribution of the hardness values.

The analysis of quartiles and Gaussian curves demonstrates that the 1% and 2% of HEA samples have a more consistent and predictable hardness distribution. The 0.5% HEA concentration composite possesses a wider spread and more variability, indicating continuous microstructural modifications. On the other hand, the B4C.2 sample has less variability, confirming the SEM results. These results prove the idea that HEA doping

improves the B_4C ceramic's mechanical performance, with the greatest results shown for higher HEA concentrations.

4. Conclusions

Focusing on the electrochemical and mechanical performances of B_4C ceramics doped with varying concentrations (0.5%, 1%, 2% and 3%) of CoCrFeNiMo HEA, the principal findings are described as follows:

- When CoCrFeNiMo high-entropy alloy is added to the B_4C ceramic matrix, a denser structure is obtained. A more refined grain structure was obtained because of this doping procedure. HEA addition leads to a more compact configuration and the inhibition of grain expansion in comparison to monolithic B_4C, resulting in notable microstructure alterations. Of all the samples studied, the smaller average grain size and the denser configuration were achieved in the 2% HEA concentration sample.
- Electrochemical tests revealed that corrosion resistance improved progressively with higher HEA content. The 3% HEA-doped B_4C demonstrates the highest resistance in artificial seawater conditions. The enhanced performance is attributed to the formation of a more compact and protective passive layer, effectively mitigating material corrosion.
- The statistical microhardness analysis of all composites revealed that even though every sample followed a normal distribution (suggesting a homogeneous structure), the 0.5% and 3% HEA concentrations had a less uniform and predictable hardness distribution, which suggests ongoing microstructural adjustments. The Vickers hardness of the B4C-doped composites were higher as the HEA percentage increased, indicating a strict relation between doping and hardness.

All the tests carried out clearly determine that increasing the HEA content implies better performance regarding corrosion resistance and mechanical properties. The 3% HEA B_4C composite exhibited the best results across all different tests, while the 0.5% HEA B_4C sample showed the poorest performance. The study finally determines the potential of CoCrFeNiMo HEA-doped B_4C ceramics for applications that involve mechanical strength and corrosion resistance. It highlights the outstanding behavior of all composites in aggressive environments, especially the 3% HEA-doped composite.

Author Contributions: Conceptualization A.D.R.-C.; methodology, A.D.R.-C.; software, A.D.R.-C.; validation, J.C.M.-R. and G.G.; formal analysis, A.D.R.-C. and B.C.O.; investigation, A.D.R.-C.; resources, J.C.M.-R. and G.G.; data curation, A.D.R.-C.; writing—original draft preparation, A.D.R.-C.; writing—review and editing, A.D.R.-C.; visualization, A.D.R.-C.; supervision, J.C.M.-R. and G.G. All authors have read and agreed to the published version of the manuscript.

Funding: This research was funded by European project 2023-1-RO01-KA220-HED-000159985: Smart Healthcare Engineering and Government of Gran Canaria project, with the reference PROID2024010003.

Institutional Review Board Statement: Not applicable.

Informed Consent Statement: Not applicable.

Data Availability Statement: The original contributions presented in this study are included in the article. Further inquiries can be directed to the corresponding author.

Acknowledgments: We hereby acknowledge the European project 2023-1-RO01-KA220-HED-000159985: Smart Healthcare Engineering and Government of Gran Canaria project, with the reference PROID2024010003.

Conflicts of Interest: The authors declare no conflicts of interest.

References

1. Yavas, B.; Sahin, F.; Yucel, O.; Goller, G. Effect of Particle Size, Heating Rate and CNT Addition on Densification, Microstructure and Mechanical Properties of B_4C Ceramics. *Ceram. Int.* **2015**, *41*, 8936–8944. [CrossRef]
2. Domnich, V.; Reynaud, S.; Haber, R.A.; Chhowalla, M. Boron Carbide: Structure, Properties, and Stability under Stress. *J. Am. Ceram. Soc.* **2011**, *94*, 3605–3628. [CrossRef]
3. Suri, A.K.; Subramanian, C.; Sonber, J.K.; Ch Murthy, T.S.R. Synthesis and Consolidation of Boron Carbide: A Review. *Int. Mater. Rev.* **2010**, *55*, 4–38. [CrossRef]
4. Pérez, S.; Tamayo, P.; Rico, J.; Alonso, J.; Thomas, C. Effect of Fibers and Boron Carbide on the Radiation Shielding Properties of Limestone and Magnetite Aggregate Concrete. *Prog. Nucl. Energy* **2024**, *175*, 105320. [CrossRef]
5. Tamayo, P.; Thomas, C.; Rico, J.; Pérez, S.; Mañanes, A. Radiation Shielding Properties of Siderurgical Aggregate Concrete. *Constr. Build. Mater.* **2022**, *319*, 126098. [CrossRef]
6. Zhang, W. A Review of Tribological Properties for Boron Carbide Ceramics. *Prog. Mater. Sci.* **2021**, *116*, 100718. [CrossRef]
7. Zorzi, J.E.; Perottoni, C.A.; Da Jornada, J.A.H. Hardness and Wear Resistance of B_4C Ceramics Prepared with Several Additives. *Mater. Lett.* **2005**, *59*, 2932–2935. [CrossRef]
8. Cantor, B.; Chang, I.T.H.; Knight, P.; Vincent, A.J.B. Microstructural Development in Equiatomic Multicomponent Alloys. *Mater. Sci. Eng.* **2004**, *375*, 213–218. [CrossRef]
9. Yeh, J.W. Recent Progress in High-Entropy Alloys. *Ann. Chim. Sci. Mater.* **2006**, *31*, 633–648. [CrossRef]
10. Kozhakhmetov, Y.; Skakov, M.; Kurbanbekov, S.; Uazyrkhanova, G.; Kurmantayev, A.; Kizatov, A.; Mussakhan, N. High-Entropy Alloys: Innovative Materials with Unique Properties for Hydrogen Storage and Technologies for Their Production. *Metals* **2025**, *15*, 100. [CrossRef]
11. de Oliveira, T.G.; Fagundes, D.V.; Capellato, P.; Sachs, D.; da Silva, A.A.A.P. A Review of Biomaterials Based on High-Entropy Alloys. *Metals* **2022**, *12*, 1940. [CrossRef]
12. Castro, D.; Jaeger, P.; Baptista, A.C.; Oliveira, J.P. An Overview of High-entropy Alloys as Biomaterials. *Metals* **2021**, *11*, 648. [CrossRef]
13. Gawel, R.; Rogal, Ł.; Smoła, G.; Grzesik, Z. High-Temperature Oxidation and Diffusion Studies on Selected Al–Cr–Fe–Ni High-Entropy Alloys for Potential Application in Thermal Barrier Coatings. *Intermetallics* **2024**, *169*, 108273. [CrossRef]
14. Yang, H.; Shao, Z.; Lu, Q.; Cui, C.; Xu, L.; Yang, G. Development of Reduced-Activation and Radiation-Resistant High-Entropy Alloys for Fusion Reactor. *Int. J. Refract. Met. Hard Mater.* **2024**, *121*, 106674. [CrossRef]
15. Chakraborty, P.; Sarkar, A.; Ali, K.; Jha, J.; Jothilakshmi, N.; Arya, A.; Tewari, R. Design and Development of Low Density, High Strength ZrNbAlVTi High Entropy Alloy for High Temperature Applications. *Int. J. Refract. Met. Hard Mater.* **2023**, *113*, 106222. [CrossRef]
16. Xu, Z.Q.; Ma, Z.L.; Wang, M.; Chen, Y.W.; Tan, Y.D.; Cheng, X.W. Design of Novel Low-Density Refractory High Entropy Alloys for High-Temperature Applications. *Mater. Sci. Eng.* **2019**, *755*, 318–322. [CrossRef]
17. Nartita, R.; Ionita, D.; Demetrescu, I. A Modern Approach to HEAs: From Structure to Properties and Potential Applications. *Crystals* **2024**, *14*, 451. [CrossRef]
18. Naveen, L.; Umre, P.; Chakraborty, P.; Rahul, M.R.; Samal, S.; Tewari, R. Development of Single-Phase BCC Refractory High Entropy Alloys Using Machine Learning Techniques. *Comput. Mater. Sci.* **2024**, *238*, 112917. [CrossRef]
19. Wakai, E.; Noto, H.; Shibayama, T.; Furuya, K.; Ando, M.; Kamada, T.; Ishida, T.; Makimura, S. Microstructures and Hardness of BCC Phase Iron-Based High Entropy Alloy Fe-Mn-Cr-V-Al-C. *Mater. Charact.* **2024**, *211*, 113881. [CrossRef]
20. Li, C.; Ma, Z.; Tong, S.; Liu, J.; Zhang, W.; Shen, G.; Wang, S.; Zhao, H.; Ren, L. Mechanical-Thermal Coupling Fatigue Failure of CoCrFeMnNi High Entropy Alloy. *J. Mater. Res. Technol.* **2024**, *30*, 3430–3437. [CrossRef]
21. Matsuzaka, T.; Hyakubu, A.; Kim, Y.S.; Matsugaki, A.; Nagase, T.; Ishimoto, T.; Ozasa, R.; Kim, H.S.; Mizuguchi, T.; Gokcekaya, O.; et al. Development of an Equiatomic Octonary TiNbTaZrMoHfWCr Super-High-Entropy Alloy for Biomedical Applications. *Mater. Chem. Phys.* **2024**, *316*, 129120. [CrossRef]
22. Wu, Y.; Du, C.; Yu, Z.; Wang, R.; Ren, X. Effect of Cu Content on the Microstructure and Mechanical Properties of $Fe_{20}Co_{30}Ni_{10}Cr_{20}Mn_{20}$ FCC-Typed HEAs. *Mater. Sci. Eng.* **2024**, *897*, 146336. [CrossRef]
23. Yen, C.C.; Lin, S.Y.; Ting, C.L.; Tsai, T.L.; Chen, Y.T.; Yen, S.K. Passivation Mechanisms of $CoCrFeNiMo_x$ (x = 0, 0.1, 0.2, 0.3) High Entropy Alloys and MP35N in 3.5 Wt% NaCl Aerated Aqueous Solutions. *Corros. Sci.* **2024**, *228*, 111812. [CrossRef]
24. Dong, D.; Jiang, W.; Wang, X.; Ma, T.; Zhu, D.; Wang, Y.; Huo, J. Enhanced Mechanical Properties of High Pressure Solidified $CoCrFeNiMo_{0.3}$ High Entropy Alloy via Nano-Precipitated Phase. *Intermetallics* **2024**, *166*, 108192. [CrossRef]
25. Zin, V.; Montagner, F.; Miorin, E.; Mortalò, C.; Tinazzi, R.; Bolelli, G.; Lusvarghi, L.; Togni, A.; Frabboni, S.; Gazzadi, G.; et al. Effect of Mo Content on the Microstructure and Mechanical Properties of $CoCrFeNiMo_x$ HEA Coatings Deposited by High Power Impulse Magnetron Sputtering. *Surf. Coat. Technol.* **2024**, *476*, 130244. [CrossRef]
26. Guo, K.; Sun, Y.; Cheng, W.; Gu, J.; Chen, Y.; Zhang, S. Effect of Rare Earth La_2O_3 on the Microstructure and Corrosion Resistance of CoCrFeNiMoSi High Entropy Alloys. *Surf. Interfaces* **2024**, *44*, 103683. [CrossRef]

27. Brito-Garcia, S.; Mirza-Rosca, J.; Geanta, V.; Voiculescu, I. Mechanical and Corrosion Behavior of Zr-Doped High-Entropy Alloy from CoCrFeMoNi System. *Materials* **2023**, *16*, 1832. [CrossRef]
28. Semikolenov, A.; Shalnova, S.; Klinkov, V.; Andreeva, V.; Salynova, M.; Larionova, T.; Tolochko, O. Effect of al Content on Phase Compositions of FeNiCoCrMo$_{0.5}$Al$_x$High Entropy Alloy. *Metals* **2021**, *11*, 1734. [CrossRef]
29. Brito-García, S.; Jiménez-Marcos, C.; Mirza-Rosca, J.; Voiculescu, I. Behavior of Ti-Doped CoCrFeMoNi High Entropy Alloy. *Microsc. Microanal.* **2023**, *29*, 439–444. [CrossRef]
30. Li, Y.; Zhang, J.; Huang, X.; Liu, J.; Deng, L.; Han, P. Influence of Laser Power on Microstructure Evolution and Properties of Laser Cladded FeNiCoCrMo HEA Coatings. *Mater. Today Commun.* **2023**, *35*, 105615. [CrossRef]
31. Wu, H.; Zhang, S.; Wang, Z.Y.; Zhang, C.H.; Chen, H.T.; Chen, J. New Studies on Wear and Corrosion Behavior of Laser Cladding FeNiCoCrMo$_x$ High Entropy Alloy Coating: The Role of Mo. *Int. J. Refract. Metals. Hard. Mater.* **2022**, *102*, 105721. [CrossRef]
32. Wang, W.; Wang, J.; Sun, Z.; Li, J.; Li, L.; Song, X.; Wen, X.; Xie, L.; Yang, X. Effect of Mo and Aging Temperature on Corrosion Behavior of (CoCrFeNi)$_{100-X}$Mo$_x$ High-Entropy Alloys. *J. Alloys Compd* **2020**, *812*, 152139. [CrossRef]
33. Fu, Y.; Huang, C.; Du, C.; Li, J.; Dai, C.; Luo, H.; Liu, Z.; Li, X. Evolution in Microstructure, Wear, Corrosion, and Tribocorrosion Behavior of Mo-Containing High-Entropy Alloy Coatings Fabricated by Laser Cladding. *Corros. Sci.* **2021**, *191*, 109727. [CrossRef]
34. Dai, C.; Luo, H.; Li, J.; Du, C.; Liu, Z.; Yao, J. X-Ray Photoelectron Spectroscopy and Electrochemical Investigation of the Passive Behavior of High-Entropy FeCoCrNiMo$_x$ Alloys in Sulfuric Acid. *Appl. Surf. Sci.* **2020**, *499*, 143903. [CrossRef]
35. Wang, L.; Mercier, D.; Zanna, S.; Seyeux, A.; Laurent-Brocq, M.; Perrière, L.; Guillot, I.; Marcus, P. Study of the Surface Oxides and Corrosion Behaviour of an Equiatomic CoCrFeMnNi High Entropy Alloy by XPS and ToF-SIMS. *Corros. Sci.* **2020**, *167*, 108507. [CrossRef]
36. Rico-Cano, A.D.; Mirza-Rosca, J.C.; Ocak, B.C.; Goller, G. Corrosion Behavior and Microhardness of a New B_4C Ceramic Doped with 3% Volume High-Entropy Alloy in an Aggressive Environment. *Metals* **2025**, *15*, 79. [CrossRef]
37. Rico-Cano, A.D.; Mirza-Rosca, J.C.; Ocak, B.C.; Goller, G. Corrosion Behavior of New B_4C Ceramic Doped with High-Entropy Alloy in an Aggressive Environment. *Microsc. Microanal.* **2024**, *30*, ozae044.666. [CrossRef]
38. *ASTM E112-96*; Standard Test Methods for Determining Average Grain Size. ASTM International: West Conshohocken, PA, USA, 2004.
39. *ASTM G5-94*; Standard Reference Test Method for Making Potentiostatic and Potentiodynamic Anodic Polarization Measurements. ASTM: West Conshohocken, PA, USA, 2004.
40. *ASTM G5-87*; Recommended Practice for Making Potentiostatic and Potentiodynamic Polarization Measurements, Annual Book of Standards. ASTM International: West Conshohocken, PA, USA, 2002.
41. *ISO 16773-1-4:2016*; Electrochemical Impedance Spectroscopy (EIS) on Coated and Uncoated Metallic Specimens n.d. ISO: Geneva, Switzerland, 2016.
42. *ISO 14577-1:2015*; Metallic Materials—Instrumented Indentation Test for Hardness and Materials Parameters—Part 1: Test Method n.d. ISO: Geneva, Switzerland, 2015.
43. German, R.M.; Suri, P.; Park, S.J. Review: Liquid Phase Sintering. *J. Mater. Sci.* **2009**, *44*, 1–39. [CrossRef]
44. Wagner, C.; Traud, W. "On the Interpretation of Corrosion Processes through the Superposition of Electrochemical Partial Processes and on the Potential of Mixed Electrodes," with a Perspective by F. Mansfeld. *Corrosion* **2006**, *62*, 843.
45. Xu, M.; Zheng, Z.; Han, D.; Ma, R.; Du, A.; Fan, Y.; Zhao, X.; Cao, X. Improvement of Cracking Resistance of Hot-Dip Zn-Al-Mg Coatings by Heat Treatment. *Mater. Today Commun.* **2023**, *36*, 106521. [CrossRef]
46. Wang, J.; Han, D.; Qiao, Z.; Zheng, Z.; Ma, R.; Du, A.; Fan, Y.; Zhao, X.; Yu, H.; Cao, X. Study on the Microstructure and Corrosion Resistance of Hot-Dip Al-Zn-Si-XMg Coating. *Surf. Coat. Technol.* **2025**, *496*, 131654. [CrossRef]
47. Uzun, A.; Asikuzun, E.; Gokmen, U.; Cinici, H. Vickers Microhardness Studies on B_4C Reinforced/Unreinforced Foamable Aluminium Composites. *Trans. Indian Inst. Met.* **2018**, *71*, 327–337. [CrossRef]
48. Cramer, C.L.; Cakmak, E.; Unocic, K.A. Hardness Measurements and Interface Behavior of SiC-B_4C-Si Multiple Phase Particulate Composites Made with Melt Infiltration and Additive Manufacturing. *J. Compos. Sci.* **2023**, *7*, 172. [CrossRef]
49. Ma, H.; Liang, Y.; Fu, H. Effect of B_4C Addition on Microstructure and Wear Resistance of Laser Cladding NiCrBSi Coatings. *JOM* **2023**, *75*, 515–525. [CrossRef]

4

Documento de autoría

ULPGC Universidad de Las Palmas de Gran Canaria | Escuela de Doctorado

AUTORSHIP DOCUMENT FOR COMPENDIUM THESIS

The undersigned, as co-authors of the published paper entitled "Corrosion Behavior of New B4C Ceramic Doped with High-Entropy Alloy in an Aggressive Environment", published in Microscopy and Microanalysis on 24/07/2024:

- We recognize as main author to Mr. Alberto Daniel Rico Cano, with ID number 44727996B.
- We renounce to use this publication as main nucleus of other doctoral theses, without prejudice to the fact that said publications may be presented as complementary merits in the doctoral theses that the other authors of said publications may present.

Las Palmas de Gran Canaria on 30/04/2025

Gultekin Goller

Firma

Borak Cagri Ocak

Firma

MIRZA ROSCA JULIANA CLAUDIA - 45360672A

Firmado digitalmente por MIRZA ROSCA JULIANA CLAUDIA - 45360672A
Fecha: 2025.05.09 13:10:02 +01'00'

Julia Claudia Mirza Rosca

Firma

ULPGC Universidad de Las Palmas de Gran Canaria | Escuela de Doctorado

AUTORSHIP DOCUMENT FOR COMPENDIUM THESIS

The undersigned, as co-authors of the published paper entitled "Corrosion Behavior and Microhardness of a New B4C Ceramic Doped with 3% Volume High-Entropy Alloy in an Aggressive Environment", published in Metals on 17/01/2025:

- We recognize as main author to Mr. Alberto Daniel Rico Cano, with ID number 44727996B.
- We renounce to use this publication as main nucleus of other doctoral theses, without prejudice to the fact that said publications may be presented as complementary merits in the doctoral theses that the other authors of said publications may present.

Las Palmas de Gran Canaria on 30/04/2025

Gultekin Goller

Firma

Burak Cagri Ocak

Firma

MIRZA ROSCA JULIANA CLAUDIA - 45360672A

Firmado digitalmente por MIRZA ROSCA JULIANA CLAUDIA - 45360672A
Fecha: 2025.05.09 13:10:48 +01'00'

Julia Claudia Mirza Rosca

Firma

ULPGC Universidad de Las Palmas de Gran Canaria | Escuela de Doctorado

AUTORSHIP DOCUMENT FOR COMPENDIUM THESIS

The undersigned, as co-authors of the published paper entitled "Impact of CoCrFeNiMo High-Entropy-Alloy Doping on the Mechanical and Electrochemical Properties of B4C Ceramic", published in Applied Sciences on 25/04/2025:

- We recognize as main author to Mr. Alberto Daniel Rico Cano, with ID number 44727996B.
- We renounce to use this publication as main nucleus of other doctoral theses, without prejudice to the fact that said publications may be presented as complementary merits in the doctoral theses that the other authors of said publications may present.

Las Palmas de Gran Canaria on 30/04/2025

Gultekin Goller

Firma

Burak Cagri Ocak

Firma

MIRZA ROSCA JULIANA CLAUDIA - 45360672A

Firmado digitalmente por MIRZA ROSCA JULIANA CLAUDIA - 45360672A
Fecha: 2025.05.09 13:09:16 +01'00'

Julia Claudia Mirza Rosca

Firma

5

Otras publicaciones y eventos científicos

5. Otras publicaciones y eventos científicos

A continuación se listan, en cada uno de los apartados, el resto de los eventos científicos en los que he participado activamente para el correcto desarrollo de esta tesis doctoral, ya sea como autor o coautor. Se nombran por orden cronológico en cada uno de los distintos apartados.

5.1. Publicaciones aceptadas pendientes de publicarse

- Microscopy and Microanalysis - The Effect of Zn Addition on Bioabsorbable Mg Alloys
- Microscopy and Microanalysis - Comparison and Evaluation of the Corrosion Behavior of Two Innovative B_4C Samples Doped with 0.5% and 3% FeNiCoCrMo High-Entropy Alloy

5.2. Publicaciones en revistas sin índice de impacto

- IGSCONG'21 (online) - Microstructure and Corrosion Behavior of TiMoZrXSi Biomaterial Focused on Hip Prosthesis
- NTSA'21 (online) -
- DENTISTRY AND ORAL HEALTH'21 - Comparative study of different worldwide materials for prosthodontic restoration
- BRAMAT'24 - EIS study of HEA doped B_4C ceramic in artificial sea water

5.3. Participaciones en congresos (poster o presentación oral)

- IGSCONG'21 (online) - Microstructure and Corrosion Behavior of TiMoZrXSi Biomaterial Focused on Hip Prosthesis
- NTSA'21 (online) -
- DENTISTRY AND ORAL HEALTH'21 (online) - Comparative study of different worldwide materials for prosthodontic restoration
- M&M'24 - Corrosion Behavior of New B_4C Ceramic Doped with High-Entropy Alloy in an Aggressive Environment
- BRAMAT'24 - EIS study of HEA doped B_4C ceramic in artificial sea water

1 Comparison and Evaluation of the Corrosion Behavior of Two Innovative B₄C Samples Doped with 0.5% and 3% FeNiCoCrMo High-Entropy Alloy
Status: Complete - Submission locked for review (Submitted 02/18/2025, 6:02 AM)
Accepted: 04/07/2025, 10:12 PM

Preview Submission 1 | Resend Submission 1 Confirmation Email

2 The Effect of Zn Addition on Bioabsorbable Mg Alloys
Status: Complete - Submission locked for review (Submitted 02/18/2025, 7:40 AM)
Accepted: 04/07/2025, 10:12 PM

Preview Submission 2 | Resend Submission 2 Confirmation Email

Submission Title: The Effect of Zn Addition on Bioabsorbable Mg Alloys

SUBMISSION PREVIEW: THE EFFECT OF ZN ADDITION ON BIOABSORBABLE MG ALLOYS

The Effect of Zn Addition on Bioabsorbable Mg Alloys

Submission ID: **2063221**

Symposium Type: **Featured Syposium**

Requested Presentation Type: **Poster Presentation**

Submission Status: **Complete / Locked**

Author(s)

FS

Francisco Miguel Sanchez-Sosa

Position:
MSc student

Organization:
University of Las Palmas de Gran Canaria

Role:
Co-Author

AR

Alberto Daniel Rico-Cano

Position:
PhD Student

Organization:
University of Las Palmas de Gran Canaria

Role:
Presenting Author

JM

Julia Claudia Mirza-Rosca

Position:
University professor

Organization:
University of Las Palmas de Gran Canaria

Role:
Co-Author

VG

Victor Geanta

Position:
University professor

Organization:
Politehnica University of Bucharest

Role:
Co-Author

IV

Ionelia Voiculescu

Position:
University professor

Organization:
Politehnica University of Bucharest

Role:
Co-Author

Submission Details

Track & Symposium Selection

Cross-Disciplinary Symposia

Please select the symposium that you would like to be included in. :

C01 - Microscopy and Microanalysis of Interfaces and/or Interactions Among Organic and Inorganic Matter

Invited Submission

- No

More than 10 Authors?

- This session has 10 or fewer authors.

Have you submitted to an M&M conference in the past? If so, when?

Yes, in 2024.

Uploaded File(s)

Paper Upload for Published Proceedings

C01 - The Effect of Zn Addition on Bioabsorbable Mg Alloys.docx

Upload Figures (Image Files)

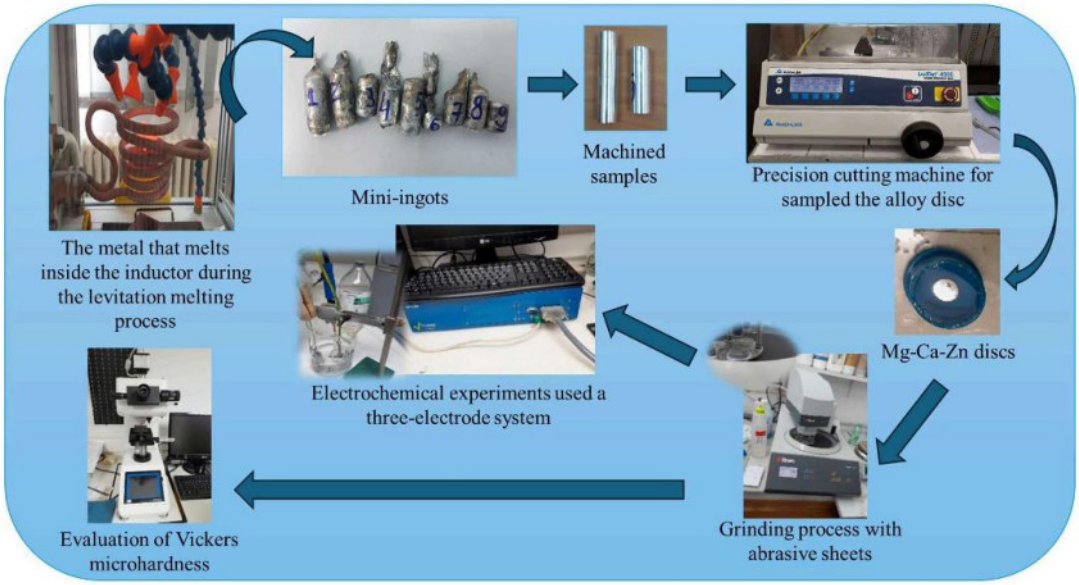

Fig. 1. Obtaining Mg-base alloys in levitation, samples' preparation and testing.

Figure 1.jpg

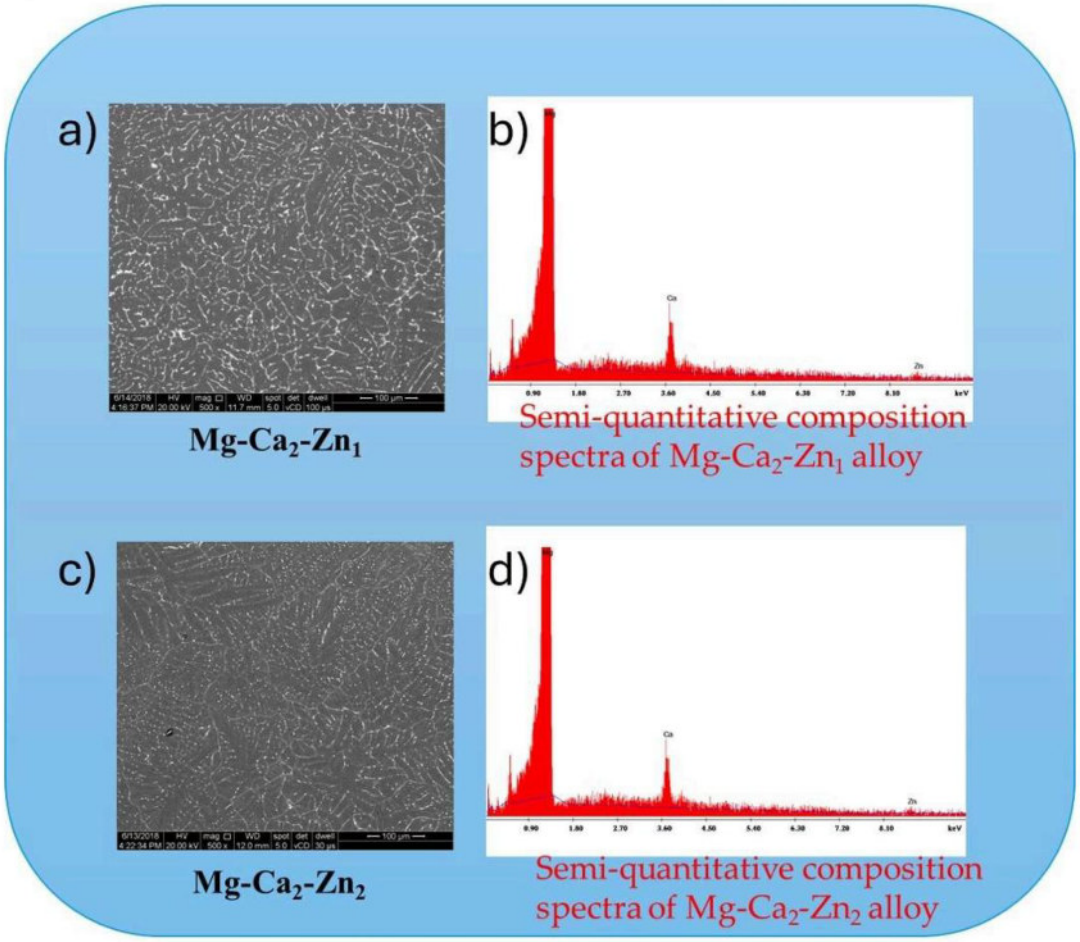

Fig. 2. SEM microstructure of Mg-Ca-Zn alloys.

Figure 2.jpg

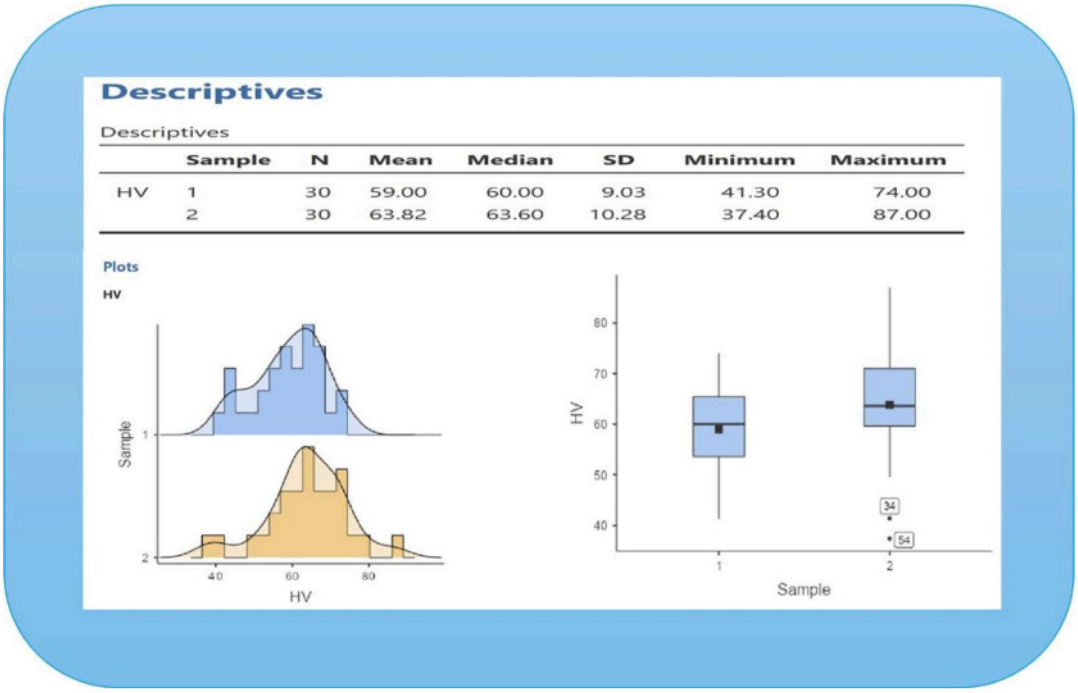

Fig. 3. Microhardness statistics.

Figure 3.jpg

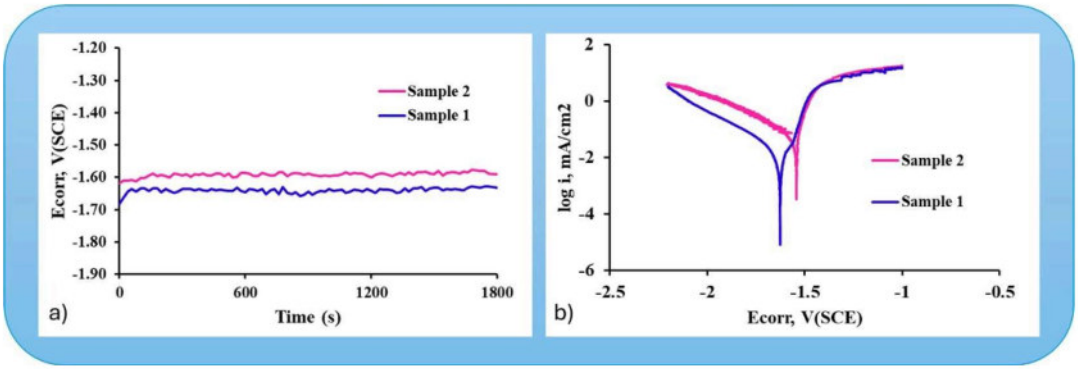

Fig. 4. Electrochemical testing of the samples.

Figure 4.jpg

License to Publish - Required for Paper Upload

I understand that should my submission/abstract be accepted to the M&M 2025 meeting, it will be published in the Microscopy & Microanalysis 2025 online Proceedings, published by Oxford University Press (OUP). No exceptions are permitted.
I understand and acknowledge.

I warrant to Microscopy Society of America and Oxford University Press that all of the following statements are true (if applicable to my work) about my submission:
I understand and acknowledge.

I warrant that this is my own original work and does not duplicate any previously published work, including my own.
I understand and acknowledge.

I warrant that this Contribution has not previously been published (in print or electronic format), and is not currently under consideration by another journal, or if it has already been submitted to any other publishers or journals, will be immediately withdrawn from them.
I understand and acknowledge.

I warrant that this Contribution will not be submitted for publication to any other journal following acceptance to the Microscopy & Microanalysis 2025 meeting (notification shall be given by April 2025). Oxford University Press will be the first publisher of this Work.
I understand and acknowledge.

I warrant that this Contribution contains nothing abusive, defamatory, libelous, obscene, fraudulent, or illegal.
I understand and acknowledge.

I warrant that I / all Authors have observed high ethical standards and obeyed publication best practices. I understand that the following are all unacceptable: data falsification or fabrication; plagiarism, including duplicate publication of your own work without proper citation; misappropriation of work.
I understand and acknowledge.

License to Publish
A) The copyright belongs to me or my employer (my employer is not Oxford University Press or Microscopy Society of America)

If your Contribution is in the public domain (U.S. Government Publication) or otherwise cannot be fully licensed as described above, please briefly indicate the reasons here:

If you selected "B" to Question 8 above, please write in the name of the person or entity that holds the current copyright.

M&M Meeting (Travel) Awards

I wish to apply for an Award Opportunity at M&M 2025.
No

Which Award Type do you wish to be considered for?

If you're applying for a student award, is a student the first author of this submission?

If you're applying for a student award, did a student produce the majority of work for this submission?

Does the submission contain two (2) figures?*

No, I am not applying for an award.

Please enter the first name of your advisor or supervisor.

Please enter the last name of your advisor or supervisor.

Please enter the email of your advisor or supervisor.

This presentation includes diamond-knife ultramicrotomy.

CIASEM M&M Travel Award
No

MAS Poster & Creative Canvas Awards

I wish to apply for an MAS Award Opportunity at M&M 2025.
No

Which Award Type do you wish to be considered for?

If you're applying for a student award, is a student the first author of this submission?

If you're applying for MAS Student Award, did a student produce the majority of work for this submission?

Please enter the first name of your advisor or supervisor.

Please enter the last name of your advisor or supervisor.

Please enter the email of your advisor or supervisor.

General Questions

At this time, I am (select one):
Student (undergraduate or graduate)

I understand that my submission must follow the format style shown in the M&M Abstract/Paper Example. If I do not follow this template, my submission may not be accepted.
I understand

I understand that if I requested a platform submission, it may be accepted as a poster presentation. (Not applicable to invited speakers.) All decisions made by Symposium Organizers are final.
I understand

I would like to receive more information about the Pre-Meeting Congress for Students, Post-docs, and Early-Career Professionals.
No

SUBMISSION PREVIEW: COMPARISON AND EVALUATION OF THE CORROSION BEHAVIOR OF TWO INNOVATIVE B₄C SAMPLES DOPED WITH 0.5% AND 3% FENICOCRMO HIGH-ENTROPY ALLOY

Comparison and Evaluation of the Corrosion Behavior of Two Innovative B₄C Samples Doped with 0.5% and 3% FeNiCoCrMo High-Entropy Alloy

Submission ID: **2063201**

Symposium Type: **Featured Syposium**

Requested Presentation Type: **Poster Presentation**

Submission Status: **Complete / Locked**

Author(s)

AR

Alberto Daniel Rico-Cano

Position:
PhD Student

Organization:
University of Las Palmas de Gran Canaria

Role:
Presenting Author

JM

Julia Claudia Mirza-Rosca

Position:
University professor

Organization:
University of Las Palmas de Gran Canaria

Role:
Co-Author

BO

Burak Cagri Ocak

Position:
University professor

Organization:
Istanbul Technical University

Role:
Co-Author

Submission Title: Comparison and Evaluation of the Corrosion Behavior of Two Innovative B₄C Samples Doped with 0.5% and 3% FeNiCoCrMo High-Entropy Alloy

GG

Gultekin Goller

Position:
University professor

Organization:
Istanbul Technical University

Role:
Co-Author

Submission Details

Track & Symposium Selection

Cross-Disciplinary Symposia

Please select the symposium that you would like to be included in. :

C03 - Microscopy and Microanalysis in Industry

Invited Submission

- No

More than 10 Authors?

- This session has 10 or fewer authors.

Have you submitted to an M&M conference in the past? If so, when?

Yes, in 2024

Uploaded File(s)

Paper Upload for Published Proceedings

C03 - Comparison and Evaluation of the Corrosion Behavior of Two Innovative B4C Samples Doped with 0.5% and 3% FeNiCoCrMo High-Entropy Alloy .docx

Upload Figures (Image Files)

Submission Title: Comparison and Evaluation of the Corrosion Behavior of Two Innovative B₄C Samples Doped with 0.5% and 3% FeNiCoCrMo High-Entropy Alloy

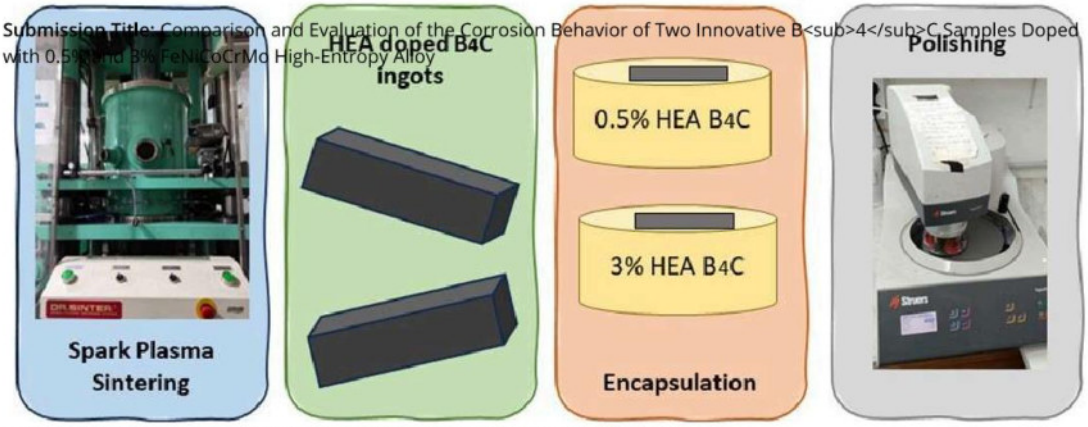

Fig. 1. Fabrication and preparation of the B4C samples under study.

Figure 1.jpg

Submission Title: Comparison and Evaluation of the Corrosion Behavior of Two Innovative B₄C Samples Doped with 0.5% and 3% FeNiCoCrMo High-Entropy Alloy

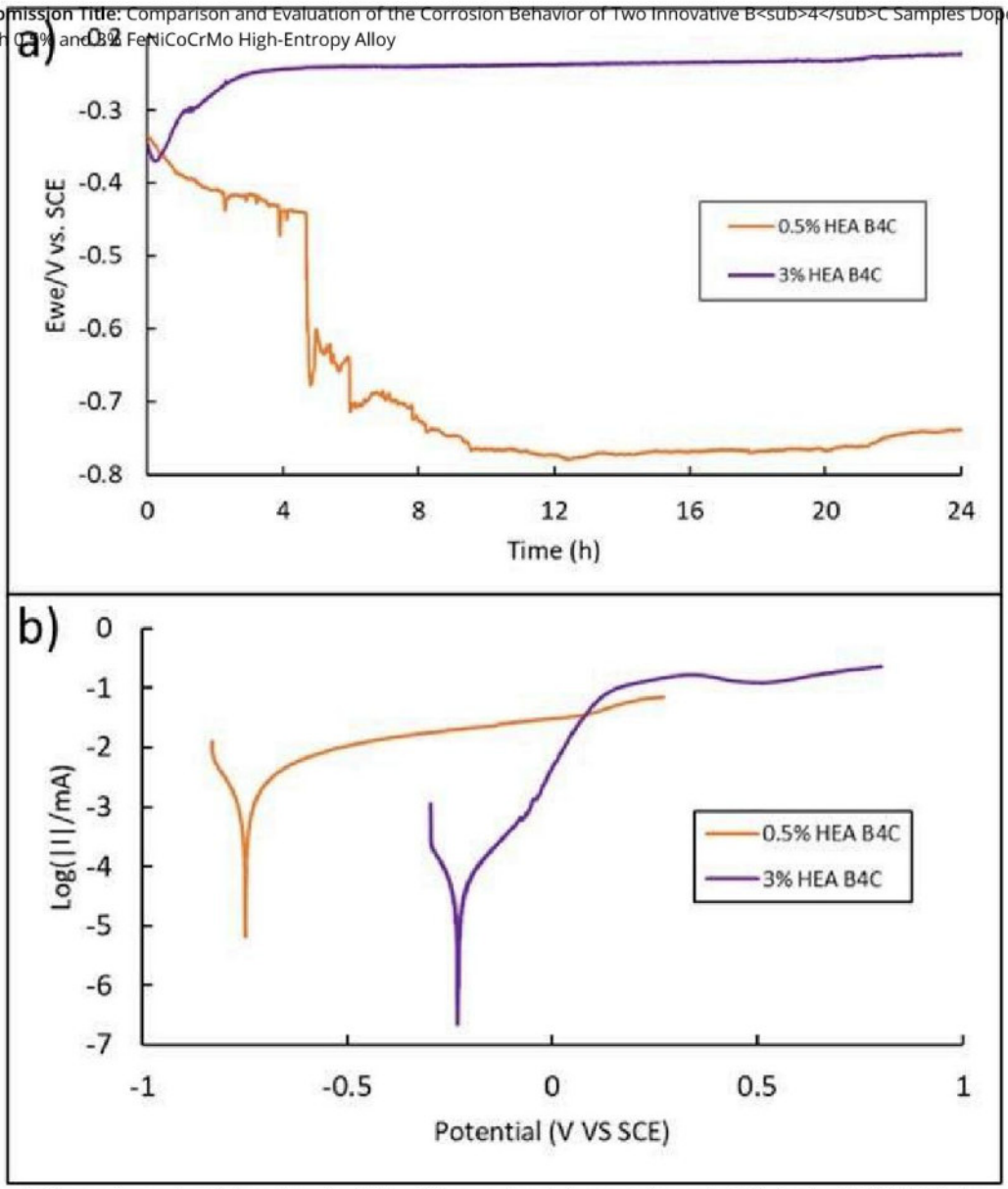

Fig. 2. Corrosion potential vs. time for 24 h of immersion (a)), corrosion rate (b)), for both B4C HEA-doped samples in 3.5% NaCl solution.

Figure 2.jpg

Submission Title: Comparison and Evaluation of the Corrosion Behavior of Two Innovative B₄C Samples Doped with 0.5% and 3% FeNiCoCrMo High-Entropy Alloy

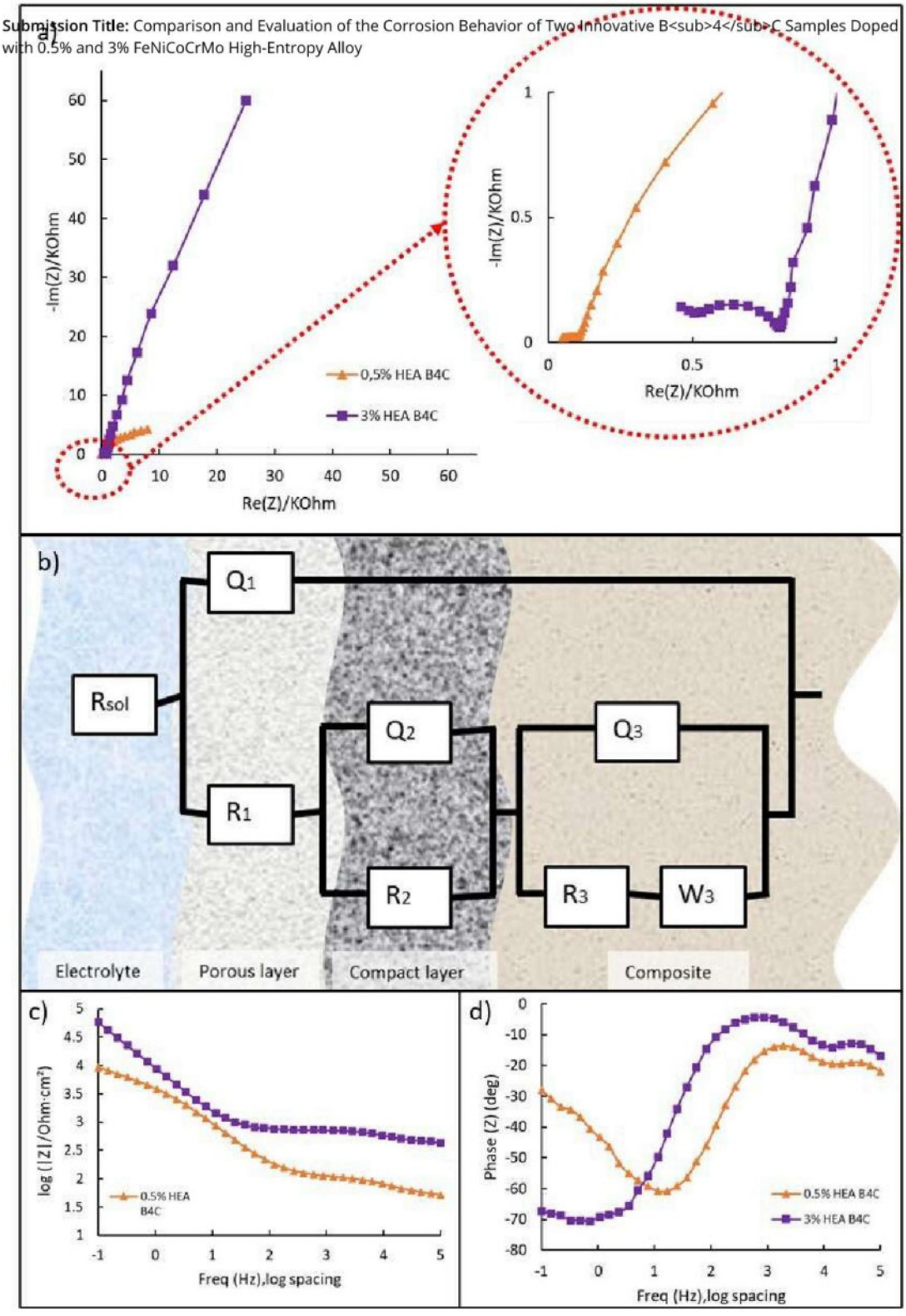

Fig. 3. Nyquist diagram (a)), equivalent electrical circuit applied (b)), Bode impedance diagram (c)), Bode phase diagram (d)), for doped samples, at Ecorr after 24 h of immersion in 3.5% NaCl solution.

Submission Title: Comparison and evaluation of the Corrosion Behavior of Two Innovative B₄C Samples Doped with 0.5% and 3% FeVNbCoCrMo High-Entropy Alloy

Figure 3.jpg

Submission Title: Comparison and Evaluation of the Corrosion Behavior of Two Innovative B₄C Samples Doped with 0.5% and 3% FeNiCoCrMo High-Entropy Alloy

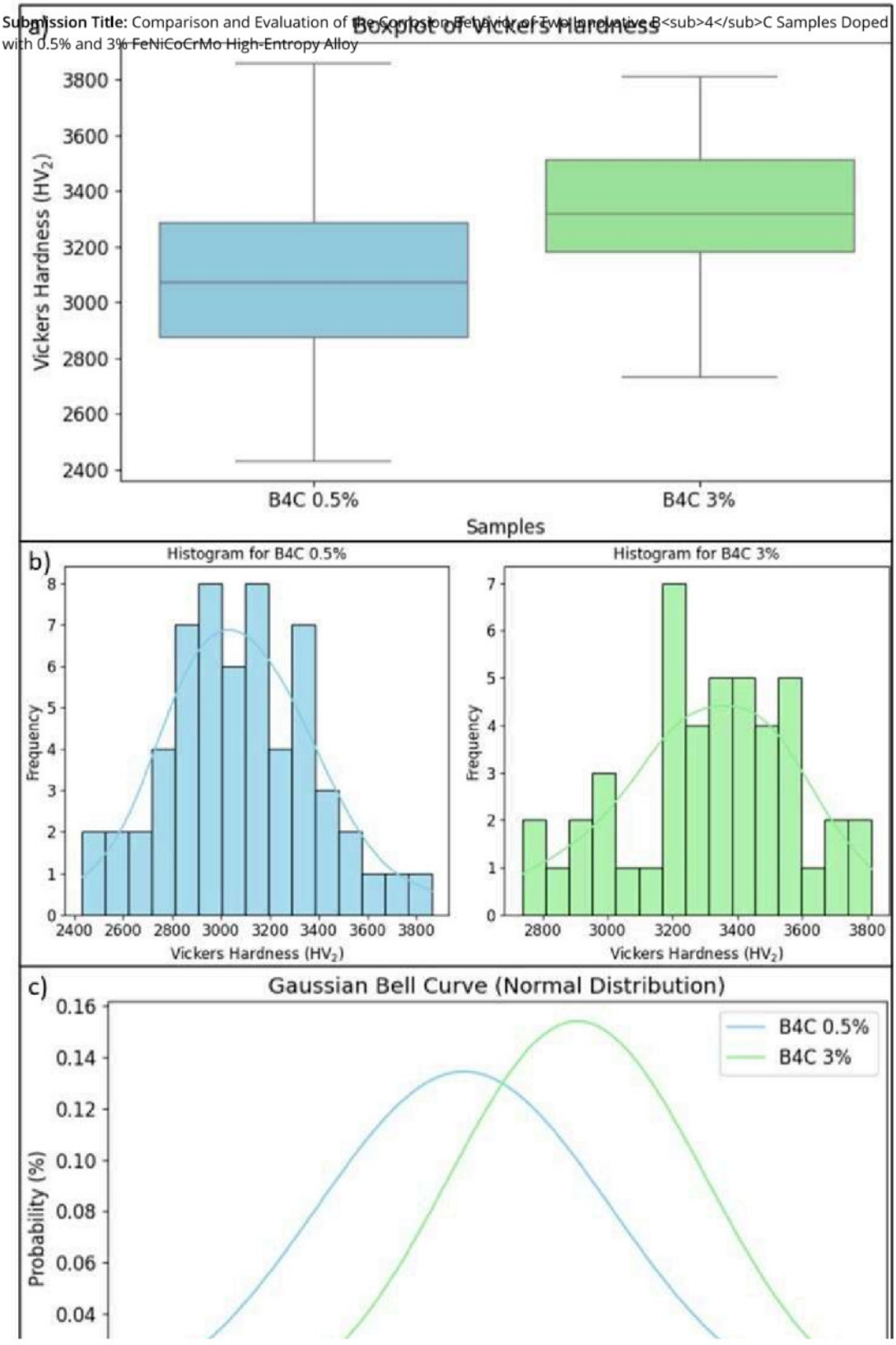

Submission Title: Comparison and Evaluation of the Corrosion Behavior of Two Innovative B₄C Samples Doped with 0.5% and 3% FeNiCoCrMo High-Entropy Alloy

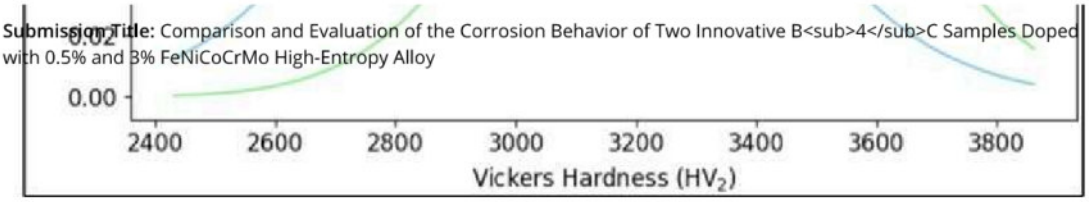

Fig. 4. Distribution of Vickers hardness data through its quartiles (a), frequency of Vickers hardness values within certain intervals (bins) (b)) probability distribution of the hardness values (c)), comparison for B4C doped samples.

Figure 4.jpg

License to Publish - Required for Paper Upload

I understand that should my submission/abstract be accepted to the M&M 2025 meeting, it will be published in the Microscopy & Microanalysis 2025 online Proceedings, published by Oxford University Press (OUP). No exceptions are permitted.
I understand and acknowledge.

I warrant to Microscopy Society of America and Oxford University Press that all of the following statements are true (if applicable to my work) about my submission:
I understand and acknowledge.

I warrant that this is my own original work and does not duplicate any previously published work, including my own.
I understand and acknowledge.

I warrant that this Contribution has not previously been published (in print or electronic format), and is not currently under consideration by another journal, or if it has already been submitted to any other publishers or journals, will be immediately withdrawn from them.
I understand and acknowledge.

I warrant that this Contribution will not be submitted for publication to any other journal following acceptance to the Microscopy & Microanalysis 2025 meeting (notification shall be given by April 2025). Oxford University Press will be the first publisher of this Work.
I understand and acknowledge.

I warrant that this Contribution contains nothing abusive, defamatory, libelous, obscene, fraudulent, or illegal.
I understand and acknowledge.

I warrant that I / all Authors have observed high ethical standards and obeyed publication best practices. I understand that the following are all unacceptable: data falsification or fabrication; plagiarism, including duplicate publication of your own work without proper citation; misappropriation of work.
I understand and acknowledge.

License to Publish
A) The copyright belongs to me or my employer (my employer is not Oxford University Press or Microscopy Society of America)

If your Contribution is in the public domain (U.S. Government Publication) or otherwise cannot be fully licensed as described above, please briefly indicate the reasons here:

If you selected "B" to Question 8 above, please write in the name of the person or entity that holds the current copyright.

Submission Title: Comparison and Evaluation of the Corrosion Behavior of Two Innovative B₄C Samples Doped with 0.5% and 5% FeNiCrCo High-Entropy Alloy

M&M Meeting (Travel) Awards

I wish to apply for an Award Opportunity at M&M 2025.
No

Which Award Type do you wish to be considered for?

If you're applying for a student award, is a student the first author of this submission?

If you're applying for a student award, did a student produce the majority of work for this submission?

Does the submission contain two (2) figures?*

No, I am not applying for an award.

Please enter the first name of your advisor or supervisor.

Please enter the last name of your advisor or supervisor.

Please enter the email of your advisor or supervisor.

This presentation includes diamond-knife ultramicrotomy.

CIASEM M&M Travel Award
No

MAS Poster & Creative Canvas Awards

I wish to apply for an MAS Award Opportunity at M&M 2025.
No

Which Award Type do you wish to be considered for?

If you're applying for a student award, is a student the first author of this submission?

If you're applying for MAS Student Award, did a student produce the majority of work for this submission?

Please enter the first name of your advisor or supervisor.

Please enter the last name of your advisor or supervisor.

Please enter the email of your advisor or supervisor.

General Questions

At this time, I am (select one):
Student (undergraduate or graduate)

Submission Title: Comparison and Evaluation of the Corrosion Behavior of Two Innovative B₄C Samples Doped with 0.5% and 3% FeNiCoCrMo High-Entropy Alloy

I understand that my submission must follow the format style shown in the M&M Abstract/Paper Example. If I do not follow this template, my submission may not be accepted.
I understand

I understand that if I requested a platform submission, it may be accepted as a poster presentation. (Not applicable to invited speakers.) All decisions made by Symposium Organizers are final.
I understand

I would like to receive more information about the Pre-Meeting Congress for Students, Post-docs, and Early-Career Professionals.
No

Uluslararası Lisansüstü Çalışmalar Kongresi

International Graduate Studies Congress

17-20 Haziran/June

2021

IGSCONG`21

Bildiri Kitabı

Proceedings Book

ISBN: 978-605-68187-0-7

IGSCONG'21

IGSCONG'21, 17-20 June 2021

Microstructure and Corrosion Behavior of TiMoZrXSi Biomaterial Focused on Hip Prosthesis

C. Jiménez-Marcos[1], A.D. Rico-Cano[1], N.R. Florido-Suárez[1], J.C. Mirza-Rosca[1*], P. Vizureanu[2]

[*]: julia.mirza@ulpgc.es, ORCID: 0000-0003-0623-3318

[1]: *Department of Mechanical Engineering, University of Las Palmas de Gran Canaria, Las Palmas de Gran Canaria, Spain*

[2]: *Department of Technologies and Equipment for Materials Processing, "Gheorghe Asachi" Technical University of Iasi, Iasi, Romania*

ABSTRACT

Introduction

Biomaterials are designed to act with biological systems by evaluating, treating or replacing some tissue, organ or body function. Since the hip supports 9 to 12 times a person's weight, hip prostheses need to be made mainly of metallic materials.

Currently, the most used metallic material for orthopedic applications is titanium with the respective alloys given which provide better properties. Titanium alloys are classified into alpha, alpha-beta and beta alloys which depend on the predominant alpha and beta phases in the microstructure at room temperature [1]. Nonetheless, the alloy Ti6Al4V presents certain difficulties since aluminum can cause, in high concentrations, dementia or problems to the central nervous system in addition to vanadium which is a toxic element and can produce adverse effects on tissues [2].

Purpose

A study of two samples with different percentage composition, T1 (73 Ti, 20 Mo, 7 Zr, 0 Si percentage) and T2 (72 Ti, 20 Mo, 7 Zr, 1 Si percentage), produced by a Vacuum Arc Remelting (VAR) method, is developed to evaluate the potential biomedical applications of these alloys focusing on hip replacement.

Experimental

As a previous step to electrochemical and metallographic tests, several processes should be performed, such as to embed into an epoxy resin cylinder the samples for cutting and their subsequent polishing in two stages: polishing with SiC abrasive papers of progressive grain size from 280 to 1200 grit and final polishing with 0.1 micrometer alpha alumina suspension.

However, the metallographic test is carried out for two different types of grit emery paper, P800 and P1200. In both tests, the samples must have a mirror finish polished. Once the samples are prepared, images are taken by utilizing the metallographic microscope, 10 and 20 times amplification of the actual size of a part of the samples. Then, these samples are submerged from 15 to 35 seconds, in a dissolution of a reactive agent called Kroll (water, hydrofluoric acid, nitric acid) and they are observed again through the microscope.

On the other hand, electrochemical test consists in inserting a specimen into an electrochemical cell together with Saturated Calomel Electrode (SCE) as reference and Pt electrode as counter electrode, Corrosion potential (Ecorr) was determined and Electrochemical Impedance Spectroscopy (EIS) was applied [3].

Results

In the metallographic test, the images taken before the corrosive agent attack show some porosity and scratches on the samples surface. Nevertheless, two different phases of the structure of the compositional variants under study can be observed after chemical etching. Moreover, in the corrosion tests, the samples are immersed in Ringer Grifols solution which simulates the physiological fluid of the human body. All the electrochemical tests are processed by the Ec Lab program to accomplish the values and the graphics. In the linear polarization test, potential E versus time graphics are obtained to determine the tendency to passivation or corrosion of each sample. Besides, the EIS method is performed on each specimen at different potentials to obtain the Bode Impedance graphics.

Conclusions

The two samples show a positive behavior in contact with physiological fluids, therefore, their possible use in various medical devices should continue to be studied. T2 sample, which has a lower percentage of titanium and silicon, show a greater ease of stabilization, although the two samples tend to passivation. However, in the EIS method, using Bode-impedance graphics, the higher the impedance value result, the higher its corrosion resistance. Sample T1 has higher corrosion resistance because its impedance value is upper than T2, its process occurs in one stage and the impedance phases of the different values given during the EIS are similar. The metallographic study confirms the two-phase amorphous structure of the samples for different polishing finishes. In view of the data collected and the conclusions presented, it is not possible to establish a clear relationship between the degree of concentrations of titanium and silicon in the alloys and the behavior against electrochemical corrosion.

Keywords— *Biomaterial; Bode Impedance; Corrosion Potential; Linear Polarization; Electrochemical Impedance Spectroscopy; Metallographic Test.*

References

1. de Lera, D. D. (2013). Biomateriales: el titanio en odontología. Cuadernos del Tomás, (5), 233-258.
2. Dalmau Borrás, A. (2013). Caracterización y estudio del comportamiento electroquímico de aleaciones biomédicas de titanio.
3. Ríos, M. L., Perdomo, P. S., Voiculescu, I., Geanta, V., Crăciun, V., Boerasu, I., & Rosca, J. M. (2020). Effects of nickel content on the microstructure, microhardness and corrosion behavior of high-entropy AlCoCrFeNix alloys. Scientific Reports, 10(1), 1-11.

CERTIFICATE
OF PARTICIPATION

THIS IS THE CERFICATE THAT

A.D. Rico-Cano

participated at International Graduate Studies Congress (IGSCONG'21)
and made a presentation (oral) entitled

Microstructure and Corrosion Behavior of TiMoZrXSi Biomaterial Focused on Hip Prosthesis

the contrubution is awarded with this certificate.

Dr.M. Cem ALDAG
Member of the Organizing Committee

Assoc. Prof. Dr.M. Nuri SEYMAN
Head of the Organizing Committee

Date of Achievment: 17-20 June 2021

The paper has been reviewed, accepted, presented and discussed during the conference and included in the conference proceedings.


International Conference on New Trends in Science and Applications (NTSA)
BOOK OF ABSTRACT PROCEEDING
ORAL
October 12-13
2021
EDITORS
Mohammed Al-Hashimi, Ph.D. FRSC
Nadia Nebbache, Ph.D.
Niyazi Bulut, Ph.D.
ISBN 978-605-80511-2-6
9 786058 051126

Book of Abstracts of the International Conference on New Trends in Science and Applications (NTSA)

BOOK OF ABSTRACT PROCEEDINGS (ORAL)

EDITORS

Mohammed Al-Hashimi, Ph.D. FRSC

Nadia Nebbache, Ph.D.

Niyazi Bulut, Ph.D.

Published, October 2021

http://pcfm-conference.com *bulut_niyazi@yahoo.com*

ISBN: 978-605-80511-2-6

OP-13

Microhardness and Flexural Strength Behavior of TiMoZrxSi Biomaterial Focused on HIP Prosthesis

C. Jiménez-Marcos, A.D. Rico-Cano, N.R. Florido-Suárez, J.C. Mirza-Rosca, P. Vizureanu*

Department of Mechanical Engineering, University of Las Palmas de Gran Canaria, Las Palmas de Gran Canaria, Spain
**Department of Technologies and Equipment for Materials Processing, "Gheorghe Asachi"Technical University of Iasi, Iasi, Romania*

julia.mirza@ulpgc.es

Introduction: Nowadays, due to the great weight borne by the hip and the problems caused by the current biomaterials used, new alloys with a low modulus of elasticity and low cytotoxicity are being researched and developed. It has therefore been decided to further investigate the possible biomedical applications of T1 (73% Ti, 20% Mo, 7% Zr, 0% Si) and T2 (72% Ti, 20% Mo, 7% Zr, 1% Si) samples.
Experimental: To perform the three-point bending and microhardness tests, the specimens are embedded in an epoxy resin cylinder, then cut into sheets for re-embedding and polished with silicon carbide emery papers and 0.1 micrometer of alumina suspension [1]. Three-point bending test to find the value of the modulus of elasticity of each specimen and the microhardness test with at least 5 indentations to calculate and express as Vickers hardness (HV) were performed [2].
Results: Once the techniques have been applied, it can be observed in the three-point bending test that the value obtained for the modulus of elasticity of one of the three specimens tested in sample T1 is much higher than that of the others, and the same occurs in sample T2, where the values of thetwo specimens tested are very different from each other. Furthermore, the graphs of Vickers hardnessversus scan length for both samples show widely dispersed maxima and minima, as the surfaces of the samples show soft and hard areas and it is confirmed that the hardness increases the higher the applied load and the higher the percentage of silicon.
Conclusions: Therefore, the values of the modulus of elasticity found for each sample are very different from each other, making the results inconclusive. However, in the case of microhardness, both samples perform well under the different loads applied, although sample T2 has a higher resistance to deformation.

References

[1] Jiménez Marcos, C., Rico Cano, A. D., Florido Suárez, N. R., Mirza Rosca, J. C. & Vizureanu, P. Microstructure and Corrosion Behavior of TiMoZrXSi Biomaterial Focused on Hip Prosthesis. *IGSCONG'21. PROCEEDINGS BOOK*, 599-600 (2021). **ISBN:978-605-68187-0-7**

[2] López Ríos, M., Socorro Perdomo, P. P., Voiculescu, I., Geanta, V., Crăciun, V., Boerasu, I. & Mirza Rosca, J.C. Effects of nickel content on the microstructure, microhardness and corrosion behavior of high-entropy AlCoCrFeNix alloys. *Sci Rep* **10**, 21119 (2020).

CERTIFICATE

OF ATTENDANCE

International Conference on New Trends in Science and Applications (NTSA)

Alberto Rico Cano

We would like to thank you for valuable contributions as a Participant with a presentation at the **International Conference on New Trends in Science and Applications (NTSA)**
Virtual conference, ***October 12-13, 2021***

Mohammed Al-Hashimi Ph.D. FRSC	Nadia Nebbache Ph.D.	Niyazi Bulut Ph.D.

UNITED RESEARCH FORUM
(CONNECT WITH RESEARCH WORLD)

Proceedings of

2nd International E-Conference on

DENTISTRY AND ORAL HEALTH

November 22, 2021 I Webinar

Address:
United Research Forum,
1-75 Shelton Street Covent Garden, WC2H 9JQ, LONDON, ENGLAND

UNITED RESEARCH FORUM
(CONNECT WITH RESEARCH WORLD)

CONTENTS

Comparative study of different worldwide materials for prosthodontic restoration

A. Rico-Cano[1], N. Florido-Suarez[1], A. Saceleanu[2]
[1]University of Las Palmas de Gran Canaria, Las Palmas de Gran Canaria, Spain
[2]Lucian Blaga University, Sibiu, Romania

Hello and good afternoon, my name is Alberto Rico and I am PhD student from the mechanical engineer department, at the university of las Palmas de Gran Canaria, situated in the island of Gran Canaria, Canary Islands, Spain.

The title of the paper I am about to expose is "**Comparative study of different worldwide materials for prosthodontic restoration".**

Many alloys are available for prosthodontic restorations and among them nickel-based alloys are widely used in the porcelain-fused-to-metal and casting crown and bridge. This is due to their simple fabrication process, low cost and, not less important, to their corrosion resistance. Therefore, study this alloys behavior in contact with physiological fluids is very important, if not, corrosion products can cause serious problems to our health, such as local inflammation or damage to our immune system.

Even the nickel-chromium alloys form a thin protective oxide film on the surface, they show unstable galvanic corrosion and also, they corrode in physiological solutions such as balanced salt, human saliva, artificial saliva and artificial sweat solutions. Despite all these, the use of Ni-Cr dental alloys is increasing. Many types of Ni-Cr alloys are found in the world markets and contain Fe, Mo, Mn, Cu, Nb, Al and Si in their composition.

The present paper made a comparative study of six Ni-Cr dental alloys from USA, Romania and Germany that are worldwide used prosthodontic restoration, studying how they react in artificial physiological fluids, in this time, Ringer solution.

First, we cut the samples in order to obtain 5 cylindric specimens of 2 mm long. Then, microstructure analysis, Open Circuit Potential (E_{OC}), Potentiodynamic Polarization and Electrochemical Impedance Spectroscopy (EIS) techniques were applied.

All alloys examined are under the influence of an anodic control, due to the formation of protective layers, most likely of oxide, on the surface of the alloys. The alloys studied can be divided into two categories according to the type of corrosion observed. A uniform general corrosion behavior was found at the surface of the two Ni-Cr alloys (as we can see in sample 1 and 2 microstructure

analysis images, before and after being chemically attacked, both with almost the same chromium percentage). In the other hand, localized points of corrosion were found in the others Ni-Cr alloys. The Electrochemical Impedance Spectroscopy shows on the Nyquist diagram a capacitive arc on each sample, and the Bode Impedance spectrum indicate that for high frequencies the impedance logarithm tends to become constant.

In terms of susceptibility to corrosion, findings in this study show from the impedance spectra analysis that all alloys investigated have more than adequate corrosion resistance in artificial saliva. Being sample 1 and 2 the alloys with greater corrosion resistance, meanwhile, sample 5 and 6, probably by their high copper percentage (which is used to increase the alloy moldability, making it easier to manipulate), shows the lowest corrosion resistance, probably becoming toxic if expose to physiological fluids for long time.

Thank you very much for listening, I hope this presentation was adequate to expose and understand the techniques and results found. Hope seeing you all soon at the Canary Island.

Keywords: dental alloys, corrosion, Ni-Cr, EIS

1. Alberto Rico Cano
2. Ph.D. student/ Mechanical Eng. Dept./ University of Las Palmas de GC

3. Alberto Daniel Rico Cano is Ph.D student at the Mechanical Engineer Department of Las Palmas de Gran Canaria. Master in renewable energies at the Universidad Europea de Canarias in 2019 and degree in Mechanical Engineering at the ULPGC in 2018. He worked designing the European Comision Sustainable Energy and Climate Action Plan (SECAP) for two councils of Gran Canaria as energy advisor, participated in two research conferences and has published two articles on a new biomaterial, applied in the medical field.

4. Contact information: Nanomaterials Laboratory, Campus Univ. Tafira, Spain, 35017, alberto.rico101@alu.ulpgc.es, +34 691472214.

5. Category: Poster presentation
6. Session Name: Dental Material Sciences Dental Medicine

UNITED RESEARCH FORUM (CONNECT WITH RESEARCH WORLD)

2nd International E-Conference on

DENTISTRY AND ORAL HEALTH

November 22, 2021 I Webinar

Comparative study of different worldwide materials for prosthodontic restoration

A. Rico-Cano[1]*, N. Florido-Suarez[1], A. Saceleanu[2]

[1]University of Las Palmas de Gran Canaria, Las Palmas de Gran Canaria, Spain

[2]Lucian Blaga University, Sibiu, Romania

Many alloys are available for prosthodontic restorations and among them nickel-based alloys are widely used in the porcelain-fused-to-metal and casting crown and bridge. This is due to their simple fabrication process, low cost and, not less important, to their corrosion resistance. Even the nickel-chromium alloys form a thin protective oxide film on the surface, they show unstable galvanic corrosion and also they corrode in physiological solutions such as balanced salt, human saliva, artificial saliva and artificial sweat solutions. Despite all these, the use of Ni-Cr dental alloys is increasing. Many types of Ni-Cr alloys are found in the world markets and contain Fe, Mo, Mn, Cu, Nb, Al and Si in their composition. The present paper made a comparative study of six Ni-Cr dental alloys from USA, Romania and Germany using microstructure analysis, Open Circuit Potential (EOC), Potentiodynamic Polarization and EIS technique. All alloys examined are under the influence of an anodic control, due to the formation of protective layers, most likely of oxide, on the surface of the alloys. The alloys studied can be divided into two categories according to the type of corrosion observed. A uniform general corrosion behavior that was found at the surface of the two Ni-Cr alloys and a localized in points corrosion found in the others Ni-Cr alloys. In terms of susceptibility to corrosion, findings in this study show from the impedance spectra analysis that all alloys investigated have more than adequate corrosion resistance in artificial saliva.

Keywords: dental alloys, corrosion, Ni-Cr, EIS

Biography:

Alberto Daniel Rico Cano is Ph.D student at the Mechanical Engineer Department of Las Palmas de Gran Canaria. Master in renewable energies at the Universidad Europea de Canarias in 2019 and degree in Mechanical Engineering at the ULPGC in 2018. He worked designing the European Comision Sustainable Energy and Climate Action Plan (SECAP) for two councils of Gran Canaria as energy advisor, participated in two research conferences and has published two articles on a new biomaterial.

2nd International E-Conference on Dentistry and Oral Health

November 22nd– 23rd, 2021 | United Research Forum, London, UK

Comparative study of different worldwide materials for prosthodontic restoration

A. Rico-Cano[1], N. Florido-Suarez[1], A. Saceleanu[2]
[1]University of Las Palmas de Gran Canaria, Las Palmas de Gran Canaria, Spain
[2]Lucian Blaga University, Sibiu, Romania

MATERIALS	Composition (wt%)								
	Ni	Cr	Mo	Fe	Nb	Si	Cu	Mn	Al
SAMPLE 1	60.1	24.3	10.1	2.1	1			2	
SAMPLE 2	60.8	23.9	8.8	2.4	3.8				
SAMPLE 3	63.4	23.2	3	9		1			
SAMPLE 4	72.1	20		7.5					
SAMPLE 5	64.9	17.9				1.8	9.9	3.6	1.5
SAMPLE 6	53.4	14.4				1.5	9.5	19.4	1.6

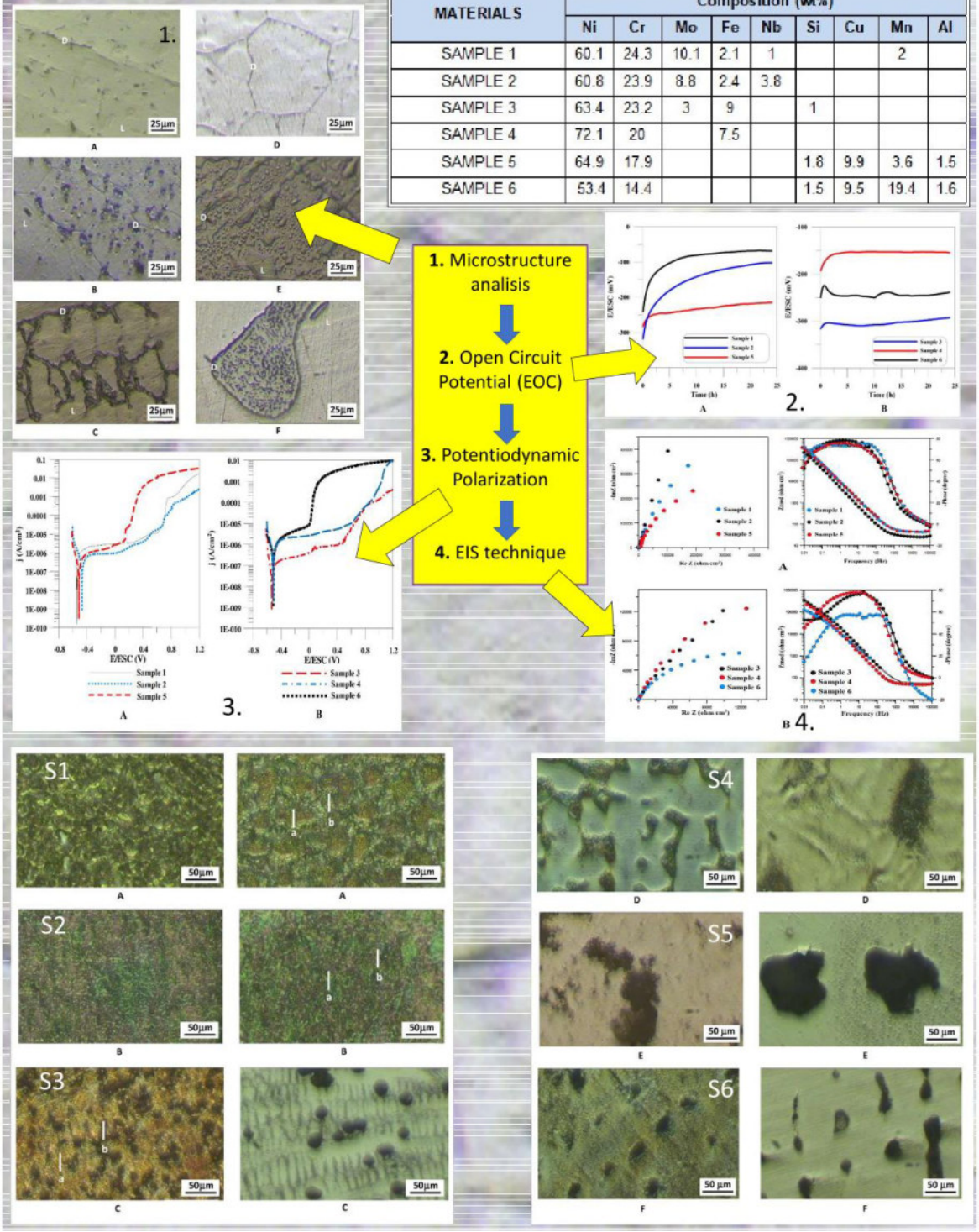

CERTIFICATE OF RECOGNITION

United Research Forum wish to thank

Mr. Alberto Rico Cano

University of Las Palmas de Gran Canaria, Spain

For his phenomenal and worthy **Poster Presentation** on

"Comparative study of different worldwide materials for prosthodontic restoration"

at

2nd International E-Conference on Dentistry and Oral Health during on November 22, 2021.

Dr. Vicky Jocelyne Ama Moor
University of Yaounde, Cameroun

Dr Vanga
CEO, United Research Forum, UK


M&M 2024
MICROSCOPY & MICROANALYSIS
July 28-August 1 • Cleveland, OH
ifes
international field emission society
MAS
Microanalysis Society
MSA
Microscopy Society of America
LOOK INSIDE FOR:
Plenary Sessions &
Program Highlights
Registration Fees
Special M&M Hotel Rates
Onsite Program Guide &
Exhibitor Information
2024
https://mmconference.microscopy.org

Scientific Program

P Physical Sciences Poster Sessions – Tuesday cont.

POSTER # 207

476 *Transmission Electron Microscopy Exploration of Solution-Grown Lead Oxide Nanosheets: Unveiling Crystallinity and Defects;* **Udupa Manjunatha**, N Ravishankar

POSTER # 208

477 *Transmission Electron Microscopy of Crystalline Nanorods of Molecules in Ammonium Urates;* **Hector Calderon**, WeiWei Tang

P04.P1 Science and Applications of High-Entropy Materials

POSTER # 209

478 *Corrosion Behavior of New B4C Ceramic Doped with High-Entropy Alloy in an Aggressive Environment;* **Alberto Daniel Rico-Cano**, Julia Mirza-Rosca, Burak Cagri Ocak, Gultekin Goller

POSTER # 210

479 *Electrochemical Comparison Between HEA Films in Different Deposition Conditions;* **Julia Mirza-Rosca**, Ionelia Voiculescu, Doina Craciun, Valentin Craciun

POSTER # 211

480 *In-depth Analysis of Structural Heterogeneity in High Entropy Bulk Metallic Glasses Using 4D-STEM;* **Minhazul Islam**, Ji Young Kim, Geun-Hee Yoo, Soohyun Im, Gabriel Calderon Ortiz, Eun Soo Park, Jinwoo Hwang

POSTER # 212

481 *Synthesis of CrMnFeCoNiAlx Alloy by Mechanical Alloying and Sintering by High-Frequency Induction;* **Leonardo Baylón García**, C.G. Garay-Reyes, X. Atanacio-Sánchez, P. A. Guerrero-Seañez, I. Estrada-Guel, A. Martínez-García, J.M. Mendoza-Duarte, M.A. Ruiz-Esparza-Rodriguez, R. Martínez-Sánchez

POSTER # 213

482 *The Influence of the Re-Melting on the Microstructure and Corrosion Resistance of New Welding Material;* **George Simion**, Matteo Bertapelle, Julia Mirza-Rosca, Ionelia Voiculescu, Elena Scutelnicu

P09.P1 Advances in In Situ TEM Characterization of Dynamic Processes in Materials

POSTER # 214

483 *Analyzing Structural Dynamics in Nanocrystalline Thin Films using In-Situ 4D-STEM: A Statistical Approach;* **Yuan Tian**, Yutong Bi, Mingjie Xu, Evgeniy Boltynjuk, Horst Hahn, Jian Han, David Srolovitz, Xiaoqing Pan

POSTER # 215

484 *Atomic Force Microscopy Imaging of Individual CO Molecules Adsorbed on a Cu(111) Surface;* **Dingxin Fan**, Pengcheng Chen, Nan Yao

POSTER # 216

485 *Deep learning Driven Analysis of a Structural Phase Transformation in CrSBr;* **Dawn Ford**, Mads Weile, Thang Pham, Aubrey Penn, Frances Ross, Julian Klein

POSTER # 217

486 *Electrochemical Transmission Electron Microscopy (EC-TEM) of Capacitance-Induced Electrodeposition and Coarsening on Graphene;* **Serin Lee**, Shu Fen Tan, Frances Ross

POSTER # 218

487 *Flexible Framework for Customized Autonomous Acquisition of In-Situ Spectrum Image Series Using DigitalMicrograph;* **Liam Spillane**, Shelly Michele Conroy

POSTER # 219

488 *He Bubble Evolution in LiAlO2: A Comparison of Human and Artificial Intelligence Based Analysis;* **Kip Wheeler**, Eric Lang, Christopher Field, Nathan Madden, Ryan Schoell, Ryan Pena, David Senor, Andrew Casella, Khalid Hattar

POSTER # 220

489 *In situ Electron Energy Loss Spectroscopy (EELS) Studies of Laser-induced Graphene Oxide Reduction in a Dynamic Transmission Electron Microscope (DTEM);* **Israt Ali**, Kenneth Beyerlein

POSTER # 221

490 *In Situ light Injection Study on Stacked WS2/WSe2 /hBN Hetero-Bilayers;* **Sriram Sankar**, Medha Dandu, Piyush Haluai, Takashi Taniguchi, Kenji Watanabe, Archana Raja, Sandhya Susarla

POSTER # 222

491 *In situ TEM Investigation of Graphitization Mechanism on Nickel Catalyst;* **Jaemin Kim**, Seungwoo Son, Myeonggi Choe, Zonghoon Lee

POSTER # 223

492 *In Situ TEM Study on Temperature-dependent Growth of Carbon Nanofiber and Nanotube from Ethanol Vapor;* **Handolsam Chung**, Myeonggi Choe, Wonjun Kim, Younggeun Jang, Zhaoying Wang, Zonghoon Lee

POSTER # 224

493 *In-situ Heating Technique with the FIB-TEM Compatible MEMS Specimen Holder;* **Toshie Yaguchi**, Akiko Wakui, Katsuji Ito, Hiroyuki Asakura, Yasuhira Nagakubo, Meng Li, Zhiwei Shan

POSTER # 225

494 *In-situ Observation of the Effect of Grain Boundary Defects on Dynamics of Incoherent Twin Boundaries in FCC Crystals;* **Yutong Bi**, Yuan Tian, Xiaoguo Gong, Eugen Rabkin, Jian Han, David Srolovitz, Xiaoqing Pan, Jonathan Zimmerman

POSTER # 226

495 *Solid State Phase Transformations in Materials for Carbon Capture and Conversion Revealed Using Electrothermal S/TEM Holders;* **William Bowman**, Jenna Wardini, Jenny Martinez

POSTER # 227

496 *Standard Calibrations and Prediction for Thermal Gradients during In Situ Transmission Electron Microscopy Heating Experiments;* **Yi-Chieh Yang**, Sriram Vijayan, Murat Yesibolati, Joerg Jinschek

POSTER # 228

497 *Understanding Redox Behavior in STCH Water Splitters Using In-Situ Monochromated EELS and Atomic Resolution EDS;* **Arielle Clauser**, Keith King, Dan Lowry, Sean Bishop, Anthony McDaniel, Joshua Sugar

MICROSCOPY & MICROANALYSIS Cleveland
M&M 2024 July 28-August 1 Cleveland, OH

Corrosion Behavior of New B4C Ceramic Doped with High-Entropy Alloy in an Aggressive Environment

A.D. Rico-Cano[1], J.C. Mirza-Rosca[1,2*], B.C. Ocak[3], G. Goller[3]

[1] Mechanical Engineering Department, University of Las Palmas de Gran Canaria, Las Palmas de Gran Canaria, Spain
[2] Transilvania University of Brasov, Materials Engineering and Welding Department, Brasov, Romania
[3] Department of Metallurgical and Materials Engineering, Istanbul Technical University, Maslak, Istanbul, Turkey
*Corresponding author: julia.mirza@ulpgc.es

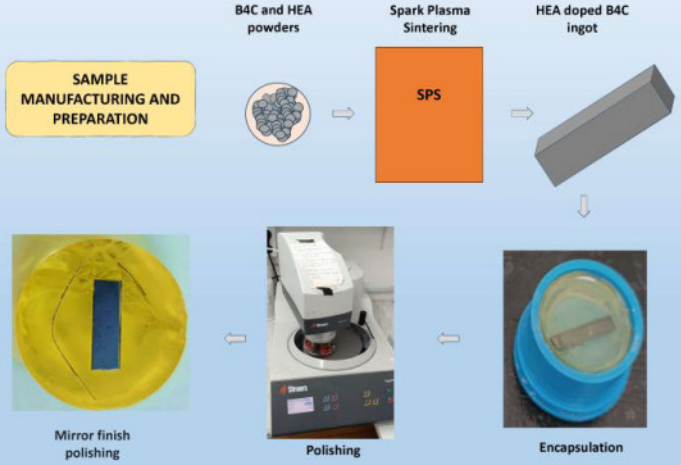

TEST AND RESULTS

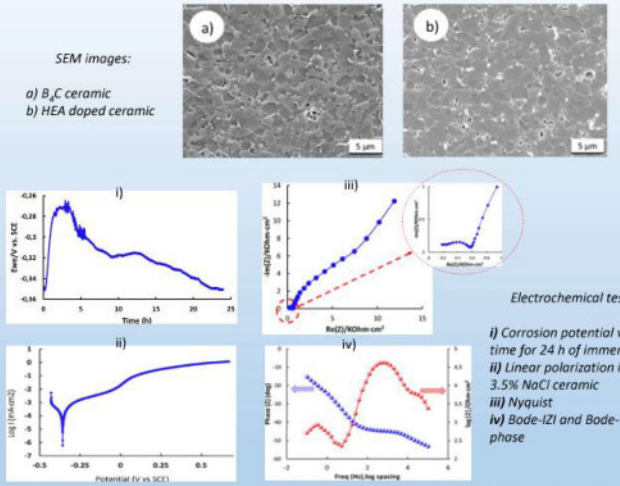

Electrochemical tests:

i) *Corrosion potential vs. time for 24 h of immersion*
ii) *Linear polarization in 3.5% NaCl ceramic*
iii) *Nyquist*
iv) *Bode-IZI and Bode-phase*

The behavior of a high entropy alloy doped B4C in artificial sea water (3.5% NaCl) was studied and the main conclusions are listed as follows:
- The doping of B4C ceramic with CoCrFeMoNi high entropy alloy led to a more compact microstructure in comparison to the solid B4C material, inhibits grain expansion and results in a finer grain structure.
- The doped sample has a very high resistance to corrosion in artificial sea water.
- The chemical process which takes place at immersion of the doped sample in artificial sea water has two steps with an important diffusional component.

Transilvania University of Brasov
ULPGC · UNIVERSIDAD DE LAS PALMAS DE GRAN CANARIA
İTÜ

ULPGC Universidad de Las Palmas de Gran Canaria | Escuela de Doctorado

BraMat 2024

13TH INTERNATIONAL CONFERENCE ON MATERIALS SCIENCE & ENGINEERING

Brașov - ROMANIA
March 13 - 16, 2024

PROGRAM OVERVIEW

Conference's Partners:
Namicon, Sartorom, Struers, AMS 2000, Global Source, Nanoteam, Standard Service

Organized by
Materials Science and Engineering Faculty
Transilvania University of Brasov, Romania
and
Technical Sciences Academy of Romania – ASTR
Romanian Foundry Technical Association – ATTR
Romanian Welding Society - ASR

BRAMAT 2024
13TH INTERNATIONAL CONFERENCE ON MATERIALS SCIENCE & ENGINEERING
Transilvania University of Brasov - Romania
Materials Science and Engineering Faculty

EIS STUDY OF HEA DOPED B_4C CERAMIC IN ARTIFICIAL SEA WATER

Alberto Daniel Rico-Cano[1], Julia Claudia Mirza-Rosca[1,2], Burak Cagri Ocak[3], Gultekin Goller[3]

[1] Universidad de Las Palmas de Gran canaria, Dpto. de Ingeniería Mecánica, Campus Universitario Tafira, 35017, Las Palmas de gran Canaria, Spain, alberto.rico101@alu.ulpgc.es
[2] Transilvania University of Brasov, Materials Engineering and Welding Department, Brasov, Romania
[3] Istanbul Technical University, Department of Metallurgical and Materials Engineering, 34469, Maslak, Istanbul, Turkey

Keywords: Ceramic, HEA, EIS, corrosion

Abstract: Evaluating a new material's corrosion behavior is a crucial step in its development, since it allows us to determine the material's whole range of possible applications. Therefore, we decided to proceed with different electrochemical test in artificial sea water, obtaining information about corrosion resistance, corrosion rate and corrosion potential. The surface taken in analysis is a new type of material, boron carbide doped with a 3% of High-Entropy Alloy (HEA) CoCrFeNiMo, with promising mechanical properties [1]. The doping of B_4C ceramic with CoCrFeMoNi high entropy alloy led to a more compact microstructure in comparison to the solid B4C material, inhibits grain expansion and results in a finer grain structure. The doped sample has shown a promising high resistance to corrosion in artificial sea water. By electrochemical impedance spectroscopy [2-3], it was demonstrated that the chemical process which takes place at immersion of the doped sample in artificial sea water has two steps with an important diffusional component, ending with the creation of a passive film as shown in Fig. 1.

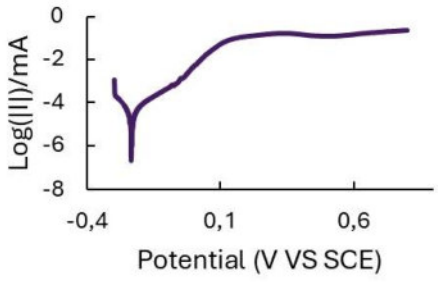

Fig. 1. Linear polarization Rate of doped B_4C sample.

Selective references:
1.B. C. Ocak and G. Goller, *Investigation the effect of FeNiCoCrMo HEA addition on properties of B4C ceramic prepared by spark plasma sintering*, Journal of the European Ceramic Society, 41(13), Oct. 2021, p. 6290-6301.
2. J. Cabrera-Peña, S.J. Brito-Garcia, J.C. Mirza-Rosca, G.M. Callico, *Electrical Equivalent Circuit Model Prediction of High-Entropy Alloy Behavior in Aggressive Media*, Metals (Basel). 13 (2023) 1204.
3. S.J. Brito-Garcia, J.C. Mirza-Rosca, C. Jimenez-Marcos, I. Voiculescu, *Impact of Ti Doping on the Microstructure and Mechanical Properties of CoCrFeMoNi High-Entropy Alloy*, Metals (Basel). 13 (2023) 854.

Acknowledgements: I hereby acknowledge the project SHENG: 2023-1-RO 01- KA220- HED-000159985, for allowing me to participate in this project.

BRAMAT 2024
13TH INTERNATIONAL CONFERENCE ON MATERIALS SCIENCE & ENGINEERING
Transilvania University of Brasov - Romania
Materials Science and Engineering Faculty

EIS STUDY OF HEA DOPED B_4C CERAMIC IN ARTIFICIAL SEA WATER

Alberto Daniel Rico-Cano[1], Julia Claudia Mirza-Rosca[1,2], Burak Cagri Ocak[3], Gultekin Goller[3]

[1] *Universidad de Las Palmas de Gran canaria, Dpto. de Ingeniería Mecánica, Campus Universitario Tafira, 35017, Las Palmas de gran Canaria, Spain, alberto.rico101@alu.ulpgc.es*
[2] *Transilvania University of Brasov, Materials Engineering and Welding Department, Brasov, Romania*
[3] *Istanbul Technical University, Department of Metallurgical and Materials Engineering, 34469, Maslak, Istanbul, Turkey*

SAMPLE PREPARATION

B4C and HEA powders → Spark Plasma Sintering → HEA doped B_4C ingot → Encapsulation → Polishing → Mirror finish polishing

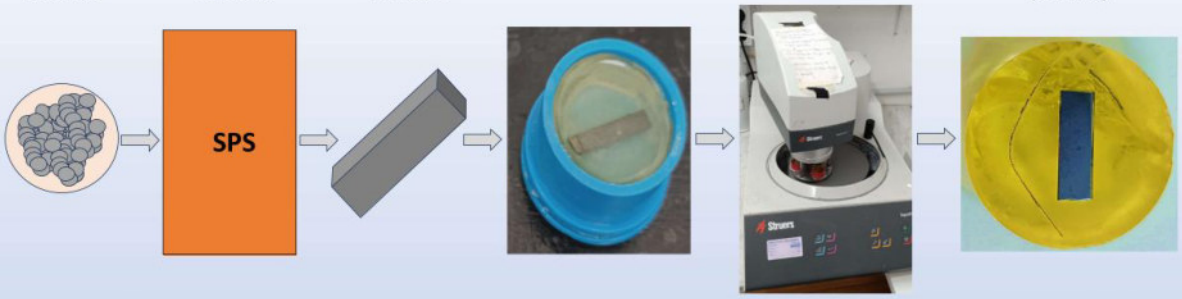

TEST AND RESULTS

Nyquist

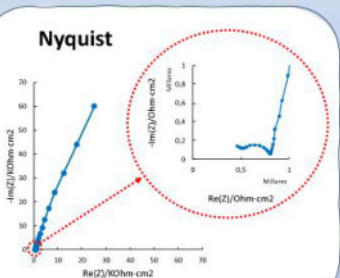

Bode impedance and phase

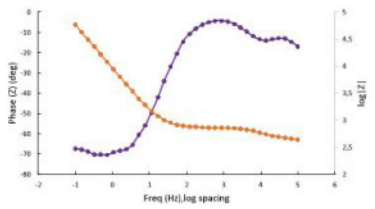

Electrochemical cell

Linear polarization

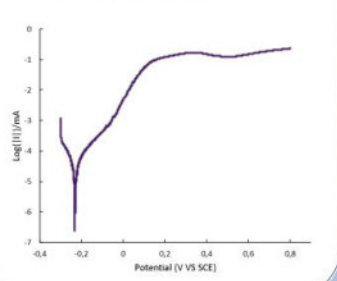

Corrosion potential

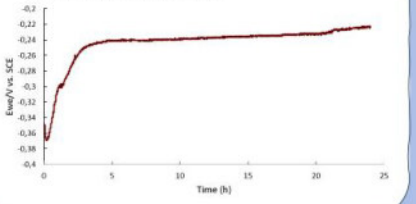

The behavior of a high entropy alloy doped B4C in artificial sea water (3.5% NaCl) was studied and the main conclusions are listed as follows:
- The doping of B4C ceramic with CoCrFeMoNi high entropy alloy led to a more compact microstructure in comparison to the solid B4C material, inhibits grain expansion and results in a finer grain structure.
- The doped sample has a very high resistance to corrosion in artificial sea water.
- The chemical process which takes place at immersion of the doped sample in artificial sea water has two steps with an important diffusional component.

Erasmus+ Co-funded by the European Union
ULPGC · UNIVERSIDAD DE LAS PALMAS DE GRAN CANARIA
Transilvania University of Brasov
İTÜ

Acknowledgements: ERASMUS 2023-1-RO01-KA220-HED-000159985: Smart Healthcare Engineering

Transilvania University of Brasov
FACULTY OF MATERIALS SCIENCE AND ENGINEERING

BraMat 2024
13TH INTERNATIONAL CONFERENCE ON MATERIALS SCIENCE & ENGINEERING

CERTIFICATE OF PARTICIPATION

13th International conference on materials science & engineering

13-16 March 2024, Brasov, Romania

The research entitled: ***EIS STUDY OF HEA DOPED B_4C CERAMIC IN ARTIFICIAL SEA WATER,*** authors: Alberto Daniel Rico-Cano, Julia Claudia Mirza-Rosca, Burak Cagri Ocak, Gultekin Goller, was presented by Alberto Daniel Rico-Cano, at BraMat 2024 international conference, organized by Materials Science and Engineering Faculty of Transilvania University of Brasov.

The extended conference program is available on the BraMat 2024 conference website: http://www.bramat.ro.

Paper identifying number: I.O.01

Section: Metallic materials and composites (Section I)

ROMÂNIA MINISTERUL EDUCAȚIEI UNIVERSITATEA TRANSILVANIA DIN BRAȘOV FACULTATEA DE ȘTIINȚA ȘI INGINERIA MATERIALELOR

Prof. dr. eng. Alexandru PASCU
Dean of Materials Science and Engineering Faculty
Conference chairman

6 Conclusiones

6. Conclusiones

Centrándonos en las prestaciones electroquímicas y mecánicas de la cerámica B_4C sin dopar (0% HEA) y dopada con concentraciones variables (0%, 0,5%, 1%, 2% y 3%) de CoCrFeNiMo HEA, los principales hallazgos se describen a continuación:

Cuando se añade la aleación de alta entropía CoCrFeNiMo a la matriz cerámica B_4C, se obtiene una estructura más densa. Gracias a este procedimiento de dopaje se obtuvo una estructura de grano más refinada. La adición de HEA conduce a una configuración más compacta y a la inhibición de la expansión del grano en comparación con el B_4C monolítico, lo que da lugar a notables alteraciones de la microestructura. El SEM corroboró que, de todas las muestras estudiadas, el menor tamaño medio de grano y la configuración más densa se alcanzaron en la muestra con una concentración de HEA del 2%.

Los ensayos electroquímicos revelaron que la resistencia a la corrosión mejoraba progresivamente con un mayor contenido de HEA. Todas las muestras inmersas en la solución corrosiva siguieron un proceso de corrosión en dos etapas, en el que intervino un importante componente de difusión. Inicialmente, el agua de mar artificial penetró en la superficie del material, a lo que siguió la formación de películas o capas protectoras que impiden una mayor degradación, contribuyendo a la elevada resistencia a la corrosión observada. El B_4C dopado con HEA al 3% demuestra la mayor resistencia en condiciones de agua de mar artificial. El mayor rendimiento se atribuye a la formación de una capa pasiva más compacta y protectora, que mitiga eficazmente la corrosión del material.

El análisis estadístico de microdureza de todos los materiales compuestos reveló que, aunque todas las muestras seguían una distribución normal (lo que sugiere una estructura homogénea), siendo la cerámica dopada a un 2% de HEA la que presentó menor variación, confirmando los resultados obtenidos en el SEM. Las concentraciones de HEA del 0,5% y el 3% presentaban una distribución de dureza menos uniforme y predecible, lo que sugiere ajustes microestructurales en curso. La dureza Vickers de todas las muestras B_4C fue mayor a medida que aumentaba el porcentaje de HEA, lo que indica una relación estricta dopaje y dureza.

Todas las pruebas realizadas determinan claramente que el aumento del contenido de HEA implica un mejor rendimiento en cuanto a resistencia a la corrosión y propiedades

mecánicas. El material compuesto B_4C con un 3% de HEA mostró los mejores resultados en los diferentes ensayos, mientras que la muestra B_4C con un 0,5% de HEA mostró el peor rendimiento. El estudio determina finalmente el potencial de la cerámica B_4C dopada con HEA CoCrFeNiMo para aplicaciones que implican resistencia mecánica y resistencia a la corrosión. Destaca el excelente comportamiento de todos los compuestos en ambientes agresivos, especialmente el compuesto dopado con HEA al 3%.

En definitiva, podemos determinar que la adición de la HEA a la matriz cerámica del carburo de boro, en sus propiedades mecánicas consigue una estructura más densa y mayor dureza, a medida que se aumenta el contenido de HEA, mejores estás propiedades. Sin embargo, a partir del 2% de contenido en HEA los resultados caen ligeramente, presentando la muestra con un 3% de contenido en HEA resultados ligeramente peores que la anterior. Esto cobra sentido tras el análisis del SEM, en el que se aprecia como la HEA se va depositando en los poros de la matriz cerámica. Al solidificarse la cerámica antes que la HEA, esta aun líquida, tiende a ocupar las configuraciones con menor energía, como son las intersecciones entre granos o los poros [39]. La muestra al 3% de contenido en HEA demuestra saturación de la matriz cerámica, existiendo más metal del que la configuración del carburo de boro puede absorber de manera estable y homogénea, dando lugar a una configuración más caótica.

A nivel electroquímico, no hay duda ninguna de que a mayor contenido en HEA también se consiguen mejores propiedades, siendo la muestra con un 3% de HEA la más estable en todos los ensayos realizados.

La mejora en ambas de estas características supone ampliar en gran medida el rango de aplicación de este material en usos industriales, siendo una alternativa mucho más económica que el diamante. Las muestras dopadas han conseguido una mayor densidad del material, mayor dureza y mayor resistencia a la corrosión frente al carburo de boro monolítico.

7 Bibliografía

7. BIBLIOGRAFÍA

1. Yavas, B.; Sahin, F.; Yucel, O.; Goller, G. Effect of Particle Size, Heating Rate and CNT Addition on Densification, Microstructure and Mechanical Properties of B4C Ceramics. Ceram. Int. 2015, 41, 8936–8944. Doi:10.1016/J.CERAMINT.2015.03.167.

2. Domnich, V.; Reynaud, S.; Haber, R.A.; Chhowalla, M. Boron Carbide: Structure, Properties, and Stability under Stress. J. Am. Ceram. Soc. 2011, 94, 3605–3628. Doi:10.1111/j.1551-2916.2011.04865.x.

3. Suri, A.K.; Subramanian, C.; Sonber, J.K.; Ch Murthy, T.S.R. Synthesis and Consolidation of Boron Carbide: A Review. Int. Mater. Rev. 2010, 55, 4–38.

4. Pérez, S.; Tamayo, P.; Rico, J.; Alonso, J.; Thomas, C. Effect of Fibers and Boron Carbide on the Radiation Shielding Properties of Limestone and Magnetite Aggregate Concrete. Prog. Nucl. Energy 2024, 175, 105320. Doi:10.1016/j.pnucene.2024.105320.

5. Tamayo, P.; Thomas, C.; Rico, J.; Pérez, S.; Mañanes, A. Radiation Shielding Properties of Siderurgical Aggregate Concrete. Constr. Build. Mater. 2022, 319, 126098. Doi:10.1016/j.conbuildmat.2021.126098.

6. Zhang, W. A Review of Tribological Properties for Boron Carbide Ceramics. Prog. Mater. Sci. 2021, 116, 100718.

7. Zorzi, J.E.; Perottoni, C.A.; Da Jornada, J.A.H. Hardness and Wear Resistance of B4C Ceramics Prepared with Several Additives. Mater. Lett. 2005, 59, 2932–2935. Doi:10.1016/j.matlet.2005.04.047.

8. Cantor, B.; Chang, I.T.H.; Knight, P.; Vincent, A.J.B. Microstructural Development in Equiatomic Multicomponent Alloys. Mater. Sci. Eng. 2004, 375, 213–218. Doi:10.1016/J.MSEA.2003.10.257.

9. Yeh, J.W. Recent Progress in High-Entropy Alloys. Ann. Chim. Sci. Mater. 2006, 31, 633–648. Doi:10.3166/acsm.31.633-648.

10. Kozhakhmetov, Y.; Skakov, M.; Kurbanbekov, S.; Uazyrkhanova, G.; Kurmantayev, A.; Kizatov, A.; Mussakhan, N. High-Entropy Alloys: Innovative Materials with

Unique Properties for Hydrogen Storage and Technologies for Their Production. Metals 2025, 15, 100. https://doi.org/10.3390/met15020100.

11. de Oliveira, T.G.; Fagundes, D.V.; Capellato, P.; Sachs, D.; da Silva, A.A.A.P. A Review of Biomaterials Based on High-Entropy Alloys. Metals 2022, 12, 1940. https://doi.org/10.3390/met12111940.

12. Castro, D.; Jaeger, P.; Baptista, A.C.; Oliveira, J.P. An Overview of High-entropy Alloys as Biomaterials. Metals 2021, 11, 648.

13. Gawel, R.; Rogal, Ł.; Smoła, G.; Grzesik, Z. High-Temperature Oxidation and Diffusion Studies on Selected Al–Cr–Fe–Ni High-Entropy Alloys for Potential Application in Thermal Barrier Coatings. Intermetallics 2024, 169, 108273. Doi:10.1016/J.INTERMET.2024.108273.

14. Yang, H.; Shao, Z.; Lu, Q.; Cui, C.; Xu, L.; Yang, G. Development of Reduced-Activation and Radiation-Resistant High-Entropy Alloys for Fusion Reactor. Int. J. Refract. Met. Hard Mater. 2024, 121, 106674. Doi:10.1016/J.IJRMHM.2024.106674.

15. Chakraborty, P.; Sarkar, A.; Ali, K.; Jha, J.; Jothilakshmi, N.; Arya, A.; Tewari, R. Design and Development of Low Density, High Strength ZrNbAlVTi High Entropy Alloy for High Temperature Applications. Int. J. Refract. Met. Hard Mater. 2023, 113, 106222. Doi:10.1016/J.IJRMHM.2023.106222.

16. Xu, Z.Q.; Ma, Z.L.; Wang, M.; Chen, Y.W.; Tan, Y.D.; Cheng, X.W. Design of Novel Low-Density Refractory High Entropy Alloys for High-Temperature Applications. Mater. Sci. Eng. 2019, 755, 318–322. Doi:10.1016/J.MSEA.2019.03.054.

17. Nartita, R.; Ionita, D.; Demetrescu, I. A Modern Approach to HEAs: From Structure to Properties and Potential Applications. Crystals 2024, 14, 451.

18. Naveen, L.; Umre, P.; Chakraborty, P.; Rahul, M.R.; Samal, S.; Tewari, R. Development of Single-Phase BCC Refractory High Entropy Alloys Using Machine Learning Techniques. Comput. Mater. Sci. 2024, 238, 112917. Doi:10.1016/J.COMMATSCI.2024.112917.

19. Wakai, E.; Noto, H.; Shibayama, T.; Furuya, K.; Ando, M.; Kamada, T.; Ishida, T.; Makimura, S. Microstructures and Hardness of BCC Phase Iron-Based High Entropy Alloy Fe-Mn-Cr-V-Al-C. Mater. Charact. 2024, 211, 113881. Doi:10.1016/J.MATCHAR.2024.113881.

20. Li, C.; Ma, Z.; Tong, S.; Liu, J.; Zhang, W.; Shen, G.; Wang, S.; Zhao, H.; Ren, L. Mechanical-Thermal Coupling Fatigue Failure of CoCrFeMnNi High Entropy Alloy. J. Mater. Res. Technol. 2024, 30, 3430–3437. doi:10.1016/J.JMRT.2024.04.106.

21. Matsuzaka, T.; Hyakubu, A.; Kim, Y.S.; Matsugaki, A.; Nagase, T.; Ishimoto, T.; Ozasa, R.; Kim, H.S.; Mizuguchi, T.; Gokcekaya, O.; et al. Development of an Equiatomic Octonary TiNbTaZrMoHfWCr Super-High-Entropy Alloy for Biomedical Applications. Mater. Chem. Phys. 2024, 316, 129120. Doi:10.1016/J.MATCHEMPHYS.2024.129120.

22. Wu, Y.; Du, C.; Yu, Z.; Wang, R.; Ren, X. Effect of Cu Content on the Microstructure and Mechanical Properties of Fe20Co30Ni10Cr20Mn20 FCC-Typed HEAs. Mater. Sci. Eng. 2024, 897, 146336. doi:10.1016/J.MSEA.2024.146336.

23. Yen, C.C.; Lin, S.Y.; Ting, C.L.; Tsai, T.L.; Chen, Y.T.; Yen, S.K. Passivation Mechanisms of CoCrFeNiMox (x = 0, 0.1, 0.2, 0.3) High Entropy Alloys and MP35N in 3.5 Wt% NaCl Aerated Aqueous Solutions. Corros. Sci. 2024, 228, 111812. Doi:10.1016/J.CORSCI.2023.111812.

24. Dong, D.; Jiang, W.; Wang, X.; Ma, T.; Zhu, D.; Wang, Y.; Huo, J. Enhanced Mechanical Properties of High Pressure Solidified CoCrFeNiMo0.3 High Entropy Alloy via Nano-Precipitated Phase. Intermetallics 2024, 166, 108192. Doi:10.1016/J.INTERMET.2024.108192.

25. Zin, V.; Montagner, F.; Miorin, E.; Mortalò, C.; Tinazzi, R.; Bolelli, G.; Lusvarghi, L.; Togni, A.; Frabboni, S.; Gazzadi, G.; et al. Effect of Mo Content on the Microstructure and Mechanical Properties of CoCrFeNiMox HEA Coatings Deposited by High Power Impulse Magnetron Sputtering. Surf. Coat. Technol. 2024, 476, 130244. doi:10.1016/J.SURFCOAT.2023.130244.

26. Guo, K.; Sun, Y.; Cheng, W.; Gu, J.; Chen, Y.; Zhang, S. Effect of Rare Earth La2O3 on the Microstructure and Corrosion Resistance of CoCrFeNiMoSi High Entropy Alloys. Surf. Interfaces 2024, 44, 103683. Doi:10.1016/J.SURFIN.2023.103683.

27. Brito-Garcia, S.; Mirza-Rosca, J.; Geanta, V.; Voiculescu, I. Mechanical and Corrosion Behavior of Zr-Doped High-Entropy Alloy from CoCrFeMoNi System. Materials 2023, 16, 1832. Doi:10.3390/ma16051832.

28. Semikolenov, A.; Shalnova, S.; Klinkov, V.; Andreeva, V.; Salynova, M.; Larionova, T.; Tolochko, O. Effect of al Content on Phase Compositions of FeNiCoCrMo0.5AlxHigh Entropy Alloy. Metals 2021, 11, 1734. Doi:10.3390/met11111734.

29. Brito-García, S.; Jiménez-Marcos, C.; Mirza-Rosca, J.; Voiculescu, I. Behavior of Ti-Doped CoCrFeMoNi High Entropy Alloy. Microsc. Microanal. 2023, 29, 439–444. Doi:10.1093/micmic/ozad067.208.

30. Li, Y.; Zhang, J.; Huang, X.; Liu, J.; Deng, L.; Han, P. Influence of Laser Power on Microstructure Evolution and Properties of Laser Cladded FeNiCoCrMo HEA Coatings. Mater. Today Commun. 2023, 35, 105615. Doi:10.1016/j.mtcomm.2023.105615.

31. Wu, H.; Zhang, S.; Wang, Z.Y.; Zhang, C.H.; Chen, H.T.; Chen, J. New Studies on Wear and Corrosion Behavior of Laser Cladding FeNiCoCrMox High Entropy Alloy Coating: The Role of Mo. Int. J. Refract. Metals. Hard. Mater. 2022, 102, 105721. Doi:10.1016/J.IJRMHM.2021.105721.

32. Wang, W.; Wang, J.; Sun, Z.; Li, J.; Li, L.; Song, X.; Wen, X.; Xie, L.; Yang, X. Effect of Mo and Aging Temperature on Corrosion Behavior of (CoCrFeNi)100-XMox High-Entropy Alloys. J. Alloys Compd 2020, 812, 152139. Doi:10.1016/J.JALLCOM.2019.152139.

33. Fu, Y.; Huang, C.; Du, C.; Li, J.; Dai, C.; Luo, H.; Liu, Z.; Li, X. Evolution in Microstructure, Wear, Corrosion, and Tribocorrosion Behavior of Mo-Containing High-Entropy Alloy Coatings Fabricated by Laser Cladding. Corros. Sci. 2021, 191, 109727. Doi:10.1016/J.CORSCI.2021.109727.

34. Dai, C.; Luo, H.; Li, J.; Du, C.; Liu, Z.; Yao, J. X-Ray Photoelectron Spectroscopy and Electrochemical Investigation of the Passive Behavior of High-Entropy FeCoCrNiMox Alloys in Sulfuric Acid. Appl. Surf. Sci. 2020, 499, 143903. doi:10.1016/J.APSUSC.2019.143903.

35. Wang, L.; Mercier, D.; Zanna, S.; Seyeux, A.; Laurent-Brocq, M.; Perrière, L.; Guillot, I.; Marcus, P. Study of the Surface Oxides and Corrosion Behaviour of an Equiatomic

CoCrFeMnNi High Entropy Alloy by XPS and ToF-SIMS. Corros. Sci. 2020, 167, 108507. Doi:10.1016/J.CORSCI.2020.108507.

36. Rico-Cano, A.D.; Mirza-Rosca, J.C.; Ocak, B.C.; Goller, G. Corrosion Behavior and Microhardness of a New B4C Ceramic Doped with 3% Volume High-Entropy Alloy in an Aggressive Environment. Metals 2025, 15, 79. Doi:10.3390/met15010079.

37. Rico-Cano, A.D.; Mirza-Rosca, J.C.; Ocak, B.C.; Goller, G. Corrosion Behavior of New B4C Ceramic Doped with High-Entropy Alloy in an Aggressive Environment. Microsc. Microanal. 2024, 30, ozae044.666. Doi:10.1093/mam/ozae044.666.

38. Rico-Cano, A.D.; Mirza-Rosca, J.C.; Ocak, B.C.; Goller, G. Impact of CoCrFeNiMo High-Entropy-Alloy Doping on the Mechanical and Electrochemical Properties of B4C Ceramic. Appl. Sci. 2025, 15, 4859. https://doi.org/10.3390/app15094859.

39. German, R.M.; Suri, P.; Park, S.J. Review: Liquid Phase Sintering. J. Mater. Sci. 2009, 44, 1–39. DOI: 10.1007/s10853-008-3008-0